

---

# THERMAL AND CRYSTALLINITY PROFILES IN LAMINATES MANUFACTURED WITH AUTOMATED THERMOPLASTIC TOW PLACEMENT PROCESS

by

Erin Patricia Quinlan

Department of Mechanical Engineering

McGill University, Montreal, Quebec

A thesis submitted to

McGill University

in partial fulfillment of the requirements for the degree of

Master's of Engineering



© Erin Patricia Quinlan 2011

February 2011

---

# ABSTRACT

Automated Tow Placement (ATP) is an increasingly desirable manufacturing technique for composite materials for aerospace applications. Historically, thermoset composites have been the desired material for ATP. However, high performance thermoplastics have proven they can perform as well as the thermoset matrix. The three main goals to further the research on thermoplastics used in ATP are the following. First, to model the crystallinity level of a thermoplastic composite material with Differential Scanning Calorimetry (DSC) experiments on thermoplastic films. Second, to provide a thermal analysis through the thickness of the material profile and determine cooling rates that occur in carbon fiber-thermoplastic matrix laminates during processing. Last, to measure by DSC method the post processing crystallinity levels through the thickness of a laminate manufactured in ATP.

A set of DSC experiments using isothermal and dynamic cooling measured the crystallinity levels in thermoplastic films. Each experiment was compared with models from literature. After comparing three different models, none fit well to the experimental data. In order to fit properly, the constants in the literature models had to be refit to the data collected by method of least squares; however, the models fit well for the slower cooling rates only. Experiments on ATP to measure the temperatures and calculate the cooling rates through the part thickness showed that the cooling rate is affected by the material that the composite tow is laid onto. The same manufactured parts that had thermocouples implanted were also used to test the crystallinity levels through three sections of the part thickness. There was not much difference in crystallinity level through the thickness since the material used is a high crystalline material.

Generally, the material properties are related to the crystallinity level found in the thermoplastic matrix. Since it does not require the secondary post cure step as thermoset composites require, the ATP manufacturing process for thermoplastic composites is an in-situ method. This thesis seeks to provide more clarity in modeling crystallinity levels and the ATP manufacturing process for thermoplastic composites.

---

## RÉSUMÉ

L'attrait envers la fabrication de pièces en matériaux composites par des méthodes de placement de fibre automatisés (ATP) est actuellement en pleine croissance dans les milieux aéronautiques. Traditionnellement, ce sont les matrices thermodurcissables qui ont dominées les applications d'ATP. Par contre, les matrices thermoplastiques de haute performance ont prouvés qu'elles pouvaient être comparables aux thermodurcissables. Les trois objectifs principaux de la présente recherche se décrivent comme suit : Tout d'abord, modéliser le taux de cristallinité d'une pièce en matériaux composites à l'aide d'expérimentations de calorimétrie à balayage différentiel (DSC) sur des films thermoplastiques. Ensuite, déterminer les taux de refroidissement lors de la fabrication d'un laminé de fibre de carbone-thermoplastique afin d'analyser le profile thermique d'une pièce à travers son épaisseur. Finalement, mesurer, à l'aide de la méthode DSC, les taux réels de cristallinité à travers l'épaisseur d'un laminé fabriqué par procédé ATP.

Le taux de cristallinité de films thermoplastiques ayant subies des phases de refroidissement dynamique et isotherme a été mesuré à l'aide d'une série de tests en DSC. Les résultats de chaque échantillon ont été comparés à des modèles provenant de la littérature. La comparaison a révélée qu'aucun des différents modèles ne correspondait bien aux données recueillies de façon expérimentale. Afin d'obtenir une correspondance adéquate, des méthodes de moindres carrés ont dû être utilisées sur les données expérimentales afin de recalculer les constantes proposées par les modèles. Par contre, seuls les résultats pour les taux de refroidissement les plus lents ont démontrés une bonne corrélation avec les modèles. Des expérimentations servant à mesurer les températures et à calculer les taux de refroidissement à traves l'épaisseur de pièces fabriquées par procédés ATP ont démontré que le taux de refroidissement est dépendent de la nature du matériau sur lequel les fibres sont déposées. Les mêmes pièces, dans lesquelles des thermocouples avaient été introduits lors de la fabrication, ont également été utilisées afin de mesurer les taux de cristallinité de trois sections localisées à travers l'épaisseur de ces dernières. Les différents taux de cristallinité obtenus se sont avérés être très similaires, ce qui pourrait

s'explique par le fait que, à la base, le matériau utilisé est un matériau très cristallin.

De façon générale, les propriétés des matériaux composites à matrice thermoplastiques sont reliées au taux de cristallinité de ces dernières. Les procédés de fabrication par ATP de composites à base de thermoplastiques sont considérés comme des méthodes *in-situ* puisque, à l'encontre de leurs équivalents thermodurcissables, ils ne requièrent aucun traitement particulier, tel que la cuisson, après avoir terminé la déposition des différentes couches du laminé. Le présent mémoire a pour but d'apporter plus de précisions quant à la modélisation des taux de cristallinité ainsi qu'aux procédés de fabrication par ATP de composites à matrices thermoplastiques.

---

# ACKNOWLEDGEMENTS

Throughout the time for completing this Masters Degree, there have been many people who have been involved with my life in their own special way.

To begin, I would like to express my gratitude to my supervisor Pascal Hubert. He brought me into a great research group at McGill and with his advice on my work through all the struggles over the duration of the project, has pushed to make it the best possible work to present.

At NRC, I had a couple other supervisors to support my project and advise me with manufacturing and DSC experiments: Mehdi Hojjati and Ali Yousefpour.

The CRIAQ COMP5 project funding, which this thesis is based on, is from the following companies and the Canadian government: Bell Helicopter, Bombardier Aerospace, NRC-Canada, and NSERC. Also thanks to the project's technical leader Professor Suong Hoa, from Concordia University.

Outside help on the project for modeling: Andrew Floyd from Convergent and Professor Musa Kamal and Jorge Uribe-Caladron from McGill University. Also, from NRC: Hugo Laurin, François Ferland, and Alex Chen have also been instrumental to the project for the ATP experiments. Thank you all.

All of the members of the Structures and Composites Laboratory plus FDA015 have really been a great source of support, advice, and friendship over the past couple years, especially: Loleï Khoun (notably with modeling and presentations), Xavier Gagné-Brollette (in particular with manufacturing and translating the abstract), Kaven Croft, Jim Kratz, Meysam Rahmat, Tim Centea, and Mélanie Brilliant.

To the friends outside of "the lab": Sai, Julio, Erin, Lina, Kathleen, and Alexandra. And of course, in an over simplified statement to both Nicole and Gustavo (btw, you were going to be mentioned before you even requested it), your friendships to me are very dear and special.

Finally, thanks to my family. Meagan, you are a wonderful sister and I will always be grateful for our proximity to each other when everyone else is far. Mom, thanks for always being there to listen to me at all hours whether they were late for you or late for me. Dad, thank you for giving us the best opportunities and experiences possible to succeed. I love you all so much.

“When you want something,  
all the universe conspires in helping you to achieve it”

– from *The Alchemist* by Paulo Coelho

---

# TABLE OF CONTENTS

<b>Abstract</b> .....	<b>ii</b>
<b>Résumé</b> .....	<b>iii</b>
<b>Table of Contents</b> .....	<b>vii</b>
<b>List of Figures</b> .....	<b>ix</b>
<b>List of Tables</b> .....	<b>xiv</b>
<b>List of Abbreviations and Constants</b> .....	<b>xv</b>
<b>Abbreviations:</b> .....	<b>xv</b>
<b>Constants:</b> .....	<b>xvi</b>
<b>Chapter 1: Introduction</b> .....	<b>1</b>
1.1 <i>Background</i> .....	1
1.2 <i>Project Motivation and Goals</i> .....	4
<b>Chapter 2: Literature Review</b> .....	<b>5</b>
2.1 <i>General Composite Material Research</i> .....	5
2.1.1 <i>Fiber Reinforcement</i> .....	6
2.1.2 <i>Polymer Matrix</i> .....	6
2.2 <i>Thermoplastic Crystallinity Review</i> .....	10
2.2.1 <i>Measuring Crystallinity Level</i> .....	12
2.2.2 <i>Modeling Crystalline Microstructure</i> .....	14
2.2.3 <i>Modeling Crystallinity of PEEK Material</i> .....	16
2.3 <i>Manufacturing Research</i> .....	20
2.3.1 <i>Pre-Processing</i> .....	22
2.3.2 <i>Manufacturing Stages</i> .....	22
2.3.3 <i>Experimental Work (Thermal and Crystallinity)</i> .....	24
2.3.4 <i>Modeling the ATP Manufacturing Process</i> .....	25
2.4 <i>Summary of Literature Review</i> .....	27
<b>Chapter 3: Characterizing Material</b> .....	<b>29</b>
3.1 <i>Material</i> .....	29
3.1.1 <i>Properties</i> .....	30
3.2 <i>Crystallinity Modeling</i> .....	30
3.2.1 <i>Experimental Methodology</i> .....	32
3.2.2 <i>Isothermal DSC Experiments</i> .....	32
3.2.3 <i>Dynamic DSC Experiments</i> .....	39
3.3 <i>Visualizing Crystals in Film Material</i> .....	50
3.3.1 <i>Isothermally Crystallized Sample</i> .....	50
3.3.2 <i>Dynamically Crystallized Samples</i> .....	51

3.4	<i>Summary</i> .....	53
<b>Chapter 4: Manufacturing Processing</b> .....		<b>54</b>
4.1	<i>Material Selection</i> .....	55
4.2	<i>Experimental Plan</i> .....	55
4.3	<i>Manufacturing Procedure</i> .....	58
4.3.1	Manufacturing Considerations for ATP .....	60
4.3.2	Manufacturing Measurements During ATP .....	61
4.3.3	Post Processing Measurements .....	62
4.4	<i>Results</i> .....	65
4.4.1	Temperature Profile During the Process .....	65
4.4.2	Mandrel Effect on Cooling the Material .....	75
4.4.3	Cooling Rate Summary .....	79
4.5	<i>Crystallinity Measurements of Part Post Processing</i> .....	80
4.6	<i>Summary</i> .....	82
<b>Chapter 5: Conclusions</b> .....		<b>84</b>
<b>References</b> .....		<b>87</b>
<b>Appendix A: Modeling</b> .....		<b>91</b>
6.1	<i>Isothermal modeling</i> .....	91
6.2	<i>Dynamic modeling</i> .....	92
<b>Appendix B: ATP Manufacturing</b> .....		<b>93</b>
7.1	<i>Cooling rate with respect to processing time</i> .....	93
7.2	<i>Temperature with respect to processing time</i> .....	94
7.2.1	PEEK rings: .....	95
7.2.2	PEKK rings:.....	96

---

# LIST OF FIGURES

FIGURE 1.1-1: BOEING 787 DREAMLINER AIRCRAFT IMPLEMENTS A HIGH PERCENTAGE OF COMPOSITE MATERIALS IN A COMMERCIAL AIRCRAFT FOR THE FIRST TIME [2].....	2
FIGURE 1.1-2: DIAGRAM OF THE AUTOMATED TOW PLACEMENT (ATP) MANUFACTURING PROCESS.....	3
FIGURE 2.1-1: POLYMER MATRIX WITH REINFORCEMENT FIBERS TO MAKE A COMPOSITE [3].....	5
FIGURE 2.1-2: BASIC “ETHYLENE” MOLECULAR MER UNIT OF A POLYMER.....	6
FIGURE 2.1-3: CROSS-LINK NETWORK CREATED WITH MER UNITS IN A THERMOSET POLYMER [4].....	7
FIGURE 2.1-4: CRYSTALLINE AND AMORPHOUS REGIONS OF A THERMOPLASTIC POLYMER [3].....	8
FIGURE 2.1-5: THERMOPLASTIC POLYETHYLENE POLYMER CHAINS ALIGNED NEXT TO EACH OTHER [3].....	9
FIGURE 2.2-1: GENERAL PHASE DIAGRAM OF POLYMER AND GLASS MATERIALS [3].....	10
FIGURE 2.2-2: SPHERULITIC AND EPITAXIAL CRYSTAL GEOMETRY FORMATIONS IN THE THERMOPLASTIC MATRIX OF A FIBER COMPOSITE [7].....	12
FIGURE 2.2-3: TYPICAL DSC CHART OF HEAT FLOW WITH RESPECT TO TEMPERATURE....	13
FIGURE 2.2-4: GENERAL GRAPH THAT DESCRIBES HOW TO SOLVE FOR “K” AND “N” VALUES USING $\ln(-\ln(1-X(T)))$ VERSUS $\log(T)$ AS THE Y-INTERCEPT AND SLOPE FOR EACH TEMPERATURE LINE, RESPECTIVELY.....	18
FIGURE 2.3-1: ATP ON THE FRONT FUSELAGE SECTION OF BOEING 787 DREAMLINER [30].....	21
FIGURE 2.3-2: THE THREE COMPOSITE MATERIAL PROCESSING STAGES (ADAPTED [31])	23
FIGURE 2.3-3: INFRARED THERMAL CAMERA IMAGE PROFILE OF A SINGLE PLY THAT IS HEATED BY THE ATP TORCH HEAD (MODIFIED FROM TIERNEY [27]).....	25
FIGURE 3.1-1: MER UNITS OF (A) POLY ETHER ETHER KETONE AND (B) POLY ETHER KETONE.....	30
FIGURE 3.2-1: HEAT OF CRYSTALLIZATION WITH RESPECT TO ISOTHERMAL HOLD TIME FOR THREE TEMPERATURES OF DSC TESTS ON PEEK FILM MATERIAL.....	33
FIGURE 3.2-2: COMPARING THE CRYSTALLINITY LEVEL OF ISOTHERMAL CRYSTALLINITY EXPERIMENTS TO LITERATURE VALUES [7], FOR PEEK FILM MATERIAL AS A FUNCTION OF THE ISOTHERMAL TEMPERATURE.....	34
FIGURE 3.2-3: CRYSTALLINITY LEVEL AS A FUNCTION OF ISOTHERMAL HOLD TIME FOR PEEK FILMS AT THREE TEMPERATURES.....	35

FIGURE 3.2-4: PEEK FILM ISOTHERMAL DSC CRYSTALLINITY DATA USED TO SOLVE FOR AVRAMI CONSTANTS, $N_1$ AND $N_2$ , AS THE SLOPES OF THE FITTED LINES FOR EACH TEMPERATURE .....	36
FIGURE 3.2-5: AVRAMI SHAPE CONSTANTS, $K_1$ AND $K_2$ , PLOTTED WITH RESPECT TO THE ISOTHERMAL TEMPERATURE.....	37
FIGURE 3.2-6: ISOTHERMAL CRYSTALLINITY DATA ON PEEK FILM FITTED TO THE AVRAMI MODEL BY FINDING THE AVRAMI CONSTANTS AND SHAPE FACTORS.....	38
FIGURE 3.2-7: PEEK FILM ISOTHERMAL DSC TESTS FOR THREE TEMPERATURES ARE FITTED TO THE NAKAMURA MODEL USING METHOD OF LEAST SQUARES TO FIND THE CONSTANTS.....	39
FIGURE 3.2-8: HEAT OF CRYSTALLIZATION FOR PEEK FILM MATERIAL AS A DYNAMIC DSC SCAN AT A VARIETY OF COOLING RATES.....	41
FIGURE 3.2-9: COMPARING CRYSTALLINITY LEVEL AS A FUNCTION OF MATERIAL COOLING RATE FOR THE CURRENT WORK TO LITERATURE [7] .....	42
FIGURE 3.2-10: COMPARING MODELS USING THE CONSTANTS FROM LITERATURE TO DYNAMIC EXPERIMENTAL DSC CRYSTALLINITY DATA FOR PEEK FILM AT A COOLING RATE OF $1^{\circ}\text{C}/\text{MIN}$ .....	43
FIGURE 3.2-11: COMPARING MODELS USING THE CONSTANTS FROM LITERATURE TO DYNAMIC EXPERIMENTAL DSC CRYSTALLINITY DATA FOR PEEK FILM AT A COOLING RATE OF $5^{\circ}\text{C}/\text{MIN}$ .....	44
FIGURE 3.2-12: COMPARING MODELS USING THE CONSTANTS FROM LITERATURE TO DYNAMIC EXPERIMENTAL DSC CRYSTALLINITY DATA FOR PEEK FILM AT A COOLING RATE OF $10^{\circ}\text{C}/\text{MIN}$ .....	44
FIGURE 3.2-13: CEBE MODEL FITTED TO DYNAMIC DSC EXPERIMENTAL DATA FOR PEEK FILMS AT COOLING RATES OF $0.5\text{-}5^{\circ}\text{C}/\text{MIN}$ .....	46
FIGURE 3.2-14: CEBE MODEL FITTED MODEL TO DYNAMIC DSC EXPERIMENTAL DATA FOR PEEK FILMS AT COOLING RATES OF $5\text{-}30^{\circ}\text{C}/\text{MIN}$ .....	46
FIGURE 3.2-15: TIERNEY MODEL FITTED TO DYNAMIC DSC EXPERIMENTAL DATA FOR PEEK FILMS AT COOLING RATES OF $0.5\text{-}5^{\circ}\text{C}/\text{MIN}$ .....	47
FIGURE 3.2-16: TIERNEY MODEL FITTED TO DYNAMIC DSC EXPERIMENTAL DATA FOR PEEK FILMS AT COOLING RATES OF $5\text{-}30^{\circ}\text{C}/\text{MIN}$ .....	47
FIGURE 3.2-17: NAKAMURA MODEL FITTED TO DYNAMIC DSC EXPERIMENTAL DATA FOR PEEK FILMS AT COOLING RATES OF $0.5\text{-}5^{\circ}\text{C}/\text{MIN}$ .....	48
FIGURE 3.2-18: NAKAMURA MODEL FITTED TO DYNAMIC DSC EXPERIMENTAL DATA FOR PEEK FILMS AT COOLING RATES OF $5\text{-}30^{\circ}\text{C}/\text{MIN}$ .....	49
FIGURE 3.3-1: CRYSTALS FORMED IN ISOTHERMAL DSC EXPERIMENTS ON PEEK FILM AT $325^{\circ}\text{C}$ (100x).....	51
FIGURE 3.3-2: CRYSTALS FORMED IN DYNAMIC DSC EXPERIMENTS ON PEEK FILM WHEN COOLED AT $1^{\circ}\text{C}/\text{MIN}$ (100x).....	52

FIGURE 3.3-3: CRYSTALS FORMED IN DYNAMIC DSC EXPERIMENTS ON PEEK FILM WHEN COOLED AT 10°C/MIN (100x).....	52
FIGURE 4.2-1: ATP MANUFACTURING HEAD WITH A DESCRIPTION OF THE IMPORTANT MANUFACTURING PARAMETERS TO THE ATP PROCESS .....	56
FIGURE 4.2-2: MANUFACTURING SETUP WITH THERMOCOUPLES AND WIRELESS DATA AQUISITION SYSTEM .....	58
FIGURE 4.3-1: ACTUAL CARBON FIBER/THERMOPLASTIC MATRIX RING MANUFACTURED BY ATP .....	59
FIGURE 4.3-2: MANUFACTURING SETUP THAT INCLUDES THE ATP HEAD, ANODIZED ALUMINUM MANDREL, AND THERMOCOUPLES IMBEDDED IN LAMINITE RING.....	60
FIGURE 4.3-3: EXAMPLE OF A POORLY MANUFACTURED RING THAT HAD SIGNIFICANT TOW DRIFT; THE WIRES ARE TRIMMED THERMOCOUPLE WIRES .....	61
FIGURE 4.3-4: GENERAL SECTION OF A RING MANUFACTURED OUT OF THERMOPLASTIC MATERIAL BY ATP THAT SHOWS THE GENERAL PLACEMENT OF THE THERMOCOUPLES THROUGH THE THICKNESS .....	61
FIGURE 4.3-5: MANUFACTURING RING PART ON MANDREL WITH THERMOCOUPLES IN PLACE.....	62
FIGURE 4.3-6: THE THREE SECTIONS OF THE ATP MANUFACTURED RING THAT WERE TESTED IN THE DSC.....	63
FIGURE 4.3-7: DSC CHART OBTAINED FOR A SECTION OF ATP MANUFACTURED RING.....	64
FIGURE 4.4-1: CLOSEUP OF THE NIP POINT AND OF THE THERMOCOUPLE, WHICH LAYS IN BETWEEN THE LAMINATE LAYERS.....	66
FIGURE 4.4-2: GENERAL TEMPERATURE BEHAVIOR FOR ONE LAYER DURING ATP; THE MATERIAL REHEATS AFTER A MANDREL REVOLUTION WHEN THE TORCH PASSES OVER THE MATERIAL AT THE SAME POINT AGAIN .....	67
FIGURE 4.4-3: TEMPERATURE WITH RESPECT TO PROCESSING TIME FOR ONE THERMOCOUPLE IN THE PEEK RING SHOWS THAT AS MORE LAYERS ARE DEPOSITED THE PEAK TEMPERATURE DECREASES, WHILE THE OVERALL TEMPERATURE GRADUALLY INCREASES.....	68
FIGURE 4.4-4: THERMOCOUPLE RESULTS FOR THE PEEK RING MANUFACTURED BY ATP FOR SEVEN LAYERS .....	69
FIGURE 4.4-5: THERMOCOUPLE RESULTS FOR THE PEKK RING MANUFACTURED BY ATP FOR EIGHT LAYERS.....	69
FIGURE 4.4-6: FOR EACH LAYER MEASURED, THE FREQUENCY THAT THE TEMPERATURE PEAKS INTO THE MELT CRYSTALLIZATION ZONE; THE MIDDLE LAYERS SHOW A HIGHER FREQUENCY THAN THE FIRST AND LAST LAYERS.....	70
FIGURE 4.4-7: PEEK RING AT LAYER 10 - THE COOLING AND HEATING RATES WITH RESPECT TO THE PROCESSING TIME FOLLOW AN EXPONENTIAL TREND.....	71
FIGURE 4.4-8: PEEK RING AT LAYER 41 - THE COOLING AND HEATING RATES WITH RESPECT TO THE PROCESSING TIME FOLLOW AN EXPONENTIAL TREND.....	72

FIGURE 4.4-9: A GENERAL THERMOCOUPLE CHART OF TEMPERATURE WITH RESPECT TO PROCESSING TIME, AFTER ONE REVOLUTION.....	73
FIGURE 4.4-10: THE COOLING RATES FOR THE VARIOUS LAYERS FOR THE PEEK RING AFTER EACH ROTATION WITH RESPECT TO THE PROCESSING TIME FOR ROTATIONS WHERE THE MATERIAL IS REHEATED INTO THE MELT CRYSTALLIZATION REGION.....	74
FIGURE 4.4-11: THE COOLING RATES FOR THE VARIOUS LAYERS FOR THE PEKK RING AFTER EACH ROTATION WITH RESPECT TO THE PROCESSING TIME; ONLY DISPLAYING COOLING RATES FOR THE ROTATIONS WHERE THE MATERIAL IS REHEATED INTO THE MELT CRYSTALLIZATION REGION.....	75
FIGURE 4.4-12: THE MANDREL TEMPERATURES DURING THE ATP PROCESS GRADUALLY INCREASE DURING MANUFACTURING TIME.....	76
FIGURE 4.4-13: PEEK RING AT LAYER 10 - THE “HIGH” TEMPERATURES AFTER EACH MANDREL REVOLUTION GRADUALLY DECREASES AND FALLS INTO THE MELT CRYSTALLIZATION RANGE FOR A PERIOD OF TIME WHILE THE “LOW” TEMPERATURES SLIGHTLY INCREASE WITH MANUFACTURING TIME.....	77
FIGURE 4.4-14: PEEK RING AT LAYER 21 - THE “HIGH” TEMPERATURES AFTER EACH MANDREL REVOLUTION GRADUALLY DECREASES AND FALLS INTO THE MELT CRYSTALLIZATION RANGE FOR A PERIOD OF TIME WHILE THE “LOW” TEMPERATURES SLIGHTLY INCREASE WITH MANUFACTURING TIME.....	78
FIGURE 4.4-15: PEEK RING AT LAYER 75 - THE “HIGH” TEMPERATURES AFTER EACH MANDREL REVOLUTION GRADUALLY DECREASES AND FALLS INTO THE MELT CRYSTALLIZATION RANGE FOR A PERIOD OF TIME WHILE THE “LOW” TEMPERATURES SLIGHTLY INCREASE WITH MANUFACTURING TIME.....	78
FIGURE 4.5-1: ACTUAL RING, DESCRIBING THE LOCATION OF WHERE EACH SAMPLE WAS TAKEN.....	80
FIGURE 4.5-2: MEASURED CRYSTALLINITY LEVELS OF THE THREE SECTIONS OF BOTH LAMINATE RINGS.....	81
FIGURE 7.1-1: PEEK RING COOLING RATE AT EACH LAYER VERSUS ATP PROCESSING TIME WHERE EACH DOT REPRESENTS ONE MANDREL ROTATION.....	93
FIGURE 7.1-2: PEKK RING COOLING RATE AT EACH LAYER VERSUS ATP PROCESSING TIME, WHERE EACH DOT REPRESENTS ONE MANDREL ROTATION.....	94
FIGURE 7.2-1: PEEK RING AT LAYER 41 - THE “HIGH” TEMPERATURES AFTER EACH MANDREL REVOLUTION GRADUALLY DECREASES AND FALLS INTO THE MELT CRYSTALLIZATION RANGE FOR A PERIOD OF TIME WHILE THE “LOW” TEMPERATURES SLIGHTLY INCREASE WITH MANUFACTURING TIME.....	95
FIGURE 7.2-2: PEEK RING AT LAYER 51 - THE “HIGH” TEMPERATURES AFTER EACH MANDREL REVOLUTION GRADUALLY DECREASES AND FALLS INTO THE MELT CRYSTALLIZATION RANGE FOR A PERIOD OF TIME WHILE THE “LOW” TEMPERATURES SLIGHTLY INCREASE WITH MANUFACTURING TIME.....	95

FIGURE 7.2-3: PEKK RING AT LAYER 1 - THE “HIGH” TEMPERATURES AFTER EACH  
MANDREL REVOLUTION GRADUALLY DECREASES AND FALLS INTO THE MELT  
CRYSTALLIZATION RANGE FOR A PERIOD OF TIME WHILE THE “LOW” TEMPERATURES  
SLIGHTLY INCREASE WITH MANUFACTURING TIME ..... 96

FIGURE 7.2-4: PEKK RING AT LAYER 8 - THE “HIGH” TEMPERATURES AFTER EACH  
MANDREL REVOLUTION GRADUALLY DECREASES AND FALLS INTO THE MELT  
CRYSTALLIZATION RANGE FOR A PERIOD OF TIME WHILE THE “LOW” TEMPERATURES  
SLIGHTLY INCREASE WITH MANUFACTURING TIME ..... 96

FIGURE 7.2-5: PEKK RING AT LAYER 38 - THE “HIGH” TEMPERATURES AFTER EACH  
MANDREL REVOLUTION GRADUALLY DECREASES AND FALLS INTO THE MELT  
CRYSTALLIZATION RANGE FOR A PERIOD OF TIME WHILE THE “LOW” TEMPERATURES  
SLIGHTLY INCREASE WITH MANUFACTURING TIME ..... 97

FIGURE 7.2-6: PEKK RING AT LAYER 48 - THE “HIGH” TEMPERATURES AFTER EACH  
MANDREL REVOLUTION GRADUALLY DECREASES AND FALLS INTO THE MELT  
CRYSTALLIZATION RANGE FOR A PERIOD OF TIME WHILE THE “LOW” TEMPERATURES  
SLIGHTLY INCREASE WITH MANUFACTURING TIME ..... 97

FIGURE 7.2-7: PEKK RING AT LAYER 59 - THE “HIGH” TEMPERATURES AFTER EACH  
MANDREL REVOLUTION GRADUALLY DECREASES AND FALLS INTO THE MELT  
CRYSTALLIZATION RANGE FOR A PERIOD OF TIME WHILE THE “LOW” TEMPERATURES  
SLIGHTLY INCREASE WITH MANUFACTURING TIME ..... 98

FIGURE 7.2-8: PEKK RING AT LAYER 66 - THE “HIGH” TEMPERATURES AFTER EACH  
MANDREL REVOLUTION GRADUALLY DECREASES AND FALLS INTO THE MELT  
CRYSTALLIZATION RANGE FOR A PERIOD OF TIME WHILE THE “LOW” TEMPERATURES  
SLIGHTLY INCREASE WITH MANUFACTURING TIME ..... 98

---

# LIST OF TABLES

TABLE 2.2-1: SUMMARY OF WEIGHT FRACTION “ $W_1$ ” WITH RESPECT TO THE COOLING RATE [7].....	16
TABLE 2.2-2: CONSTANTS FOR THE DIFFERENT CRYSTALLINITY MODELS ON PEEK FILM MATERIAL FROM LITERATURE [7, 23, 27].....	20
TABLE 3.1-1: MATERIAL PROPERTIES OF CYTEC’S PEEK AND PEEK FILM MATERIAL [40] .....	30
TABLE 3.2-1: SUMMARY OF THE MODELING EQUATIONS FOUND IN LITERATURE, FOR THE CONSTANT “ $k$ ”, THAT ARE USED FOR PEEK FILMS [7, 15-16, 23-25, 27-29, 33] ...	32
TABLE 4.1-1: IMPORTANT TEMPERATURES FOR BOTH MATERIALS TO CONSIDER IN MANUFACTURING [45].....	55
TABLE 4.2-1: ATP MANUFACTURING PARAMETERS FOR BOTH COMPOSITE TAPE MATERIALS.....	57
TABLE 4.4-1: COOLING RATES OF THE THREE SECTIONS OF THE COMPOSITE RINGS .....	79
TABLE 6.1-1: ISOTHERMAL $k_1$ AND $k_2$ VALUES IN AVRAMI MODEL.....	91
TABLE 6.1-2: THE NAKAMURA CONSTANTS SOLVED FOR BY METHOD OF LEAST SQUARES FOR FITTING THE MODEL TO THE ISOTHERMAL DSC DATA .....	91
TABLE 6.2-1: BEST FIT CONSTANTS FOR FITTING THE CEBE MODEL TO EXPERIMENTAL DSC DATA.....	92
TABLE 6.2-2: BEST FIT CONSTANTS FOR FITTING THE TIERNEY MODEL TO EXPERIMENTAL DSC DATA.....	92
TABLE 6.2-3: BEST FIT CONSTANTS FOR FITTING THE NAKAMURA MODEL TO EXPERIMENTAL DSC DATA.....	92

---

# LIST OF ABBREVIATIONS AND CONSTANTS

## ABBREVIATIONS:

CFRP	Carbon fiber reinforced polymers
PEEK	Poly ether ether ketone
PEKK	Poly ether ketone ketone
PEI	Polyetherimide
PET	Poly(ethylene terephthalate)
ATP	Automated Tow Placement
DSC	Differential Scanning Calorimetry
WLF	Williams, Landel, and Ferry

## CONSTANTS:

$T_g$	Glass transition temperature
$T_m$	Melting temperature
$T$	Temperature
$t$	time
$\tau$	time
$H$	Enthalpy
$H_c$	Heat of crystallinity
$H_m$	Heat of melting
$H_u$	Ultimate heat of crystallization
$X$	Crystallinity level
$X_c$	Crystallinity level
$X_i$	Initial crystallinity level
$X_\infty$	Equilibrium crystallinity level
$X_{vc}$	Volumetric crystallinity level
$X_{vc\infty}$	Equilibrium volume fraction crystallinity level
$X_{vcinf}$	Infinite volumetric crystallinity level
$k$	Avrami constant
$k_1$	Avrami constant for primary crystallization
$k_2$	Avrami constant for secondary crystallization
$n$	Avrami exponent
$n_1$	Avrami exponent for primary crystallization
$n_2$	Avrami exponent for secondary crystallization
$C_1$	Universal parameter for WLF equation
$C_2$	Universal parameter for WLF equation

$w_1$	Weight fraction for primary crystallization
$w_2$	Weight fraction for secondary crystallization
$F_{vc1}$	Fraction of crystallized polymer for primary crystallization
$F_{vc2}$	Fraction of crystallized polymer for secondary crystallization
$C_{i1}$	Coefficient for model constant, where $i=1, 2$
$C_{i2}$	Empirical parameter that depends on temperature and viscosity, where $i=1, 2$
$C_{i3}$	Free energy of nucleation constant, where $i=1, 2$

---

# CHAPTER 1: INTRODUCTION

One of the most important steps of the design process occurs when an engineer selects the best possible material from a plethora of choices for the desired application. During this material selection process, the engineer must consider how the material will behave in the desired application and complete a cost-benefit analysis. When the basic load type, i.e. tension, compression, torsion, or shear, that the part or system is put under is known, the material type for the desired application can be chosen. The main material categories encompass metals, polymers, ceramics, and glasses. Then there are composites, which is when two materials with distinctive properties are combined to make one material. A primitive example of a composite material is mud and straw, which was used to make houses. Modern composites, such as Carbon Fiber Reinforced Polymer (CFRP) composites, are a hot topic in engineering research, due to their technologically-advanced abilities.

## 1.1 BACKGROUND

CFRP composites have been heavily supported by the aerospace industry, especially for use in military aircraft. The technology has matured and proven that it is a viable material choice since the 1960's when CFRP composites were first introduced into military aircraft, such as the Boeing B52 aircraft [1]. At the time, composites were only used in less critical components in military aircraft design and all together excluded from commercial aircraft. Over the years, engineers have gained more knowledge and experience with using composite materials as they have been gradually implemented into more load bearing components on military aircraft. Eventually, composites have shown up in commercial aircraft, starting with the less critical components as done in the military aircraft. By 2010, all four

major commercial aircraft manufacturers: Boeing, Airbus, Bombardier, and Embraer, have begun to heavily implement composite materials on their newest aircraft model designs as a way of reducing weight (Figure 1.1-1). Other industrial sectors, like the automotive and sports industries also see the advantages to using these materials and are implementing them into their designs.

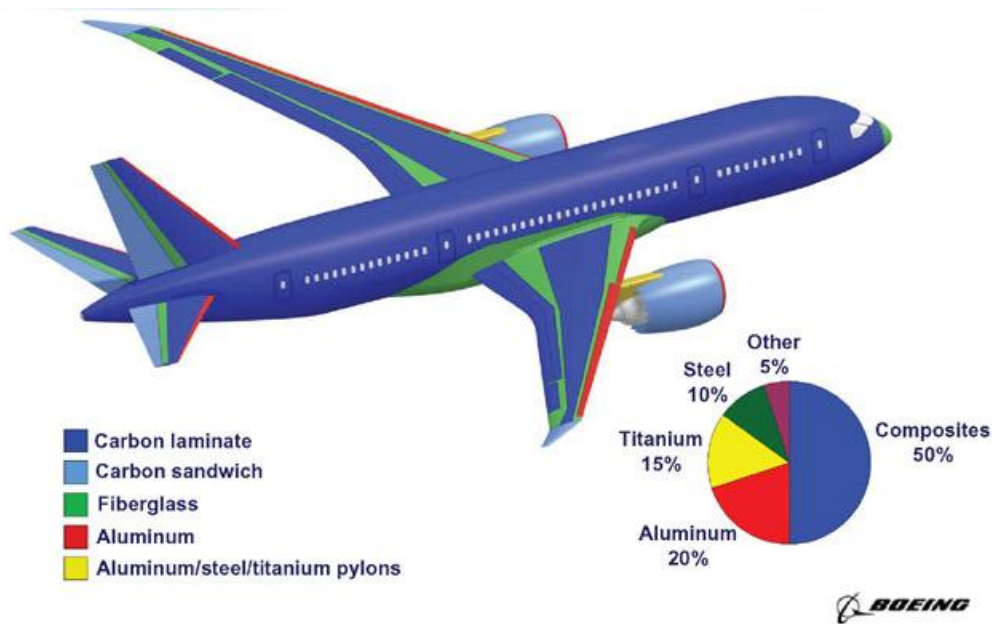
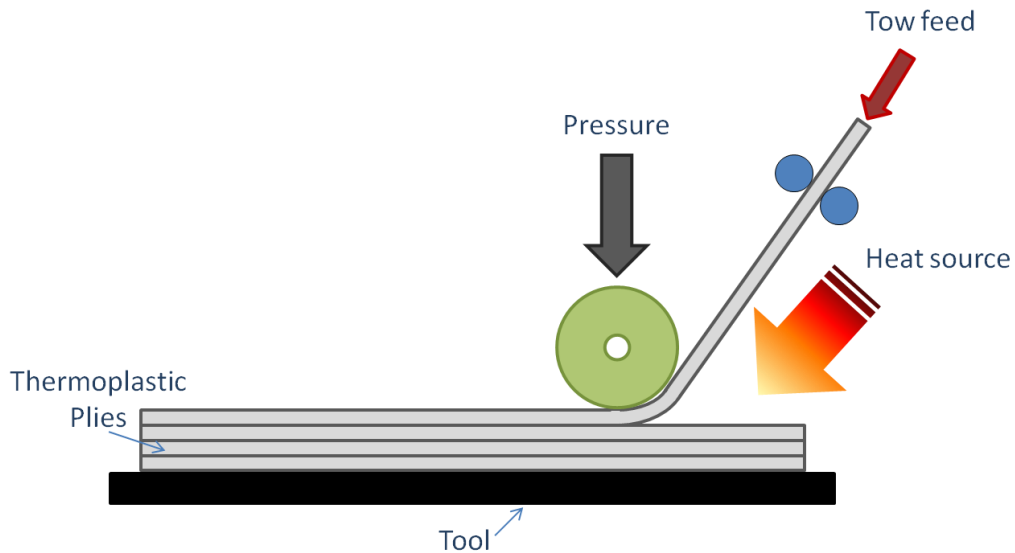


FIGURE 1.1-1: BOEING 787 DREAMLINER AIRCRAFT IMPLEMENTS A HIGH PERCENTAGE OF COMPOSITE MATERIALS IN A COMMERCIAL AIRCRAFT FOR THE FIRST TIME [2]

Composite material processing occurs simultaneously with part manufacturing. The layers of laminate fibers with the polymer are applied gradually to a part's mold. There are a variety of manufacturing methods available. The one that this thesis focuses on is Automated Tow Placement (ATP), which utilizes a robotic head to manufacture the material and part. A robotic head that contains a gas torch and roller will heat up and apply pressure to lay the pre-impregnated fibers in a tow material form from a roll

and onto a mold (Figure 1.1-2). The three processing stages in manufacturing are heating, consolidating, and cooling.



**FIGURE 1.1-2: DIAGRAM OF THE AUTOMATED TOW PLACEMENT (ATP) MANUFACTURING PROCESS**

There are two types of polymer systems that can be used as the matrix in CFRPs: thermoset and thermoplastic. Thermoset matrices are traditionally used as the matrix system. The solidifying stage differs for both polymers; thermosets cure due to a chemical reaction that creates cross-links, whereas thermoplastics crystallize due to cooling.

For thermoplastic composites, ATP is an *in-situ* processing practice while for thermosets the material would need to be put into an autoclave in order to complete the material curing process. This additional step in processing significantly increases the manufacturing cost. By using a thermoplastic material, this will allow for cheaper processing but at the expense of the material cost.

## 1.2 PROJECT MOTIVATION AND GOALS

The overall motivation in this thesis is to understand how the consequent changes in cooling rates through a thermoplastic CRFP part's layers in the ATP manufacturing process will affect the crystallinity level of the matrix in each layer. Manufacturers need to know the effects of the cooling rates that occur on the composite material since it plays a significant role on the final crystallinity level of a part manufactured by the ATP process.

In order to accomplish this, studies can model the crystallinity level of a polymer film due to the cooling rate. Next, further studies by manufacturing parts to measure the heating and cooling rates, as well as the crystallinity levels post processing can be carried out. During the investigation, this study tries to comprehend how the crystalline structure in a thermoplastic composite material is affected by the constant heating and cooling during ATP processing. This is done by modeling the cooling behavior on the polymer material and by examining the temperatures that are incurred during processing. The project objective is to model solidification behavior of thermoplastic tape per the cooling rates the material is subjected to during the ATP process.

The organization of this thesis is described as follows:

- Chapter 2 summarizes the literature on modeling crystallinity level, thermoplastic materials, and ATP manufacturing process.
- Chapter 3 describes modeling crystallinity levels of a thermoplastic material along with visualizing the crystals that found in the polymer material after it has cooled.
- Chapter 4 goes into detail on the ATP manufacturing experiment to measure the cooling rates and the crystallinity levels from manufactured laminates.
- Chapter 5 concludes the thesis and proposes future work that can be completed in this field.

---

## CHAPTER 2: LITERATURE REVIEW

Composites research covers a multitude of topics that can range from the molecular composition of a material to the structural properties that occur in a composite part or even to a manufacturing process. The material's composition correlates to the material properties and becomes a vital consideration during material selection. Also, the manufacturing process plays a crucial role when designing composite parts as the material and the part are created simultaneously. Often times there are logistical complexities when manufacturing a large part, such as an aircraft fuselage, that must be considered in the design stage. The following section presents the research that has been covered on thermoplastic matrix composite material, modeling a thermoplastic polymer's crystallinity, and a manufacturing process called Automated Tow Placement (ATP).

### 2.1 GENERAL COMPOSITE MATERIAL RESEARCH

Composite materials have at least two constituents: reinforcement and matrix. The reinforcement adds strength to the material, while the matrix keeps the reinforcement in place and transfers the load applied to the strong reinforcement constituent. The focus for this research is on a polymer-fiber blend composite material with the most emphasis on the polymer matrix system (Figure 2.1-1).

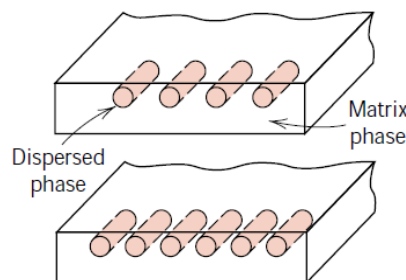


FIGURE 2.1-1: POLYMER MATRIX WITH REINFORCEMENT FIBERS TO MAKE A COMPOSITE [3]

### 2.1.1 FIBER REINFORCEMENT

The fibers will help to strengthen the matrix. Typical fiber types used can be made from carbon or glass. Also, the fibers can be infused into the matrix in a variety of sizes and orientations: long and aligned or short and random. The layup's fiber orientation will impact the overall material strength. The material used in this project had continuously long and aligned carbon fibers embedded in a polymer matrix.

### 2.1.2 POLYMER MATRIX

All polymers are molecularly composed of "mer" units, a repeated unit of a group of atoms bonded together (Figure 2.1-2). These "mers" must be composed of carbon and hydrogen atoms, and oftentimes include other atoms like fluorine or typical organic compound groups such as ether to make a "mer" unit. When all the "mers" link together, they become a "polymer" chain, where "poly" is defined as "many".

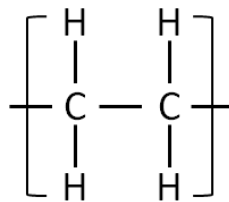


FIGURE 2.1-2: BASIC "ETHYLENE" MOLECULAR MER UNIT OF A POLYMER

There are two basic classes of polymers: thermoset and thermoplastic, which behave uniquely from each other. Both will solidify in a distinctive way; a thermoset will solidify by cross-linking whereas thermoplastics will solidify with two phases, with crystals and amorphous chains that do not move. This difference directs the manufacturing parameters and ensures that the material properties are different from each other.

### 2.1.2.1 THERMOSET VERSUS THERMOPLASTIC POLYMERS

On a molecular level, a thermoset begins as a liquid mix of monomers and additives. With a source of heat, the molecules will cross-link and the polymer will cure. The amount of cross-linking that has occurred is measured and is considered as the “Degree of Cure.” These cross-links are strong, covalent bonds between the polymer chains (Figure 2.1-3). These covalent bonds become difficult to break and thus, the thermoset cannot be melted and reformed after the polymer has been cured and solidified. Ultimately, if the material is heated up again, the material properties will degrade from what they were before the heat was added to the system.

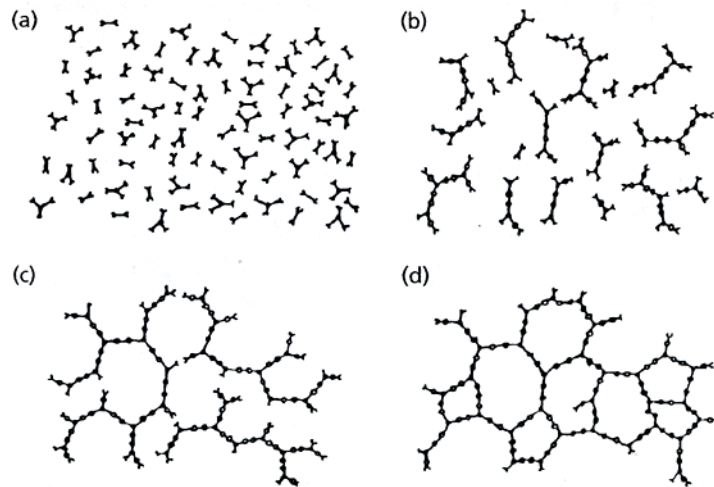
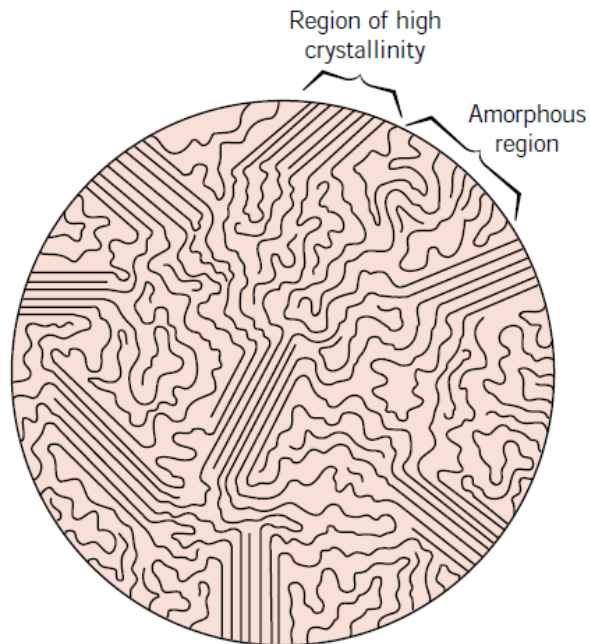


FIGURE 2.1-3: CROSS-LINK NETWORK CREATED WITH MER UNITS IN A THERMOSET POLYMER [4]

Thermoplastic polymers are long chains that are randomly oriented and when they are in the melt phase they are amorphous. As the melt solidifies the chains move and some of the chains will align themselves into an order structure known as a crystal. In the solid form, the polymer chains can be either randomly oriented or in an ordered structure (Figure 2.1-4). The names of these two types of structures would be amorphous or crystalline, respectively.



**FIGURE 2.1-4: CRYSTALLINE AND AMORPHOUS REGIONS OF A THERMOPLASTIC POLYMER [3]**

The polymer chains are attracted and aligned together by the van der Waals Forces [4]. These forces occur when the hydrogen atoms on the polymer chains are attracted to the hydrogen atoms on the neighboring chains (Figure 2.1-5).

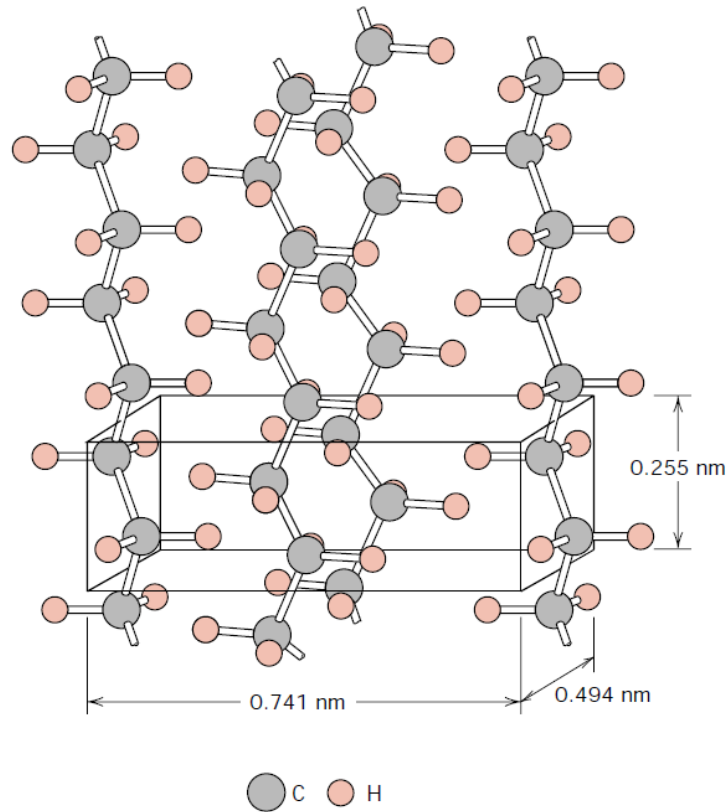


**FIGURE 2.1-5: THERMOPLASTIC POLYETHYLENE POLYMER CHAINS ALIGNED NEXT TO EACHOTHER [3]**

Thermoset polymer materials are stronger and are less expensive than thermoplastic materials. Also, thermosets can be subjected to high temperatures without the risk of melting like a thermoplastic. However, if the temperature is too high, the thermoset's material properties decay. Thermoplastics can easily return to the melt phase and be re-formed, unlike a thermoset. However, thermoplastics cannot operate at temperatures above their melting point since it will no longer be a solid. The ease of melting is due to the lack of bonding between the polymer chains. Thermoplastics can be stored at room temperature indefinitely whereas thermosets have a shelf life and must be stored in a cold environment, like a freezer to prevent curing.

## 2.2 THERMOPLASTIC CRYSTALLINITY REVIEW

Thermoplastic polymer matrix composite materials at the present time have been used sparingly compared to the thermoset polymer matrix composites, especially in the aerospace industry. However, the advent of the high performance thermoplastic polymers has allowed for thermoplastics to take the place of thermosets. Examples of thermoplastics include: polyetherimide (PEI), and poly(ethylene terephthalate) (PET), and the poly(aryl) polymers. Material crystallinity level is measured as a percentage. Thermoplastics, like PEEK, are considered “semi-crystalline” [5]. Thus, a part of the microstructure is ordered, while the other part is amorphous. Crystals form when the material cools from the melt phase into the region between the melting temperature,  $T_m$ , and the glass transition temperature,  $T_g$  (Figure 2.2-1). This region is known as the “melt crystallization zone”.

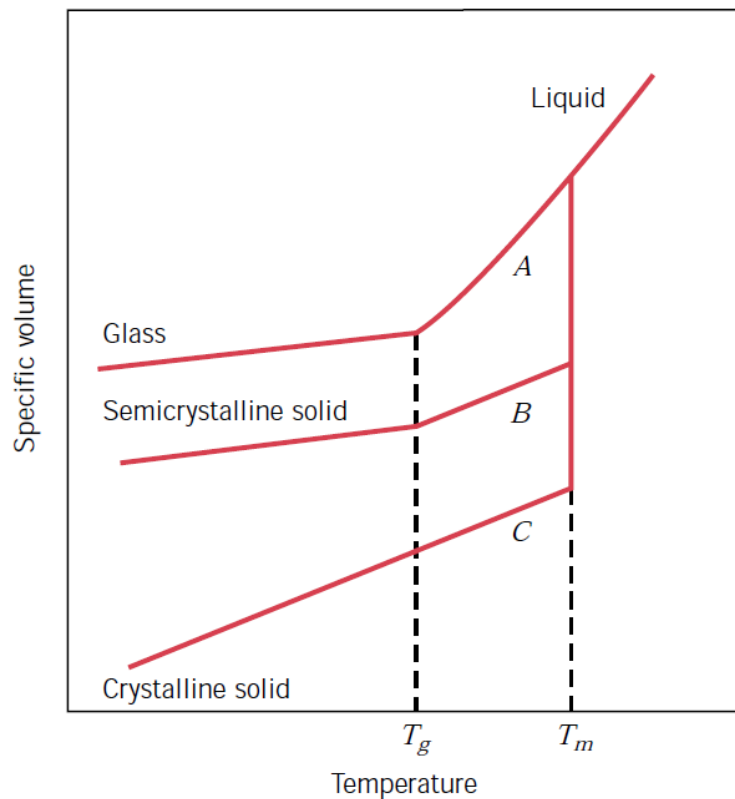


FIGURE 2.2-1: GENERAL PHASE DIAGRAM OF POLYMER AND GLASS MATERIALS [3]

There are two processing methods in which crystals can form when the polymer melt solidifies: a dynamic or an isothermal crystallization process. The dynamic process entails cooling the material at a particular cooling rate from above the  $T_m$  to a temperature well under the  $T_g$ . The material's cooling rate will affect the amount of crystals that form. Thus, a faster cooling rate yields a lower crystallinity than a slower cooling rate, as the greater amount of time allows the crystals to form. The isothermal crystallization process occurs when the material is cooled down to a temperature that is in-between the  $T_m$  and the  $T_g$ , and held at that temperature for an extended period of time. The polymer chains are mobile while in the melt crystallization region and over the extended amount of time, the chains align themselves to a crystalline structural order.

When the crystals form, there are two different crystal geometries that can appear: spheruletic or epitaxial (Figure 2.2-2). The spheruletic crystals are shaped like spheres and form first while the epitaxial crystals are rod-shaped and form soon after [4, 6]. The cooling rate will ultimately affect the percentage of each crystal type that grows and which is the more dominate crystal shape.



**FIGURE 2.2-2: SPHERULITIC AND EPITAXIAL CRYSTAL GEOMETRY FORMATIONS IN THE THERMOPLASTIC MATRIX OF A FIBER COMPOSITE [7]**

### 2.2.1 MEASURING CRYSTALLINITY LEVEL

Differential Scanning Calorimetry (DSC) is one method to determine crystallinity level in thermoplastic polymers by measuring the amount of heat released or absorbed by the sample system, in units of [W/g]. When crystals melt, heat is absorbed by the system, which is an endothermic reaction ( $\Delta H > 0$ ) and when crystals form, there is a release of energy in the form of heat, making it an exothermic reaction ( $\Delta H < 0$ ). These heat measurements are used to calculate the amount of crystals formed during the crystallization process. This “heat flow” can be plotted versus time to calculate the amount of heat given off by integrating the curve (Figure 2.2-3).

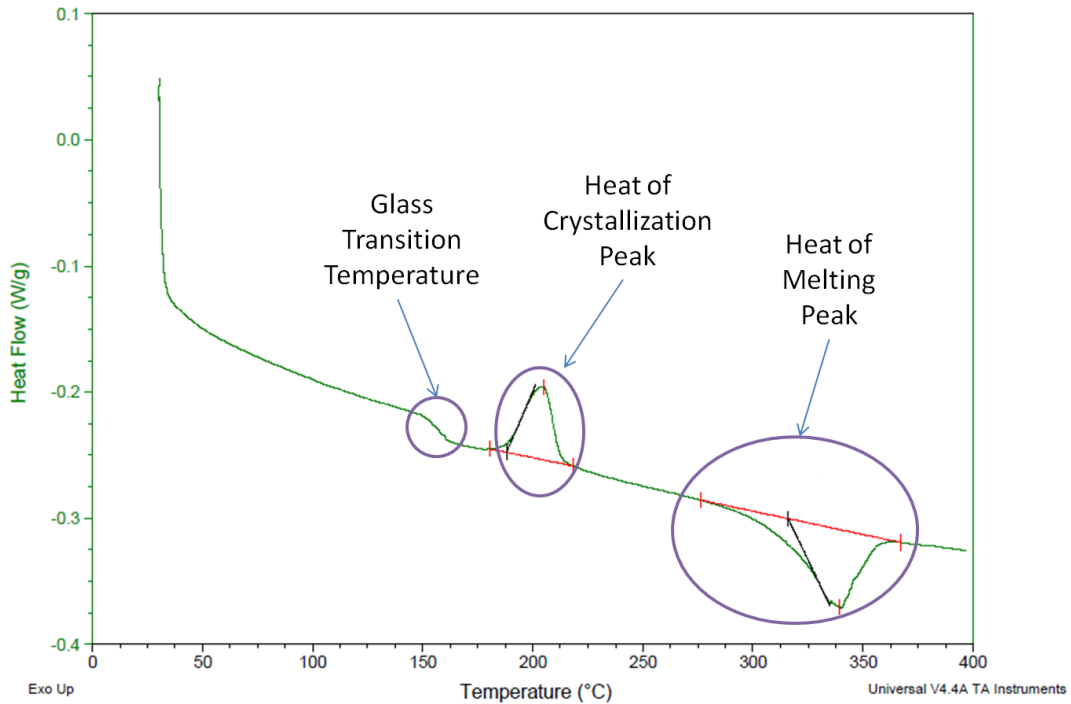


FIGURE 2.2-3: TYPICAL DSC CHART OF HEAT FLOW WITH RESPECT TO TEMPERATURE

This integration will yield the heat of the crystallization, which is a specific heat but is designated without “specific” in literature on crystallinity. It is in units of [J/g]. The areas under the “Heat of Crystallization” ( $H_c$ ) and the “Heat of Melting” ( $H_m$ ) peaks can be calculated. Each area is described as the amount of specific heat it takes the material to crystallize and the amount of specific heat it takes the material to melt, respectively. In order to calculate crystallinity level  $X_c$ , the  $H_c$  must be applied to the total ultimate heat of reaction,  $H_u$ , to calculate the percentage of crystals that have formed in the laminate during the ATP manufacturing process [5, 8].

$$X_c = \frac{H_c}{H_u}$$

1

### 2.2.2 MODELING CRYSTALLINE MICROSTRUCTURE

Modeling polymer crystallinity levels has been widely examined in many ways over the years. A basic and first model used in polymer science proposed in 1940s is the Avrami model [9].

$$\frac{X_c(t)}{X_\infty} = 1 - \exp(-k(t)^n) \quad 2$$

The Avrami equation follows the growth of crystals from when they start as nuclei over a particular time span. The “crystallinity level” measured at a particular moment in nucleation time is defined as a fraction of the amount of crystals formed at time,  $X_c(t)$ , with respect to infinite crystallinity,  $X_\infty$ . Infinite crystallinity is a special constant for thermoplastics which are always only semi-crystalline that is extrapolated from crystallinity measurements, especially which is the maximum amount of crystals that can form in the material. The variables in this model are the “k” rate constant value and the Avrami exponent, “n”, which is related to the nature of crystal growth that is in the range of 1-4 depending on the material [4].

By 1965, Hillier [10] contrasted Avrami, and showed that the crystallization was actually a two-stage crystallization process. In 1971, Ozawa [11] modified the Avrami equation crystallization form by discretizing dynamic crystallization as a series of isothermal crystallization steps. He completed his version of the model with PET material as a one-stage crystallization process [11].

Silva-Spinacé [12] proved Ozawa’s model’s limitation that it neglects secondary crystallization, for the material PET. Ahn [13] also studied PET material and found similar that Ozawa’s model is not accurate. DiLorenzo [14] pointed out that Ozawa neglected the secondary crystallization but mentioned how another researcher deemed this unimportant.

Nakamura [15-16] mentions that crystallization “cannot be a simple manner because isotherms don’t terminate like the Avrami equation

predicts". He continues to relate the crystallization constant at isothermal conditions by assuming isokinetic conditions [14]. Nakamura directly observed the polymer crystals form to fully understand the crystallization process during slow cooling rates. The main equation to calculate crystallinity level according to Nakamura is summarized here:

$$X(t) = 1 - \exp \left[ - \left\{ \int_0^t K(T(\tau)) d\tau \right\}^n \right] \quad 3$$

Nakamura's model is similar to the Avrami model; however, the term is not "k(T)" but is "K(T)". The constant "k(T)" can be related to "K(T)" as follows:

$$K(T) = k(T)^{1/n} \quad 4$$

Where "k(T)" comes from Takayanagi and Kusumoto, as stated by Nakamura [16], and in the expanded form was found to be as follows:

$$\ln k(T) = A - \frac{BT}{(T - T_g - 51.6)^2} - \frac{CT_m}{T(T_m - T)} \quad 5$$

Tobin [17-19] completed research in the mid-1970's on heterogeneous and homogenous nucleation where he looked at the growth site impingement of the crystals that form. He also described how the initial nucleation of the crystals drives the kinetics of the crystallization. Tobin points out that while Avrami's equation is useful and "reasonable", it is really only a good equation for materials with lower crystallinity levels [17].

Williams, Landel, and Ferry (WLF) equation [20] considers the mechanical and electrical relaxation process of an amorphous melted polymer. Specifically, this model considers the viscosity of a melted material with respect to its  $T_g$ . Molecular relaxation relays as movements of the polymer chains and hence how crystals form.

$$\log a_T = -\frac{C_1(T - T_S)}{C_2 + T - T_S} \quad 6$$

### 2.2.3 MODELING CRYSTALLINITY OF PEEK MATERIAL

Crystallization for PEEK must be considered as a two-stage crystallization process [5, 7, 21-24]. The models considered in this research are all parallel, two-stage crystallization kinetics models based from Avrami's equation, where the one-stage crystallization model is split into two parts with a supplementary weight fraction of the crystal type that forms during the crystallization process. The primary crystal type is: spheruletic, which is designated as the weight fraction "w<sub>1</sub>", while the secondary crystal type is epitaxial, and is the weight fraction "w<sub>2</sub>". The sum of both weight factors is equal to one.

$$w_1 + w_2 = 1 \quad 7$$

The weight factor depends on the cooling rate of the material. Summarized in the following table are constants for the weight fractions for the material PEEK [7, 21, 25].

TABLE 2.2-1: SUMMARY OF WEIGHT FRACTION "w<sub>1</sub>" WITH RESPECT TO THE COOLING RATE [7]

Cooling rate [°C/s]	Cooling rate [°C/min]-adapted	w <sub>1</sub> (PEEK-film)	w <sub>1</sub> (APC2-PEEK)
0.0 (isothermal)	0.0 (isothermal)	0.085	0.050
0.032	1.92	0.1	--
0.160	9.6	0.7	0.610
0.320	19.2	0.71	0.610
0.620	37.2	0.72	0.610
0.930	55.8	0.72	0.610
7.600	456	0.72	--
28.00	1680	0.74	--
45.00	2700	0.74	--
114.00	6840	0.75	--

The crystallinity is then solved for by implementing the weight fractions with the volume crystal fraction and the infinite volume crystal value to find the volumetric crystallinity percentage:

$$X_{vc} = X_{vc\infty}(w_1F_{vc1} + w_2F_{vc2}) \quad 8$$

“ $X_{vc}$ ” is the volumetric crystallinity and the “ $X_{vc\infty}$ ” is the infinite volumetric crystallinity, which is defined as the maximum amount of crystals that would form once the process is finished. Weight fractions “ $w_1$ ” and “ $w_2$ ” correlate to the spheruletic and epitaxial types of crystals that form during the crystallization process, respectively. The variables “ $F_{vc1}$ ” and “ $F_{vc2}$ ” are both defined as the fraction of the crystallized polymer material.

The volumetric crystallinity can be defined also as an integral of the Avrami equation with respect to the crystals that form over time:

$$X_{vc} = X_{vc\infty} \left( 1 - \exp \left[ - \int_0^t k(T) * nt^{n-1} dt \right] \right) \quad 9$$

Researchers have found differing values for the crystallization rate constant, “ $k$ ”, for the same material [7, 23, 26-28]. While the differences in the values are slight, they are significant as they provide unique modeling results. The overview of them is described in the following subsection, but the results are discussed later.

In order to solve for the “ $k$ ” and “ $n$ ” values, it is necessary to make graphs of “ $\log(-\ln(1-X(t)))$ ” versus “ $\log(t)$ ” (Figure 2.2-4) from isothermal crystallization data. The intercept and slopes will yield the “ $k$ ” and “ $n$ ” values respectively.

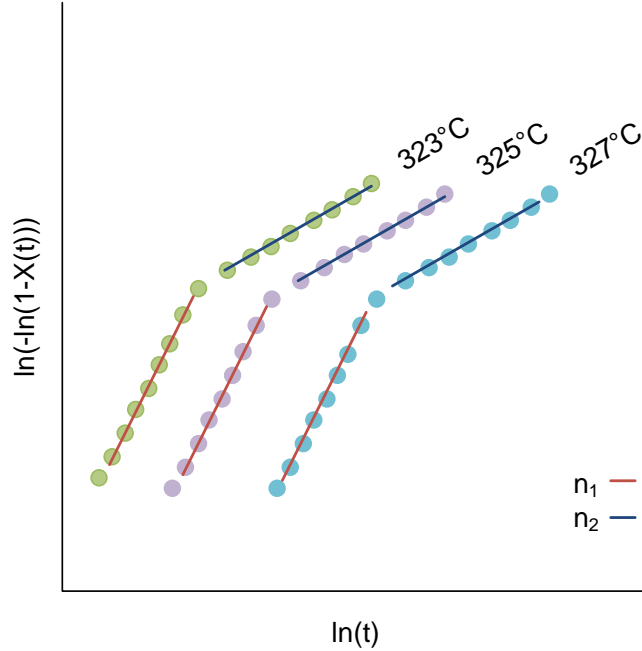


FIGURE 2.2-4: GENERAL GRAPH THAT DESCRIBES HOW TO SOLVE FOR “K” AND “N” VALUES USING LN(-LN(1-X(T))) VERSUS LOG(T) AS THE Y-INTERCEPT AND SLOPE FOR EACH TEMPERATURE LINE, RESPECTIVELY

Tierney and Gillespie [27, 29] used the model to predict crystallinity levels for high cooling rates, as this occurs in ATP and used the same constants for PEEK as Velisaris and Seferis [7, 24], except for using only one value for  $T_m$ , instead of one for each crystallization stages. Velisaris and Seferis [7, 24] separated the  $T_m$  as two different temperatures as predicted that the different crystal formations will have different melting temperatures. Velisaris and Seferis [7, 24] completed a non-isothermal kinetics model on PEEK material and used the equation as follows:

$$F_{vci} = 1 - \exp \left[ -C_{1i} \int_0^t T \exp \left\{ - \left[ \frac{C_{2i}}{T - T_g + 51.6} + \frac{C_{3i}}{T(T_{mi} - T)^2} \right] \right\} n_i t_i^{(n_i-1)} dt_i \right] \quad 10$$

The index, “i”, will be 1 or 2 for the appropriate crystallization stage. Constants describing the constant coefficient ( $C_{11}$  and  $C_{21}$ ), the empirical parameter ( $C_{12}$  and  $C_{22}$ ), the free energy of nucleation ( $C_{13}$  and  $C_{23}$ ) and the Avrami exponent ( $n_1$  and  $n_2$ ) are specific to the material modeled.

This parallel crystallization equation is partially derived from the WLF equation [4, 20], mentioned earlier. The  $C_1$  and  $C_2$  are universal parameters that are generally taken to be:  $C_1=17.44$  and  $C_2=51.6$ .  $C_2$  is a value that is seen in the parallel crystallization model.

$$\log a_T = -\frac{17.44(T - T_S)}{51.6 + T - T_S} \quad 11$$

Cebe [23, 28] based crystal structure research on growth rate, spheruletic crystal size, and surface energy of the crystals from Blundell and Osborn [5] for PEEK material. The spheruletic growth rate  $G(T)$ , of the crystals was applied to the “parallel Avrami model” from Velisaris and Seferis [7] to describe both dynamic and isothermal crystallization of PEEK.

$$k(T) \approx G(T)^n \quad 12$$

Cebe used the following relation, which is a variation from the one used by Velisaris and Seferis. The differences include doubling the temperature,  $T$ , that is multiplied by  $C_3$  and using the infinite crystal melting temperature,  $T_m^o$ , which is a different value than  $T_m$ .

$$k(T) = C_1 * \exp \left\{ - \left[ \frac{C_2}{T - T_g + 51.6} + \frac{C_3(2 * T)}{T(T_m^o - T)(T_m^o + T)} \right] \right\} \quad 13$$

Cebe found different values for the constants for a set of three cooling rates: 1, 5, and 10°C/min. Also, since Cebe’s model was slightly different from Velisaris and Seferis, all of the constants were different from Velisaris and Seferis. Likewise, some Cebe’s units for the constants are different than the units for the constants in Velisaris’ and Tierney’s models. The following table summarizes the constants values for PEEK material from the literature.

TABLE 2.2-2: CONSTANTS FOR THE DIFFERENT CRYSTALLINITY MODELS ON PEEK FILM MATERIAL FROM LITERATURE [7, 23, 27]

	Velisaris	Tierney	Cebe (1°C/min)	Cebe (5°C/min)	Cebe (10°C/min)
<b>T<sub>m1</sub></b>	593 K	611 K	389°C (662 K)		
<b>T<sub>m2</sub></b>	615 K				
<b>N<sub>1</sub></b>	2.5	2.5	3.45		
<b>N<sub>2</sub></b>	1.5	1.5	2		
<b>C<sub>11</sub></b>	2.08e10 s <sup>-n</sup>	2.08e10 s <sup>-n</sup>	1.92 s <sup>-1</sup>	1.03 s <sup>-1</sup>	0.63 s <sup>-1</sup>
<b>C<sub>12</sub></b>	4050 K	4050 K	1500 K	1540 K	1700 K
<b>C<sub>13</sub></b>	1.8e7 K <sup>3</sup>	1.8e7 K <sup>3</sup>	1.0e6 K <sup>2</sup>	8.0e5 K <sup>2</sup>	6.3e5 K <sup>2</sup>
<b>C<sub>21</sub></b>	2.08e10 s <sup>-n</sup>	2.08e10 s <sup>-n</sup>	0.68 s <sup>-1</sup>	2.03 s <sup>-1</sup>	1.06 s <sup>-1</sup>
<b>C<sub>22</sub></b>	7600 K	7600 K	1300 K	1130 K	1650 K
<b>C<sub>23</sub></b>	3.2e6 K <sup>3</sup>	3.2e6 K <sup>3</sup>	6.2e5 K <sup>2</sup>	6.1e5 K <sup>2</sup>	4.0e5 K <sup>2</sup>
<b>W<sub>1</sub></b>	Depends on cooling rate	Depends on cooling rate	0.79	0.76	0.72
<b>W<sub>2</sub></b>			0.21	0.24	0.28

### 2.3 MANUFACTURING RESEARCH

There are a variety of methods for manufacturing parts from composite material. One thing to consider during product design is how the raw materials first arrive: as two separate constituents or as one of fibers and matrix together. For the instances where the fibers are separate from the matrix pre-processing, there must be a process to infuse the resin into the fibers such as: compression molding, injection molding, or resin transfer molding (RTM). Manufacturing methods that utilize a material where the fibers have been pre-impregnated in a polymer matrix include hand layup on a mold and placing into an autoclave for further compaction and heating or Automated Tow Placement (ATP).

In ATP, a robotic head heats up and lays down the pre-impregnated tape material while simultaneously compacting it onto either a mandrel or a mold to create a desired shape. The shape can be complex since the robotic head can be programmed to lay the material down as desired. This manufacturing technique is proposed to be an *in-situ* processing practice for

thermoplastic composites. For thermosets, the material would need to be put into an autoclave in order to complete the material curing and ensure the layers are compacted well.

ATP is a good manufacturing technique especially for large-scale parts for logistical reasons since it is easier to create complex and large shapes when a robotic head can do the work. One place where this technique is applied is to make aircraft fuselages, such as Boeing's 787 Dreamliner (Figure 2.3-1).



**FIGURE 2.3-1: ATP ON THE FRONT FUSELAGE SECTION OF BOEING 787 DREAMLINER [30]**

By using ATP, the addition of strength in select areas of the part can be planned to be even more precise, since the method allows for the fiber tows to be oriented as desired. Other benefits to ATP include removing the “human error” that can occur in hand layup and accurate repeatability in manufacturing since it is an automated process. However, an ATP machine requires a large monetary investment due to the high costs to purchase, install, run, and maintain. Also, manufacturing defects can occur that are related to tow misalignment or the heat from the gas torch. If the operator is

inattentive to a defect's occurrence, the defect can have serious implications on the material's quality.

The ATP manufacturing stages that the composite material will undergo include the pre-processing, melting, consolidating, and solidifying. Modeling the manufacturing stages of the process provides insight into the manufacturing methods in order to optimize the process.

### 2.3.1 PRE-PROCESSING

The first pre-processing step deals with designing the layup pattern for the desired part to be manufactured. This pattern will then need to be programmed into the ATP machine's computer system so that the robotic head lays the material down as desired. Next, it is important to determine the processing parameters, such as torch temperature, amount of pressure for the roller, and the layup speed. Lastly, for parts manufactured on a mandrel, preheat the mandrel so that it will expand before the material is applied to facilitate in removing the composite laminate. The mandrel will shrink back to its original dimensions once it is cooled but composite laminate will not due to its low coefficient of thermal expansion.

### 2.3.2 MANUFACTURING STAGES

In manufacturing all polymer-fiber composites, the forming process will contain three critical stages: melting/heating, consolidating, and solidifying/cooling (Figure 2.3-2). Each stage plays an essential role in manufacturing a part. The solid polymer material must be melted so that the fibers can fully be submerged around the matrix. Then to insure the fibers compact together the material must be consolidated. This stage also removes the air trapped in the material, known as voids. At the end of the process, the melted material solidifies as it cools down. At completion, the polymer matrix and fiber constituent can become one solid piece. The following sections discuss the details of the processing steps.

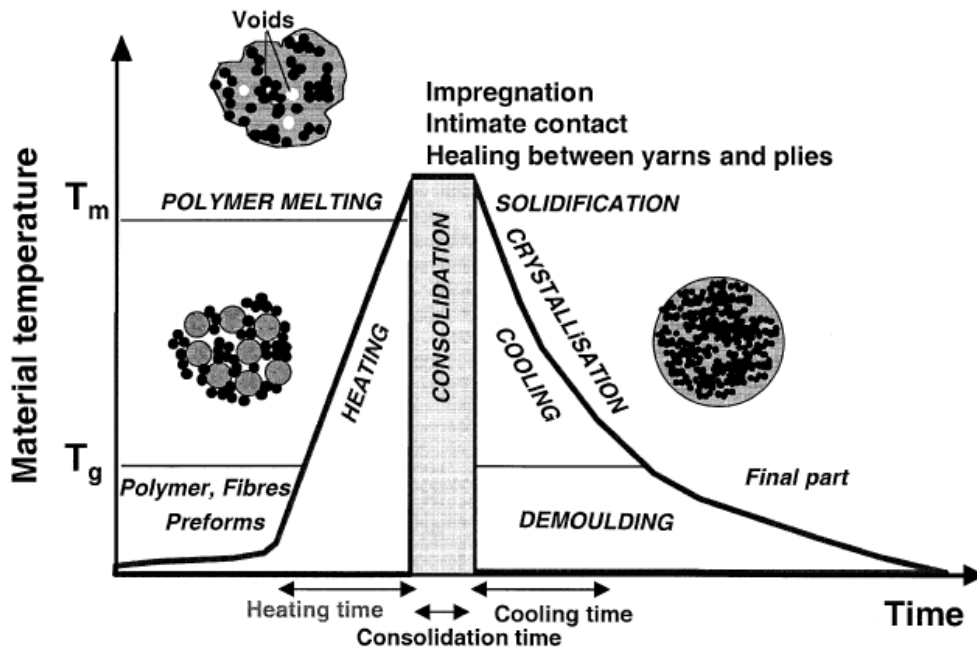


FIGURE 2.3-2: THE THREE COMPOSITE MATERIAL PROCESSING STAGES (ADAPTED [31])

### 2.3.2.1 HEATING/MELTING

The raw form of a polymer needs to be melted in order for it to be molded into a desired shape. In ATP, the heating is a localized process that is executed with a high temperature torch. The temperature needs to be high enough to allow for polymer matrix in the tow material to melt. This would mean that the temperature of the material must reach well above the melting temperature of the polymer,  $T_m$ .

### 2.3.2.2 CONSOLIDATING

When creating a laminate, each layer will require source of pressure in order to join the material plies together. During the consolidating stage, the polymer molecules in the composite's matrix will migrate across the separate ply interfaces in order to form one piece of material. A combination of heat and pressure will mobilize the molecules through the ply interfaces so that the two separate plies can become one.

There are a few methods that can provide the necessary pressure to the layers: autoclave, vacuum bag, or roller. In ATP, a roller or set of rollers, will apply pressure to lay down the tow material and consolidate the plies. The roller geometry profile must match the mold to ensure an even pressure distribution on the part. Fiber spread in the tows can also occur when there is too much pressure or improper roller alignment. Ultimately, a problem on one layer can affect the layers that are consolidated later on as well.

#### 2.3.2.3 SOLIDIFYING

To complete the manufacturing process, the polymer matrix material must harden, which occurs as the material cools down from an elevated temperature. The material is fully solidified when the material temperature is lower than the glass transition temperature,  $T_g$ . Cooling methods that can occur are natural air-cooling or forced cooling. To force cool the material in ATP processing, a “cooling shoe” can be placed at the other side of the torch and roller and cold air will be forced onto the material. Generally, the material cooling rate found in ATP for natural air cooling is 3000°C/min [29].

As mentioned earlier, the terms for solidified polymer materials is “cured” for thermosets and “crystallized” for thermoplastics. The cooling rate that a material is subjected to during processing affects a thermoplastic material’s crystallinity and in turn will affect the mechanical properties [32].

#### 2.3.2.4 POST PROCESSING

At post processing, the part has cooled completely and it is then removed from the tool. Typically parts made with ATP are put into the autoclave to finalize the compaction; however, this research is driven by making the same level of quality parts as an *in-situ*, “on the fly” manufacturing technique. Thus, the last step of the process is the cool down of the material.

### 2.3.3 EXPERIMENTAL WORK (THERMAL AND CRYSTALLINITY)

In order to evaluate the processing steps in ATP researchers have looked into the three manufacturing stages in considerable detail. The main interest in this thesis is the research completed on the thermal and subsequently crystallinity profiles of material affected by the ATP manufacturing process. Thermal profiles were taken with an infrared thermal imaging camera on one ply of PEEK composite material being heated by a heat torch from the ATP machine [25, 27, 33] (Figure 2.3-3)

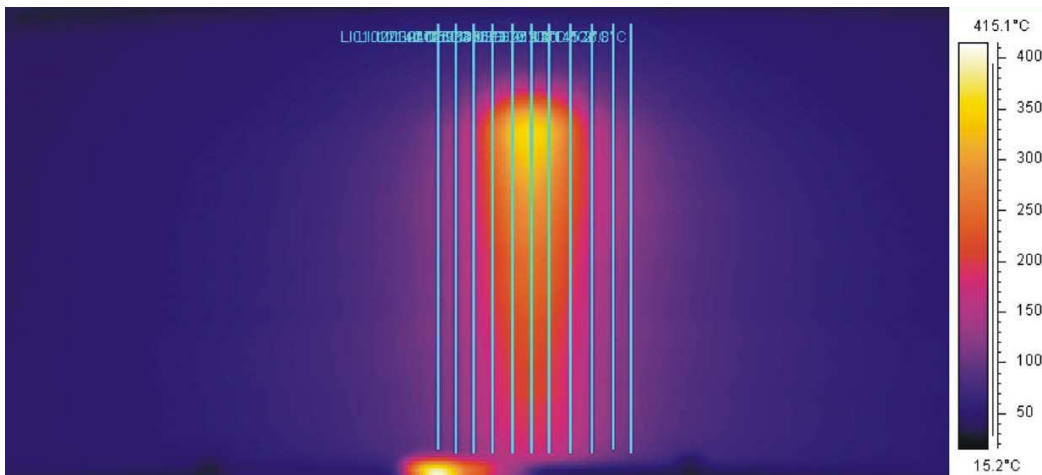


FIGURE 2.3-3: INFRARED THERMAL CAMERA IMAGE PROFILE OF A SINGLE PLY THAT IS HEATED BY THE ATP TORCH HEAD (MODIFIED FROM TIERNEY [27])

Ghasemi Nejahad et. al. [34] completed an examination on ring shaped geometry parts manufactured with ATP to test the thermal profile through the thickness. They modeled with finite elements to predict the heat flow within the material.

### 2.3.4 MODELING THE ATP MANUFACTURING PROCESS

Even though there are three manufacturing stages in ATP, this thesis focuses solely on modeling the solidification stage. The temperature profile of a laminate material as it goes through the entire manufacturing process is needed to understand how the part solidifies. The final solidification

behavior in the material depends on the heating and cooling rates that the material is subjected to during manufacturing.

Shih and Loos [35] created a finite element model of the temperature profile obtained during the processing of a ring geometry (146.1 mm or 5.75 in inner diameter). The model was based on a cylindrical transient heat transfer model with thermal conductivities and specific heat capacity. Part of the experimental set up was to measure temperatures through the thickness of a part with thermocouples. These authors were able to accurately model the temperatures that would occur in the part during ATP.

Guan and Pitchumani [36-37] completed a heat transfer analysis on the process by coupling an energy equation with a crystallization kinetics equation to obtain the temperature field and crystallinity distribution that occurs during the process. They also examined a model of the various manufacturing parameters and the effect on the end material's crystallinity level. These parameters varied the torch angle, distance, diameter, gas temperature, exit velocity, and substrate thickness.

Joshi and Lam [38] looked into 3-D modeling of pultrusion on APC2/PEEK composite material by looking into the crystallization kinetics models found from work done in various combinations from Lee, Springer, Talbott, and Mantel [8, 26, 39]. The model was input into a finite element program in order to predict the crystallinity level that the material will have post-pultrusion processing, due to the rates that the material is subjected to during processing.

Tierney and Gillespie [29] modeled the ATP process after they measured the temperature profile of PEEK-carbon fiber material during manufacturing. To measure the temperature of the material, they used a thermal imaging camera to create a visual profile of a single sheet of pre-preg that was clamped to a setup to monitor when a torch passes over the material. The torch heated one side, while the imaging camera recorded the

temperatures on the other side. The temperatures found were used to calculate the ATP process heating and cooling rates. These heating and cooling rates were then placed into the modeling equation used by Velisaris and Seferis [7] and fit a few new values for the constants to the crystallization model.

## 2.4 SUMMARY OF LITERATURE REVIEW

Composite materials research covers many areas. This chapter focused on the thermoplastic polymer matrix composites, modeling crystallinity levels in the polymer matrix, and the ATP manufacturing technique. Each of these areas focused on in the literature are the focus of the experimental work that is covered in the following chapters.

Thermoplastics have a semi-crystalline microstructure, which is defined as an alignment of the polymer chains. Crystals form during the solidification step during processing. Chapters 3 and 4 combine this foundation into how a polymer solidifies in the modeling of thermoplastic films and the manufacturing of composites with a thermoplastic matrix.

Crystallinity kinetic models explain how cooling affects the microstructure formation in thermoplastic polymers, like PEEK. Modeling crystal formation can aid in predicting the crystallinity levels in a material due to the processing cooling rates. Chapter 3 takes the crystallinity models discussed, from Velisaris, Cebe, Tierney, and Nakamura, and applies them to experimental DSC work to first validate each model and then to find the proper constants for the material grade of PEEK that is used in this thesis. There is a gap in the literature on modeling PEKK film, which also needs to be completed in order to move the research on modeling thermoplastics forward.

The ATP manufacturing process is a robotic method for laying up a pre-impregnated fiber composite material onto a mandrel. The automation provides many benefits to the composites manufacturing field such as repeatability and accuracy for complicated parts. Chapter 4 adds to research already completed on ATP manufacturing, especially for measuring the thermal profile of the laminate during manufacturing. A manufacturing method and geometry were developed to measure what occurs to the temperatures within a laminate part during the ATP process. Post processing, the cooling rates were calculated and then the crystallinity levels through the thickness of the laminate were found to determine a correlation with the cooling rates. Also, another attribute that is covered in this thesis looks at how the laminate is reheated as another ply is laid down and how this also will relate to the cooling rate of the material.

Ultimately the solidification of the polymer and the subsequent modeling of the crystallinity behavior will aid in understanding the material better for optimizing the processing techniques. Manufacturing is applying all that has been modeled to a useful product. By measuring the temperatures that occur through a laminate manufactured by ATP, details on the subject can be obtained. The following chapters provide the experimental setups for both modeling and manufacturing. The results obtained from both chapters will add more clarity to these research areas.

---

## CHAPTER 3: CHARACTERIZING MATERIAL

As mentioned in the literature review, crystallinity is defined as an ordered microstructure of polymer chains for a thermoplastic polymer. Crystallinity levels are measured as a percentage, correlate with the material's mechanical properties, and are affected by the processing conditions that occur on the material. A material with a higher crystallinity level will be stronger and have higher toughness [39]. Kinetics models help to describe the crystallization process. Thus, focusing on the crystallinity formation due to the processing will aid in optimizing the manufacturing process parameters.

### 3.1 MATERIAL

Polyaryl polymers, such as PEEK, are known to be high performance thermoplastics with a semi-crystalline microstructure. One of the special aspects of PEEK is that it is a high crystalline material, even at fast cooling rates. Also, PEEK can operate high temperature conditions like a thermoset. Crystallization occurs between  $T_m$  and  $T_g$ , must be regarded when choosing a material application where the polymer would be subjected to high heat.

The poly (aryl ether ketone) polymers have both “ether” and “ketone” groups as a part of the mer unit. These are considered as a “high performance” thermoplastic polymer since they can operate at elevated temperatures, like thermoset polymers. The two polymers examined in this study are poly ether ether ketone (PEEK) and poly ether ketone ketone (PEKK) (Figure 3.1-1).

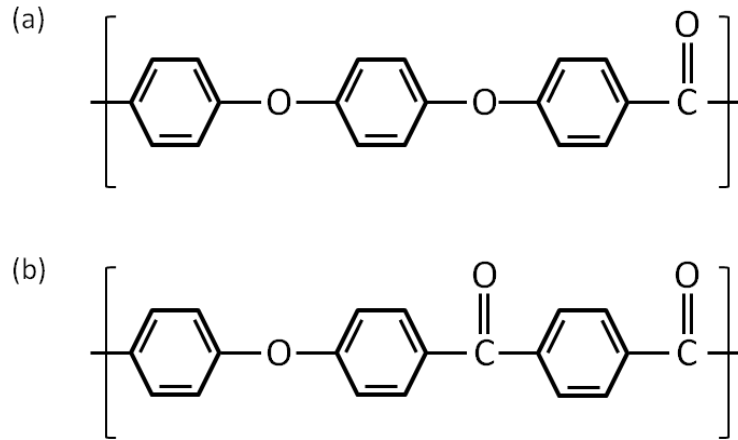


FIGURE 3.1-1: MER UNITS OF (A) POLY ETHER ETHER KETONE AND (B) POLY ETHER KETONE KETONE

### 3.1.1 PROPERTIES

The film materials were manufactured by Cytec Industries. The material properties for the two material films that are focused on in this thesis, PEEK and PEKK, are summarized in Table 3.1-1.

TABLE 3.1-1: MATERIAL PROPERTIES OF CYTEC'S PEEK AND PEEK FILM MATERIAL [40]

	<b>PEEK</b>	<b>PEKK</b>
Density [g/cm <sup>3</sup> ]	1.30	1.30
Elastic Modulus [GPa]	3.79	4.50
Strength [MPa]	103	102
Elongation [%]	11	4
Glass Transition Temperature [°C]	144	156
Melting Temperature [°C]	340	338
Processing Temperature [°C]	380	370

## 3.2 CRYSTALLINITY MODELING

During PEEK's crystallization process, spheruletic and epitaxial crystal types form. The parallel, two-stage crystallization model has been varied amongst the different researchers. Varieties of a parallel, two-stage crystallization model that is based from Avrami include: Nakamura [15-16], Cebe [23, 28], Velisaris [7, 24], and Tierney [25, 27, 29, 33]. Cebe, Velisaris, and Tierney have modeled with PEEK material, while Nakamura modeled

with high density polyethylene (HDPE). There has been some modeling presented by Ferrara [22] and was referenced by Tierney [25] on PEKK films. Experimental work has been covered by others on measuring crystallinity of PEKK films, especially two different types, from Hojjati, et.al.[41-42].

One of the original goals in this project was to include modeling of the PEKK film to add to the current research on crystallinity modeling. As it will be seen in the later sections of this chapter, the variety of models available and the fact that the models did not fit well to experimental data became the primary focus of the work. This chapter presents a comparison of the different crystallinity models with the literature constants, along with experimental data from the DSC. Next, the three crystallinity models were fit to the experimental data for PEEK film at the desired isothermal hold temperatures or cooling rates.

From the literature review in Chapter 2, the parallel, two-stage crystallinity model is what was used for the PEEK film:

$$X_{vc} = X_{vc\infty}(w_1F_{vc1} + w_2F_{vc2}) \quad 14$$

$$F_{vci} = 1 - \exp(-k_i(T) \cdot t^{ni}) \quad 15$$

$$w_1 + w_2 = 1 \quad 16$$

After comparing the literature, it was found that the constant “k” for Equation 15 was solved differently in each paper, even for the same material PEEK. Thus, it helps to visualize the differences by doing a side-by-side comparison for the constant “k”:

TABLE 3.2-1: SUMMARY OF THE MODELING EQUATIONS FOUND IN LITERATURE, FOR THE CONSTANT “K”, THAT ARE USED FOR PEEK FILMS [7, 15-16, 23-25, 27-29, 33]

Researcher	Equation	
Nakamura	$\ln k_i(T) = A_i - \frac{B_i T}{(T - T_g - 51.6)^2} - \frac{C_i T_m}{T(T_m - T)}$	17
Velisaris & Tierney	$k_i(T) = C_{1i} * T * \exp \left\{ - \left[ \frac{C_{2i}}{T - T_g + 51.6} + \frac{C_{3i}}{T(T_m - T)^2} \right] \right\}$	18
Cebe	$k_i(T) = C_{1i} * \exp \left\{ - \left[ \frac{C_{2i}}{T - T_g + 51.6} + \frac{C_{3i}(2 * T)}{T(T_m^o - T)(T_m^o + T)} \right] \right\}$	19

It is clear that Equations 17-19 are generally the same, but each has minor variations that were found to make a difference when trying to fit the model to the experimental data.

### 3.2.1 EXPERIMENTAL METHODOLOGY

PEEK material in a film form was characterized by DSC experiments to find its crystallinity levels due to processing. For running the DSC experiments, film samples that weighed 5-10 mg were cut and sealed in aluminum pans and tested in a TA Instruments Q100 DSC. There are two different methods to crystallize a material: one is isothermal crystallization and the other is dynamic crystallization.

### 3.2.2 ISOTHERMAL DSC EXPERIMENTS

An isothermal experiment holds the temperature constant for a period of time. From the melt phase, the material sample is cooled at a fast cooling rate to a temperature that is in between the  $T_m$  and  $T_g$  and held at this elevated temperature for an extended period of time, two hours. There is a range of temperatures where isothermal crystallization can occur, and for PEEK, this is between 143-343°C [43]. The method to complete the isothermal DSC experiments is summarized:

1. Melt the polymer film of 5-10 mg to 380°C at a heating rate of 10°C/min.

2. Hold film at this elevated temperature for 5 minutes to ensure all the crystals from the film are melted.
3. Rapidly cool the film at 20°C/min to one of the isothermal hold temperatures: 323, 325, and 327°C.
4. Hold at the isothermal temperature for 2 hours.
5. Cool at 10°C/min to 20°C.

The melt crystallization peak for each isothermal hold temperature is integrated in order to find the heat of crystallinity,  $H_c$ . This, as mentioned earlier with Equation 1, is used to calculate the crystallinity level due to the melt crystallization, or isothermal DSC experiment (Figure 3.2-1). The isothermal temperatures were chosen based on the fact that they provided the clearest melt crystallization peaks to be observed.

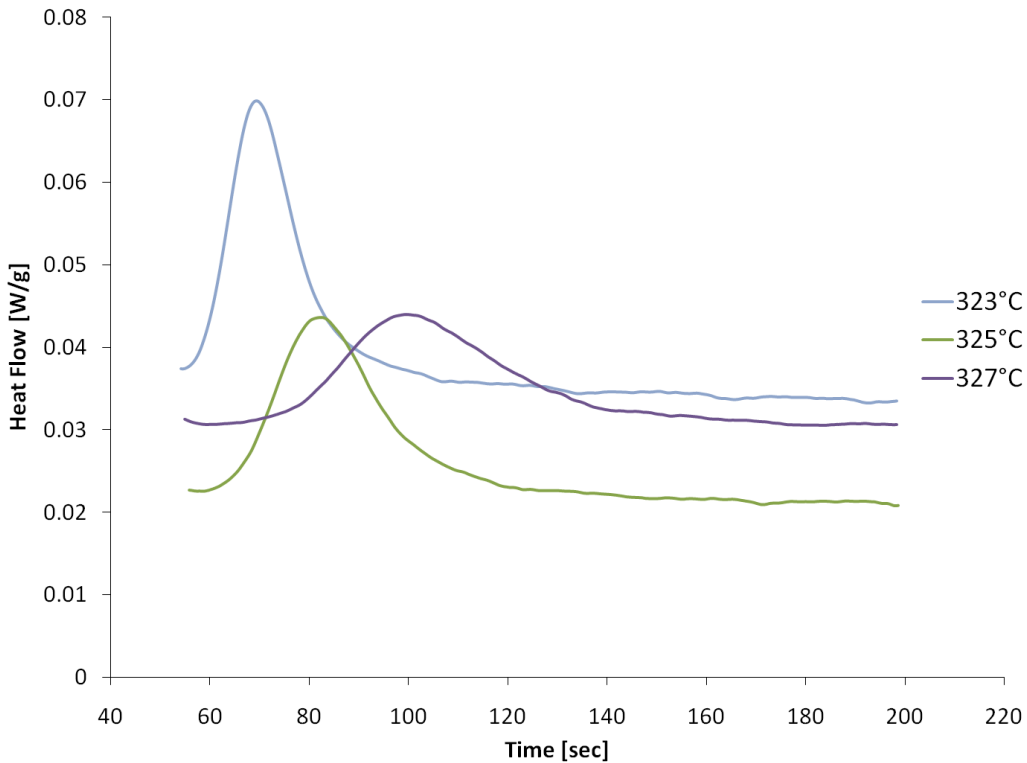


**FIGURE 3.2-1: HEAT OF CRYSTALLIZATION WITH RESPECT TO ISOTHERMAL HOLD TIME FOR THREE TEMPERATURES OF DSC TESTS ON PEEK FILM MATERIAL**

When running isothermal DSC experiments on the film samples, it was found that a small range of temperatures in the melt crystallization temperature range would produce clear crystallization peaks during the experiment. For these temperatures, the crystallinity level was calculated and interpreted. The crystallinity levels of the three isothermal hold temperatures show a general decrease with a higher isothermal temperature (Figure 3.2-2). When comparing with literature, the isothermal hold temperatures crystallinity data differ, which could signify a different grade of the material.

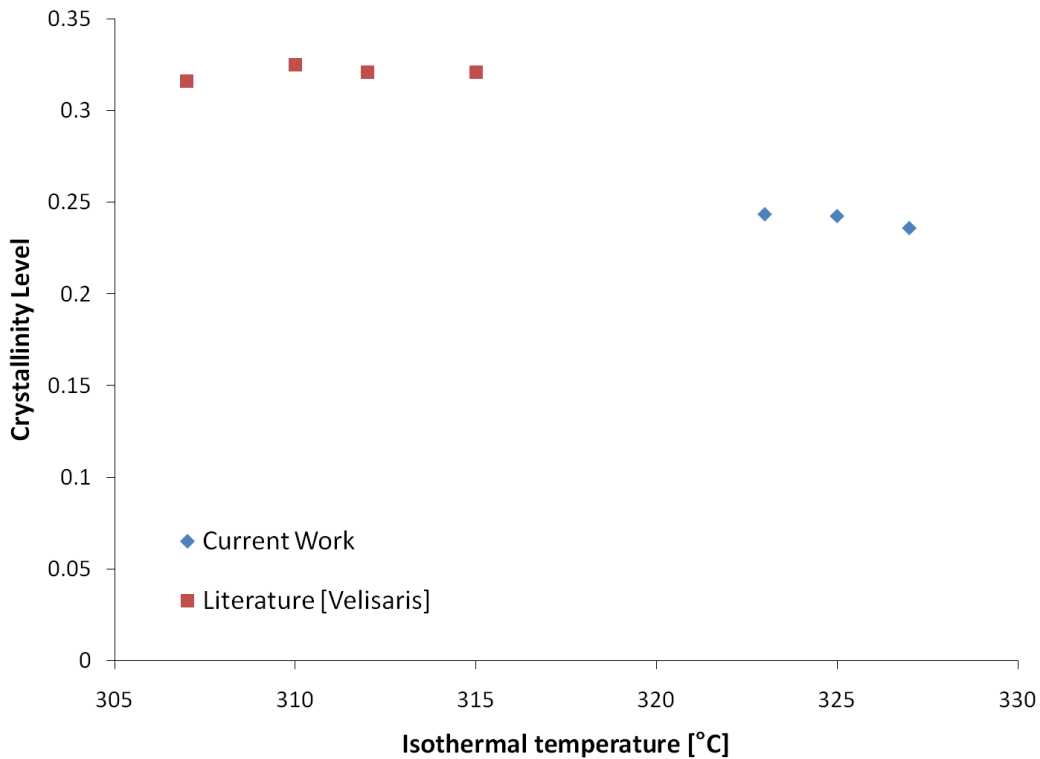


**FIGURE 3.2-2: COMPARING THE CRYSTALLINITY LEVEL OF ISOTHERMAL CRYSTALLINITY EXPERIMENTS TO LITERATURE VALUES [7], FOR PEEK FILM MATERIAL AS A FUNCTION OF THE ISOTHERMAL TEMPERATURE**

In order to determine the Avrami constants, “ $n_1$ ” and “ $n_2$ ”, the isothermal crystallization data must first be rearranged by calculating the crystallinity at the respective isothermal hold temperatures. The  $X_{vc}$  at each

moment of time through the crystallization process can be found by taking the integration of the curve as a function of time (Figure 3.2-3).

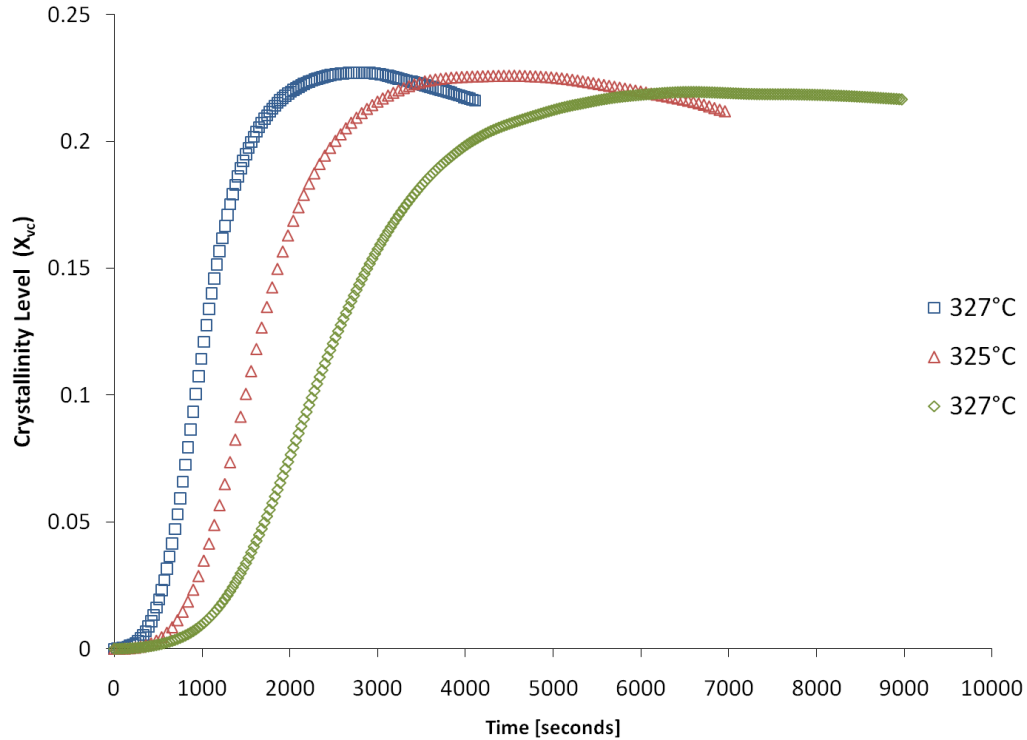


FIGURE 3.2-3: CRYSTALLINITY LEVEL AS A FUNCTION OF ISOTHERMAL HOLD TIME FOR PEEK FILMS AT THREE TEMPERATURES

As the film material is held at an elevated temperature for an extended period of time, a crystal microstructure will form. The  $X_{vcinf}$  is found to be the maximum  $X_{vc}$  value at the end of the isothermal crystallization process. By knowing how the crystals have formed with respect to time, the Avrami constant can be calculated by plotting the function  $\ln(-\ln(1-X_{vc}/X_{vcinf}))$  with respect to time as,  $\ln(t)$  (Figure 3.2-4). There are two distinct lines that form when this is plotted for PEEK material, which is the result of a parallel, two-stage crystallization process. Each line's slope correlates with the Avrami constants,  $n_1$  and  $n_2$ .

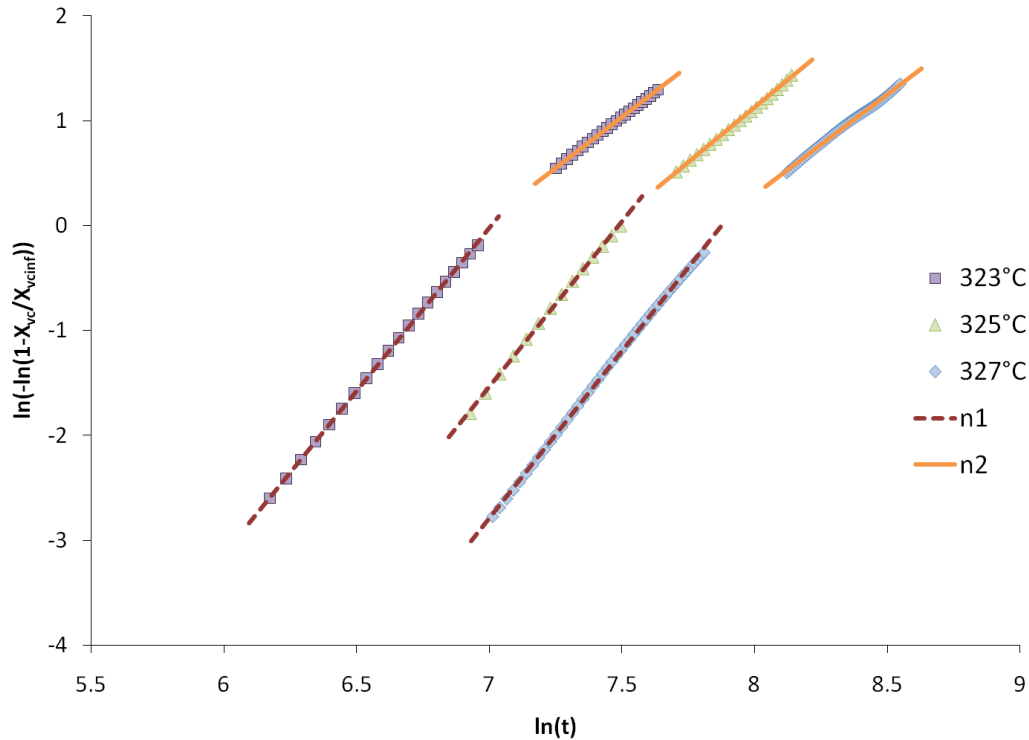


FIGURE 3.2-4: PEEK FILM ISOTHERMAL DSC CRYSTALLINITY DATA USED TO SOLVE FOR AVRAMI CONSTANTS,  $n_1$  AND  $n_2$ , AS THE SLOPES OF THE FITTED LINES FOR EACH TEMPERATURE

The experimental data for the isothermal crystallization agrees with the literature in describing that PEEK requires a parallel, two-stage crystallization kinetics equation to predict the crystallinity levels. Once the “ $n_1$ ” and “ $n_2$ ” values have been calculated, they can be used to fit both the isothermal and the dynamic crystallization data to the models. The slopes of the lines for each isothermal crystallization temperature (Figure 3.2-4) can be averaged together, and then used as the values for further crystallization modeling. Overall, for the PEEK film material, it was found that “ $n_1$ ” was 3.0 and “ $n_2$ ” was 2.0. As seen with the literature values summarized in Section 2.2, Table 2.2-3, the Avrami constants are different from those published by other researchers.

### 3.2.2.1 FITTING ISOTHERMAL DATA TO MODELS

The calculated crystallinity level due to a particular cooling rate with respect to the cooling time can easily and accurately be fitted to the Avrami equation as a two-stage function. The Avrami shape factor constants “ $k_1$ ” and “ $k_2$ ” must be solved after the Avrami exponential constants “ $n_1$ ” and “ $n_2$ ”. The Avrami shape factor is determined for each isothermal temperature, as each temperature had different “ $k_1$ ” and “ $k_2$ ” values to fit it to. To solve for the “ $k_1$ ” and “ $k_2$ ” constants, a curve of time to the “ $n$ ” with respect to “ $-\ln(1-X_{vc}/X_{vcinf})$ ” (Figure 3.2-5).

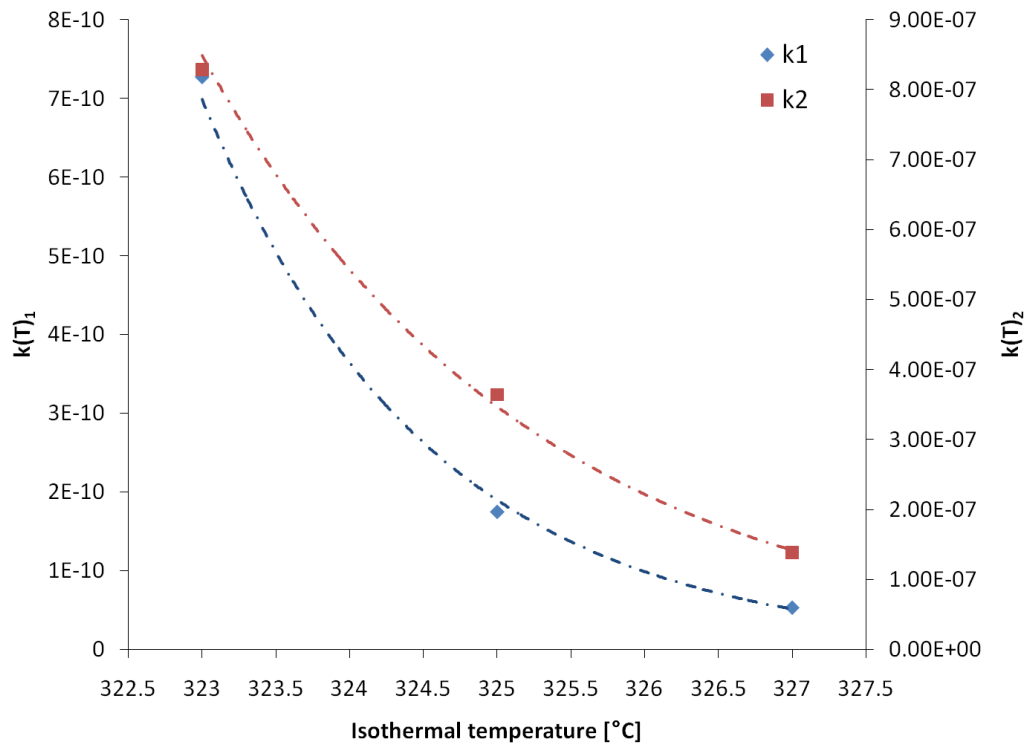
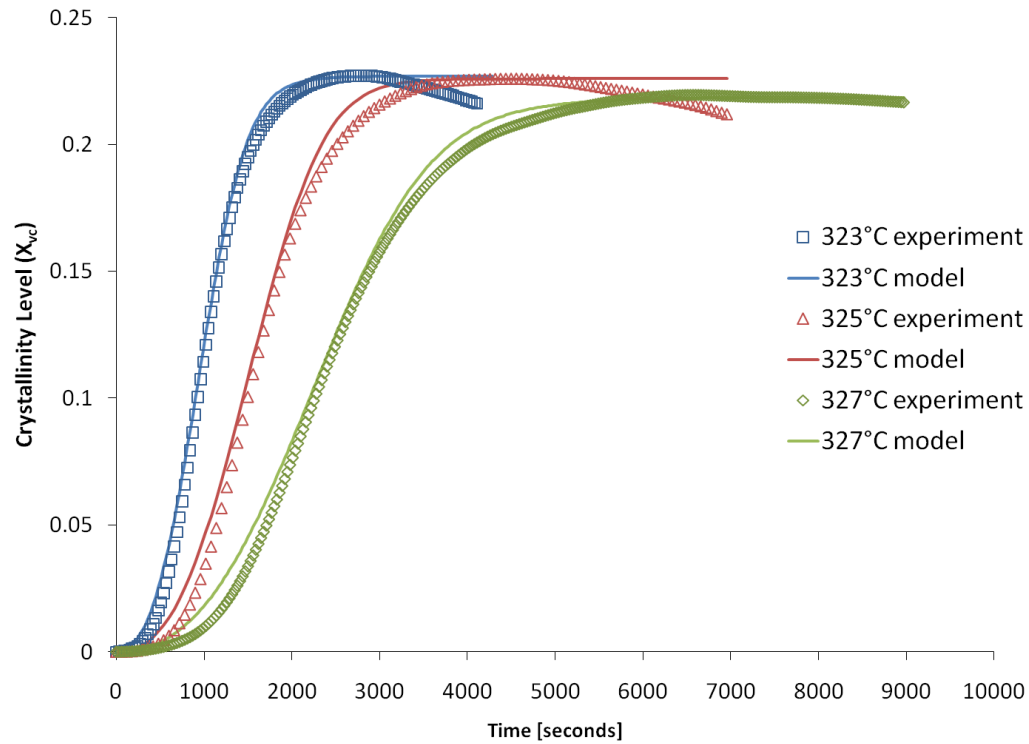


FIGURE 3.2-5: AVRAMI SHAPE CONSTANTS,  $K_1$  AND  $K_2$ , PLOTTED WITH RESPECT TO THE ISOTHERMAL TEMPERATURE

The “ $k_1$ ” and “ $k_2$ ” constants are then used in the Avrami model with the “ $n_1$ ” and “ $n_2$ ” values found earlier. Then the predicted crystallinity level can be plotted next to the experimental data to visualize the accuracy of

modeling the isothermal DSC crystallization data to the Avrami equation (Figure 3.2-6).



**FIGURE 3.2-6: ISOTHERMAL CRYSTALLINITY DATA ON PEEK FILM FITTED TO THE AVRAMI MODEL BY FINDING THE AVRAMI CONSTANTS AND SHAPE FACTORS**

Another method of modeling would be to use the Nakamura model [15-16], which was described in Section 2.2, with the constants that were solved via method of least squares. The following graph validates the Nakamura modeling equations with the experimental isothermal data (Figure 3.2-7). The constants used to fit the data are found in Appendix A, Table 6.1-2.

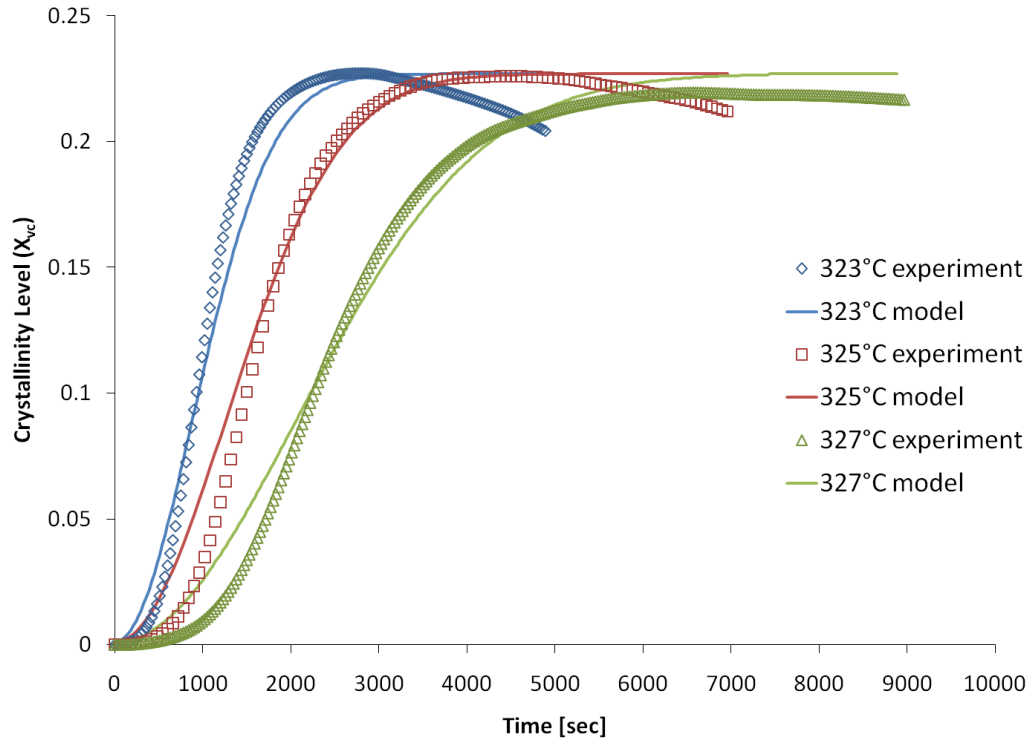


**FIGURE 3.2-7: PEEK FILM ISOTHERMAL DSC TESTS FOR THREE TEMPERATURES ARE FITTED TO THE NAKAMURA MODEL USING METHOD OF LEAST SQUARES TO FIND THE CONSTANTS**

The models show that the best fit came with the Avrami fit to the model; however, the Nakamura model fit decently well. By the method of least squares, the average of the sum difference for all three isothermal hold temperatures was 0.018.

### 3.2.3 DYNAMIC DSC EXPERIMENTS

Dynamic crystallization occurs when the melted material will solidify at a determined cooling rate. The material sample is heated from room temperature and melted to a temperature above  $T_m$ . When the liquid polymer cools, it will harden and crystallize as it passes through the temperature region between the  $T_m$  and  $T_g$ . Generally, a faster cooling rate hinders crystal nucleation and growth, thus yielding a lower crystallinity level.

To run dynamic crystallization experiments, the DSC measured the heat flows of seven film samples at a variety of cooling rates. Each of these cooling rates will yield different crystallinity levels on the film material. The method to run the DSC experiments was:

1. Melt the polymer film of 5-10 mg to 380°C at a heating rate of 10°C/min.
2. Hold film at this elevated temperature for 5 minutes to ensure all the crystals from the film are melted.
3. Cool the film to 20°C at one of the cooling rates: 0.5, 1, 2, 5, 10, 20, and 30°C/min.

The heat of crystallization peak due to the cooling rate needs to be integrated to be able to calculate the crystallinity level. The cooling rate values were chosen to be incremental, while still allowing for the maximum cooling rate that the DSC could perform, using the refrigerated cooling system. Faster cooling rates are possible to obtain if a liquid nitrogen cooling system was used; however, this was unfortunately unavailable.

#### 3.2.3.1 RESULTS

The DSC plots for heat of crystallization with respect to the time are used to calculate the total heat of the crystallization for determining the crystallinity level (Figure 3.2-8).

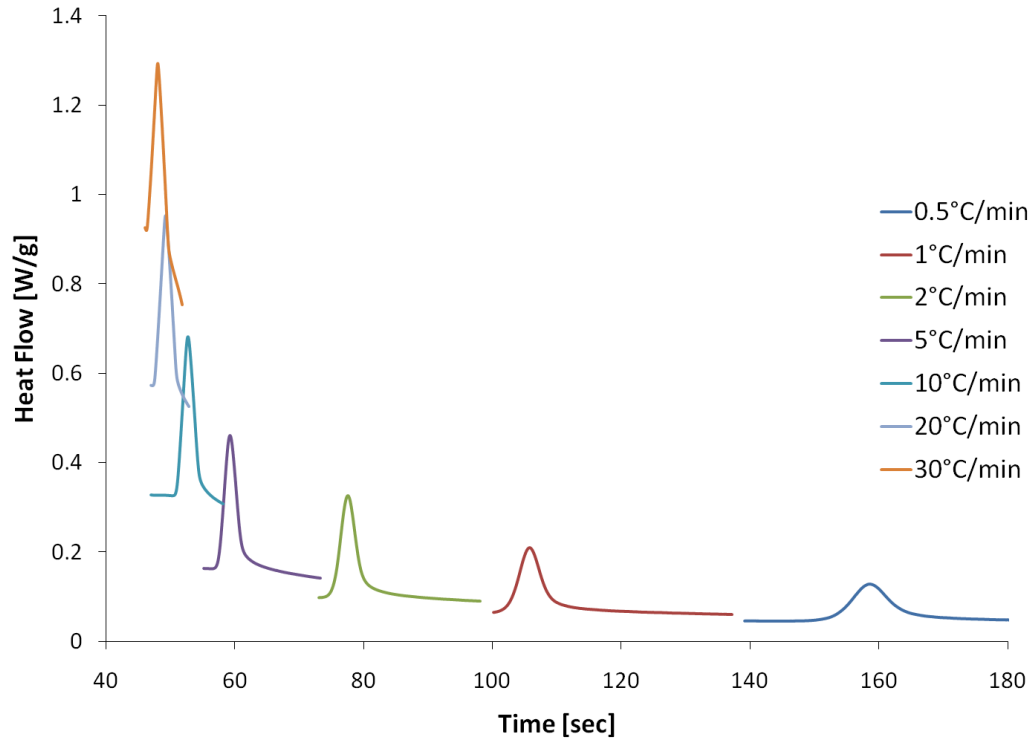


**FIGURE 3.2-8: HEAT OF CRYSTALLIZATION FOR PEEK FILM MATERIAL AS A DYNAMIC DSC SCAN AT A VARIETY OF COOLING RATES**

From the work carried out, the cooling rates of the PEEK film maintained a high crystallinity levels even at high cooling rates (Figure 3.2-9). When comparing to Velisaris, the PEEK film crystallizes at a higher percentage and due to limitations on the DSC used, the maximum cooling rate was only for 30°C/min. This signifies that there could be a difference in the grade of PEEK used based on the manufacturer or time the material was manufactured, since Velisaris' work was completed in the mid-1980's and this work was done in late 2000's.

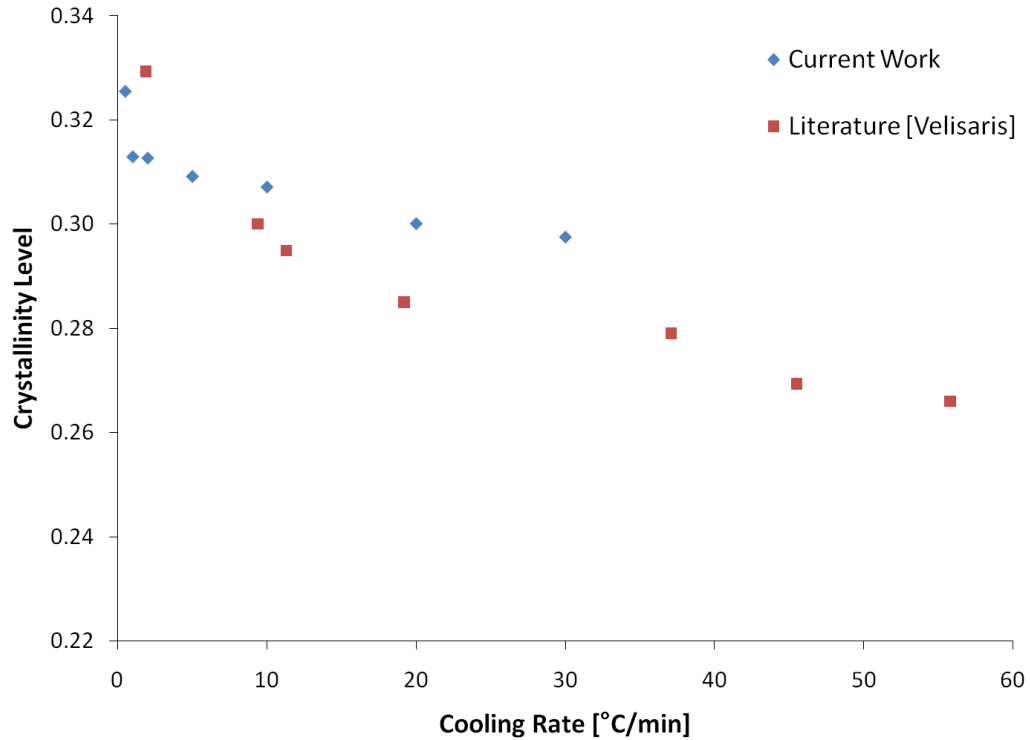


**FIGURE 3.2-9: COMPARING CRYSTALLINITY LEVEL AS A FUNCTION OF MATERIAL COOLING RATE FOR THE CURRENT WORK TO LITERATURE [7]**

### 3.2.3.2 FITTING DYNAMIC DATA TO MODELS

First the experimental data for each cooling rate as a function of time was plotted. Next, for each of the models: Velisaris, Cebe, and Tierney, the literature values of the constants were compared with the experimental data. Then, the models were fitted to the data by using the method of least squares for each of the cooling rates.

For each of the models, the first step was to test if the constant values from literature would match nicely to the experimental data from the DSC experiments. The models that were compared with to the experimental data were from Velisaris, Cebe, and Tierney, which were described in Section 2.2. The literature constants were the same for all cooling rates for Velisaris and Tierney, but Cebe had different constants for cooling rates 1, 5, and 10°C/min. Thus, the literature constants were just focused on in the

following charts (Figure 3.2-10, Figure 3.2-11, and Figure 3.2-12) for only those cooling rates.

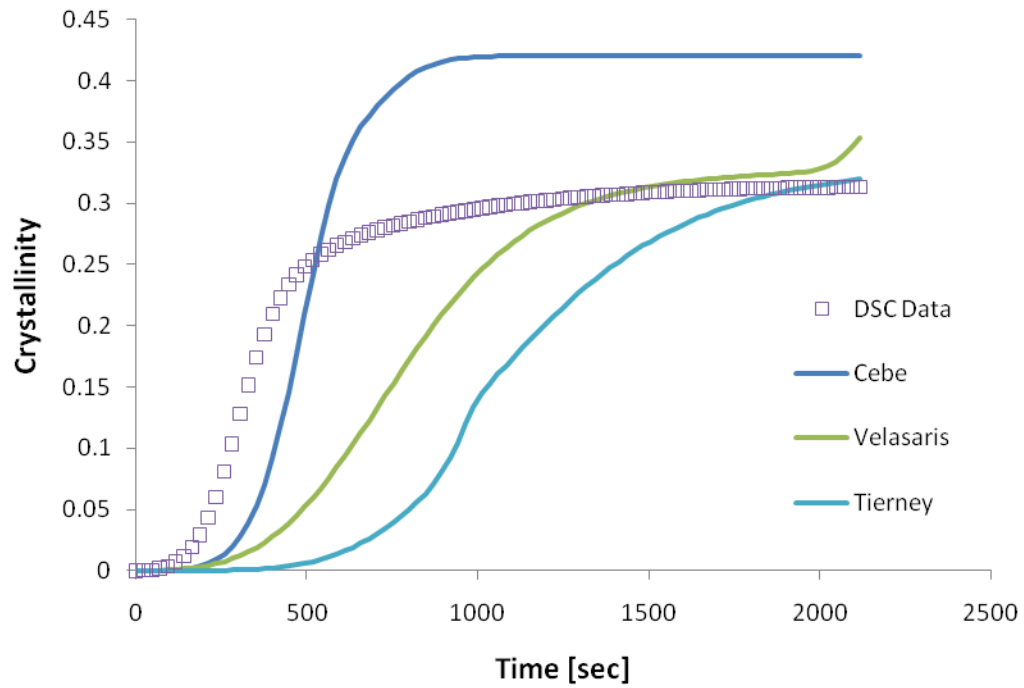


**FIGURE 3.2-10: COMPARING MODELS USING THE CONSTANTS FROM LITERATURE TO DYNAMIC EXPERIMENTAL DSC CRYSTALLINITY DATA FOR PEEK FILM AT A COOLING RATE OF 1°C/MIN**

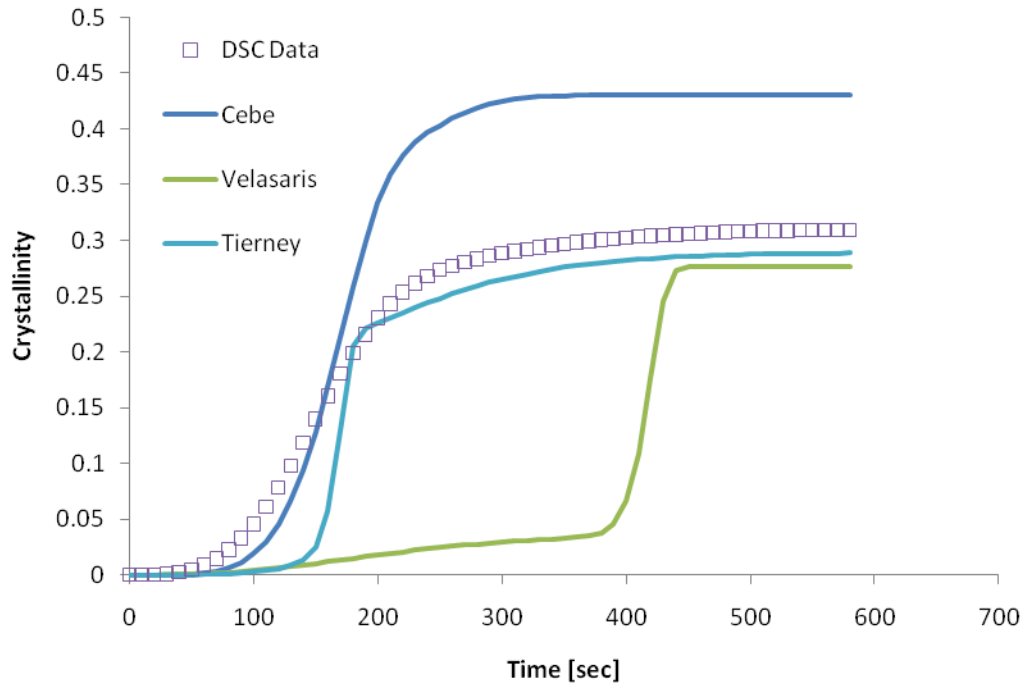


**FIGURE 3.2-11: COMPARING MODELS USING THE CONSTANTS FROM LITERATURE TO DYNAMIC EXPERIMENTAL DSC CRYSTALLINITY DATA FOR PEEK FILM AT A COOLING RATE OF 5°C/MIN**

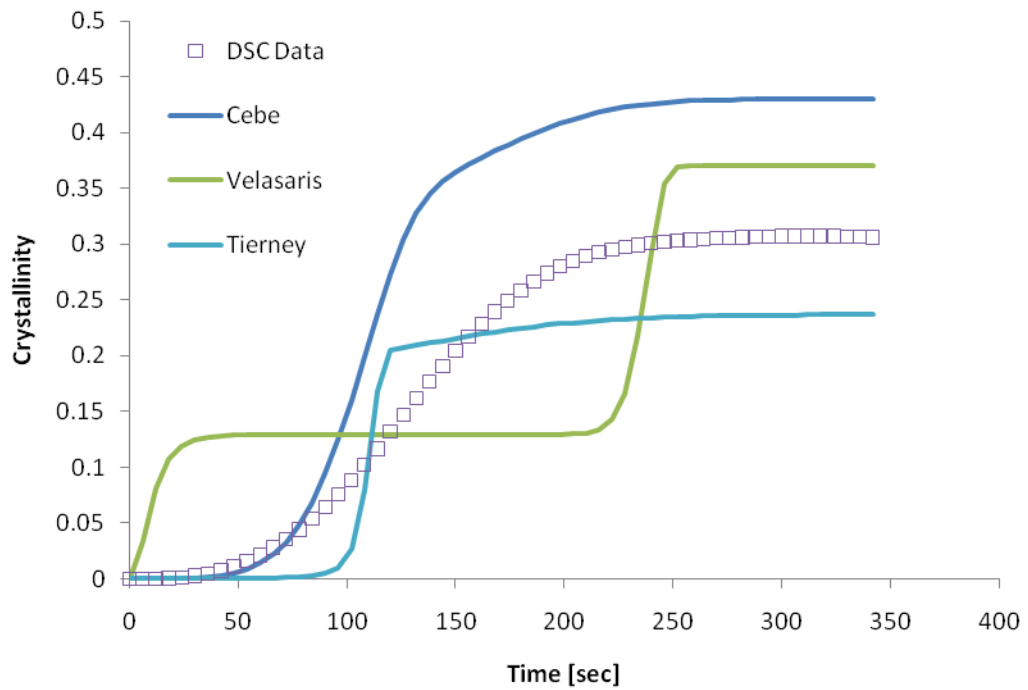


**FIGURE 3.2-12: COMPARING MODELS USING THE CONSTANTS FROM LITERATURE TO DYNAMIC EXPERIMENTAL DSC CRYSTALLINITY DATA FOR PEEK FILM AT A COOLING RATE OF 10°C/MIN**

From Figure 3.2-10, Figure 3.2-11, and Figure 3.2-12, one can see that Cebe's values predict a higher crystallinity level on the PEEK film material than what actually occurred in the DSC experiments. However, all of the shapes of the graphs are following a similar shape trend to the experimental DSC data in that it starts low and after it has an increase before it levels off. The Velisaris model does not fit well to the data at all. While, Tierney's model shows a better fit both shape-wise and maximum crystallinity level-wise, but it is still rather off. The Velisaris and Tierney models can predict the final level of crystallinity well enough, but Cebe's model with literature constants more than over predicts the crystallinity level of the material.

Part of the issue with the mismatch in properly fitting the DSC crystallinity data to the models with literature constants is due to the importance of the starting temperature at which the crystals form in the models. It was found that Velisaris started his model at a higher temperature than the temperature at which the crystals began forming in the DSC experiments on the film material. Thus, the starting temperature at which the material cools down from will affect how well the model would fit to the experimental data.

Since the models from literature did not fit so well to the DSC data with the constants from literature, the next step was to try to fit constants for each of the models to the data by using the method of least squares. The models chosen for examination were only Cebe and Tierney. Velisaris was neglected, since he used two values for  $T_m$  for the two stages of crystallization, and this was not found to be a true aspect of the process. The constants were fitted for each of the cooling rates (0.5-30°C/min) separately. The first set of graphs fits Cebe's model (Figure 3.2-13 and Figure 3.2-14) and the second set of graphs fits Tierney's model (Figure 3.2-15 and Figure 3.2-16). All of the constants for each of the cooling rates for both models are summarized in Table 6.2-1 and Table 6.2-2 in Appendix A.

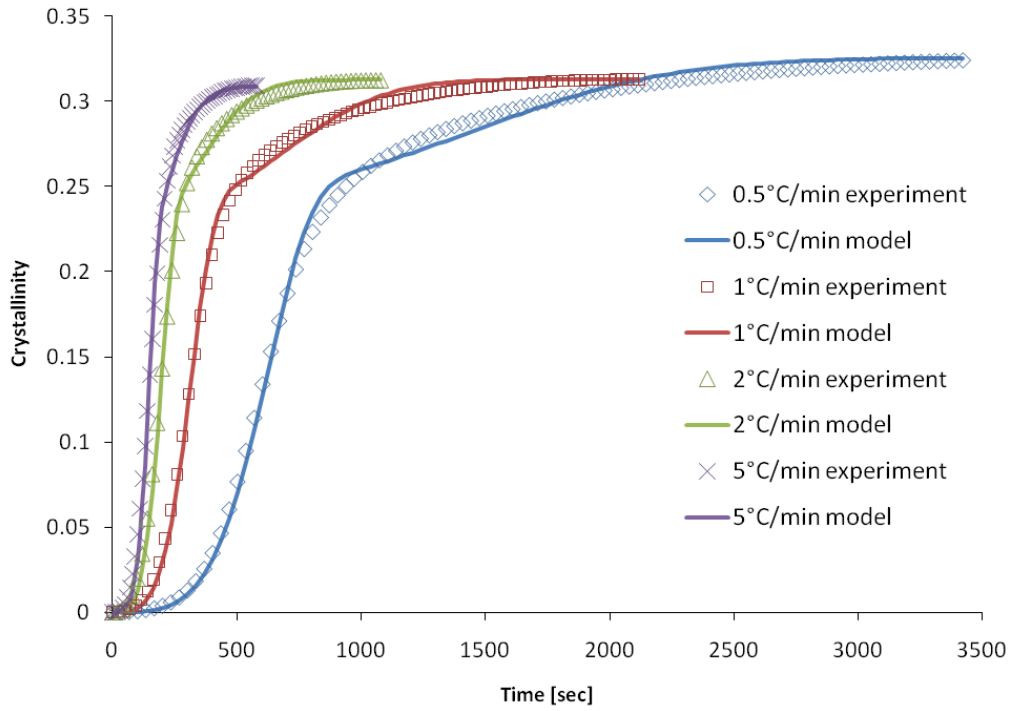


FIGURE 3.2-13: CEBE MODEL FITTED TO DYNAMIC DSC EXPERIMENTAL DATA FOR PEEK FILMS AT COOLING RATES OF 0.5-5°C/MIN

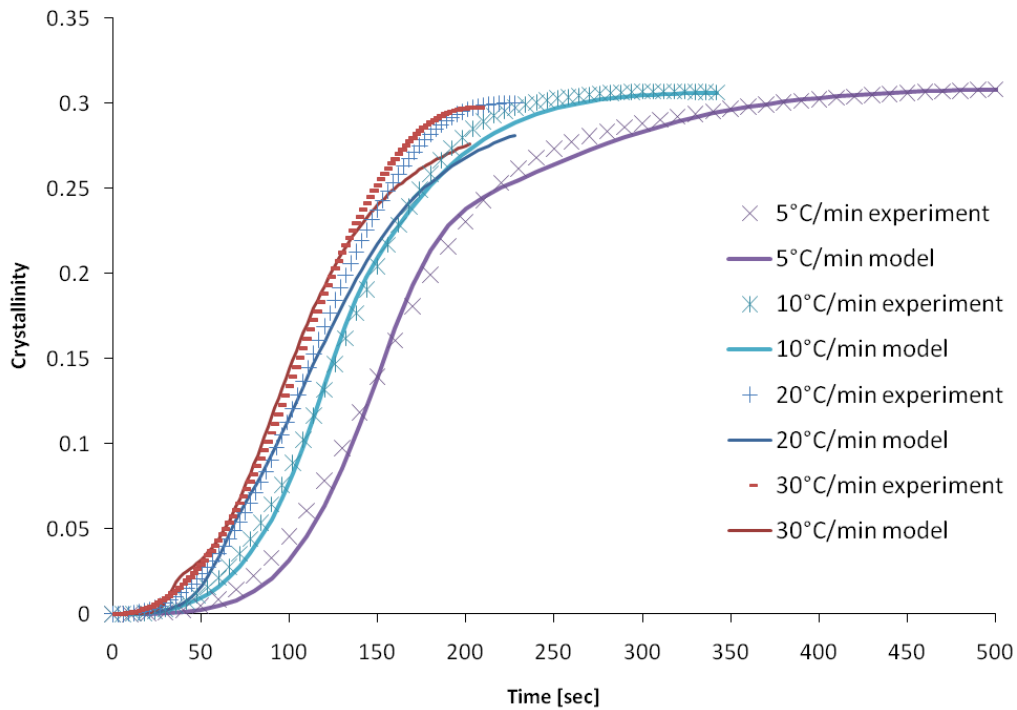


FIGURE 3.2-14: CEBE MODEL FITTED MODEL TO DYNAMIC DSC EXPERIMENTAL DATA FOR PEEK FILMS AT COOLING RATES OF 5-30°C/MIN

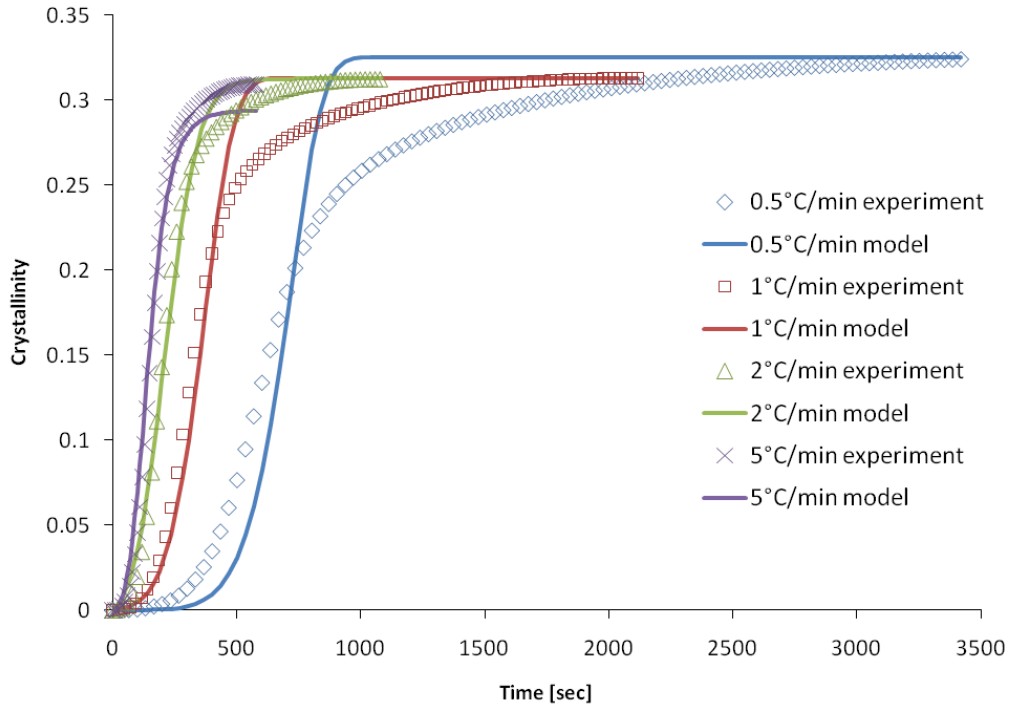


FIGURE 3.2-15: TIERNEY MODEL FITTED TO DYNAMIC DSC EXPERIMENTAL DATA FOR PEEK FILMS AT COOLING RATES OF 0.5-5°C/MIN

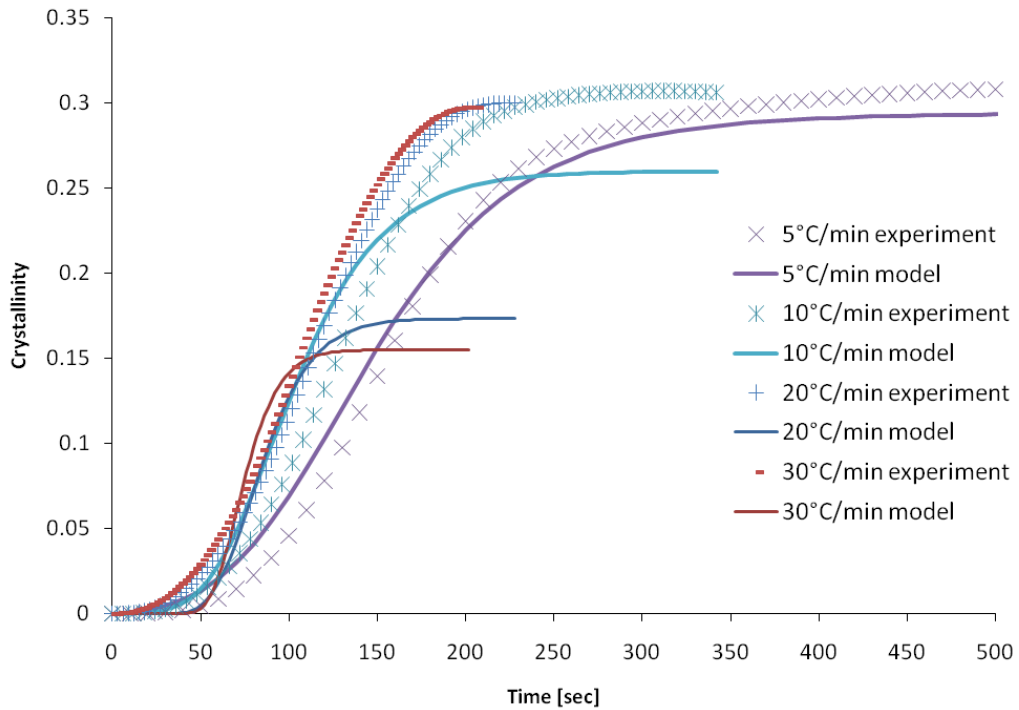


FIGURE 3.2-16: TIERNEY MODEL FITTED TO DYNAMIC DSC EXPERIMENTAL DATA FOR PEEK FILMS AT COOLING RATES OF 5-30°C/MIN

From the graphs, it is apparent that the models fit well up to the faster cooling rates and Cebe's model fit better to the data than Tierney's model. There was another model mentioned in the literature that had been used to model other thermoplastics, but had not been looked into for PEEK yet. Therefore, the Nakamura model was fit to the dynamic tests, for all the cooling rates to determine if the fit would be even better than the other two models that the data was fit to (Figure 3.2-17 and Figure 3.2-18).

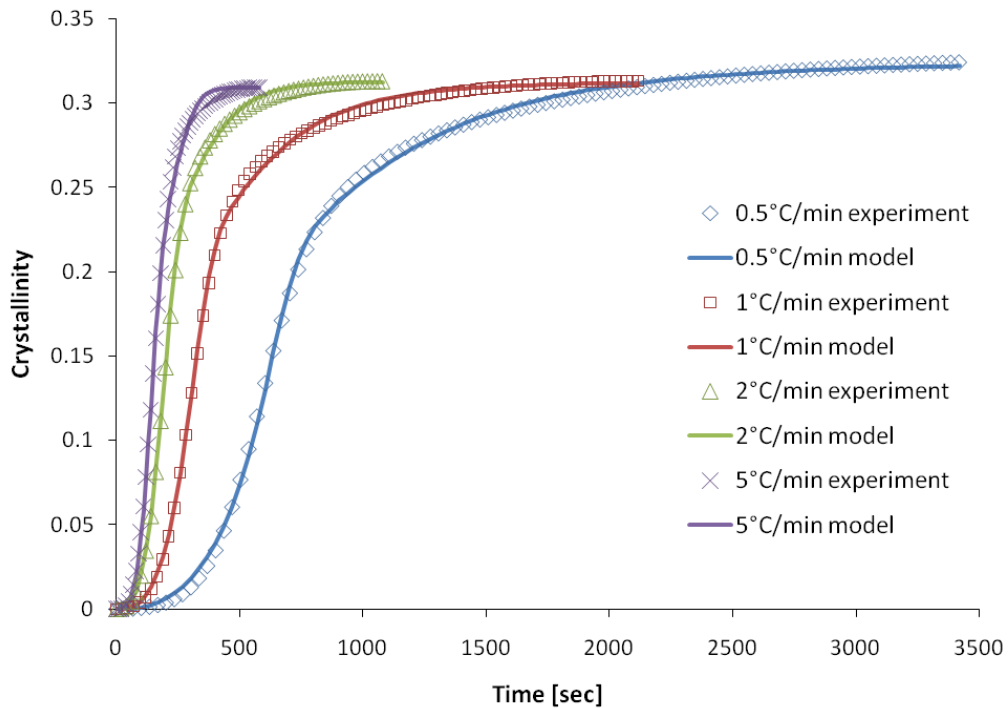
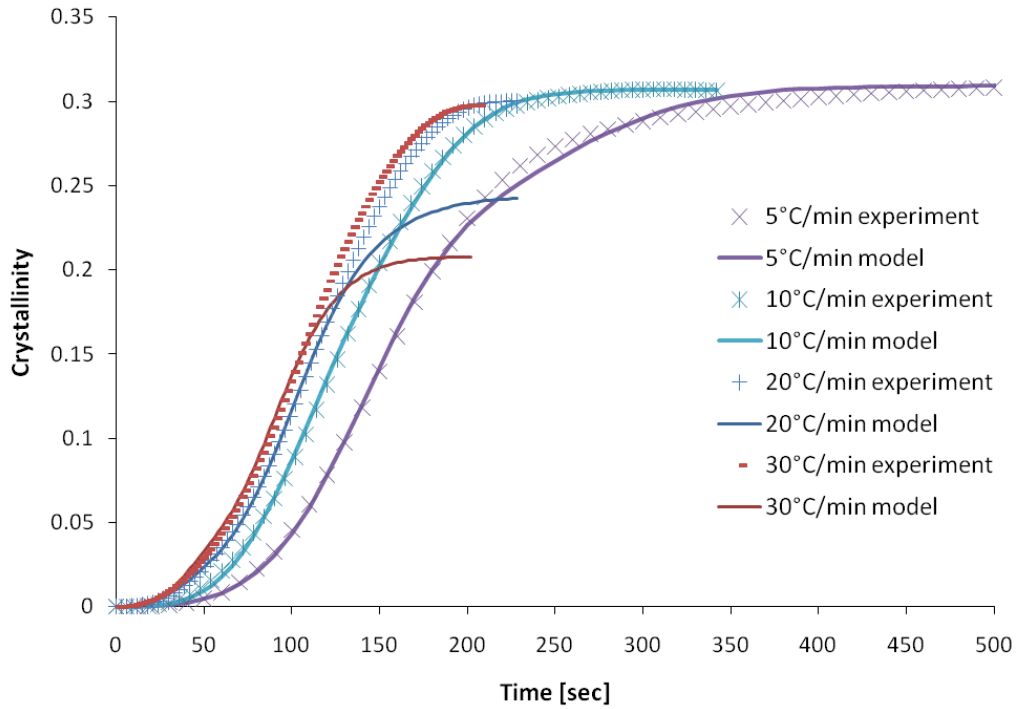


FIGURE 3.2-17: NAKAMURA MODEL FITTED TO DYNAMIC DSC EXPERIMENTAL DATA FOR PEEK FILMS AT COOLING RATES OF 0.5-5°C/MIN



**FIGURE 3.2-18: NAKAMURA MODEL FITTED TO DYNAMIC DSC EXPERIMENTAL DATA FOR PEEK FILMS AT COOLING RATES OF 5-30°C/MIN**

After the model had been fitted, it is again clear that the model matches nicely for the slower cooling rates but falls off for the fast cooling rates. These models might be good choices for predicting the crystallinity levels for materials where the material will not crystallize to a high percentage at a high cooling rate.

### 3.3 VISUALIZING CRYSTALS IN FILM MATERIAL

Due to the high percentage of crystals that form in PEEK film, the crystals can be visualized with the help of a microscope with a polarized filter over the lens. On a macroscopic level, the film material is transparent when no crystals are present, but it is translucent when there are crystals in the material. Literature has found that the crystal size for PEEK is small [44]. For observing the crystals, isothermally crystallized and dynamically crystallized samples were prepared in a TA Instruments Q800 DMA using a compression fixture. This technique was used since the DMA could apply a temperature and pressure environment to make a sample of 1.27 cm in diameter and ~8-10 layers thick (~0.5 mm). After the samples were manufactured, they were cut through the thickness using a microtome to thinly slice the plastic to be able to observe it under the microscope. The general temperature conditions applied to the samples were to create a sample by applying the temperature hold of 325°C and cooling rates 1°C/min and 10°C/min to a few sheets of the film material in a stacked formation of 1.27 cm in diameter.

#### 3.3.1 ISOTHERMALLY CRYSTALLIZED SAMPLE

At a temperature of 325°C, the material showed small crystals as they had formed due to the isothermal crystallization. Due to the magnification level, only the spheruletic crystals can be seen (Figure 3.3-1).

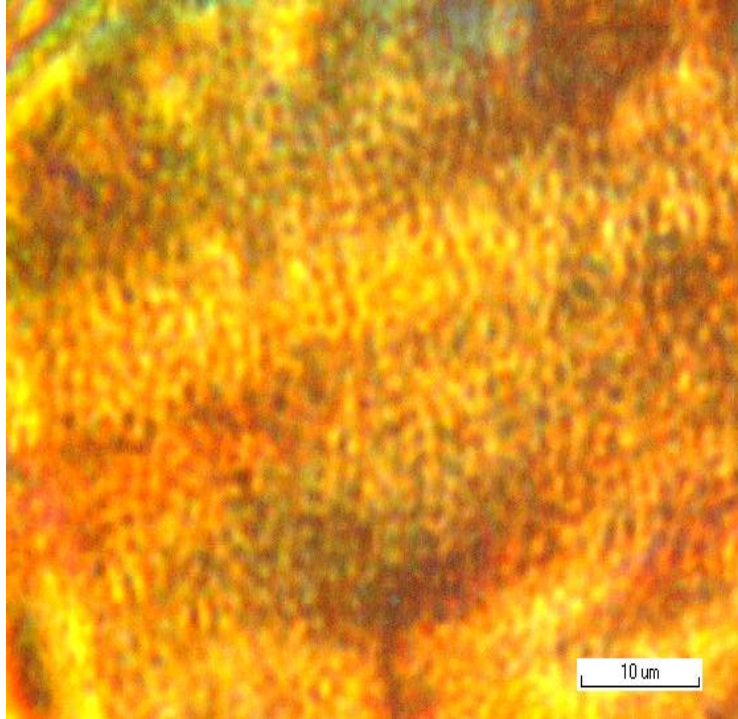


**FIGURE 3.3-1: CRYSTALS FORMED IN ISOTHERMAL DSC EXPERIMENTS ON PEEK FILM AT 325°C (100X)**

### 3.3.2 DYNAMICALLY CRYSTALLIZED SAMPLES

Crystals formed during dynamic crystallization at both cooling rates of 1°C/min and 10°C/min. Like the isothermal crystallized samples, the spherule-like crystals are the only type that can be visualized under the 100x magnification. However, it is possible to recognize that the spherule-like crystal size is larger for the 1°C/min samples than for the 10°C/min samples (Figure 3.3-2 and Figure 3.3-3).

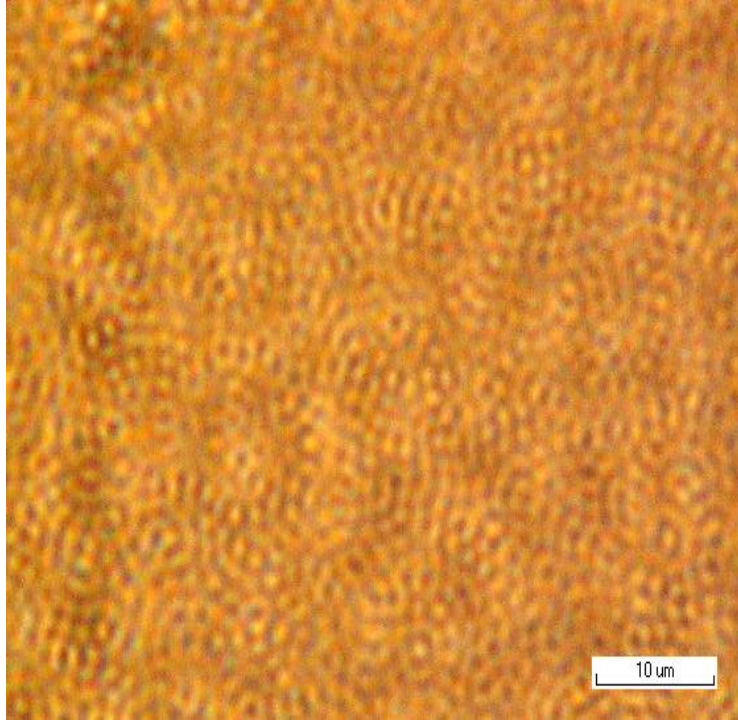


**FIGURE 3.3-2: CRYSTALS FORMED IN DYNAMIC DSC EXPERIMENTS ON PEEK FILM WHEN COOLED AT 1°C/MIN (100X)**

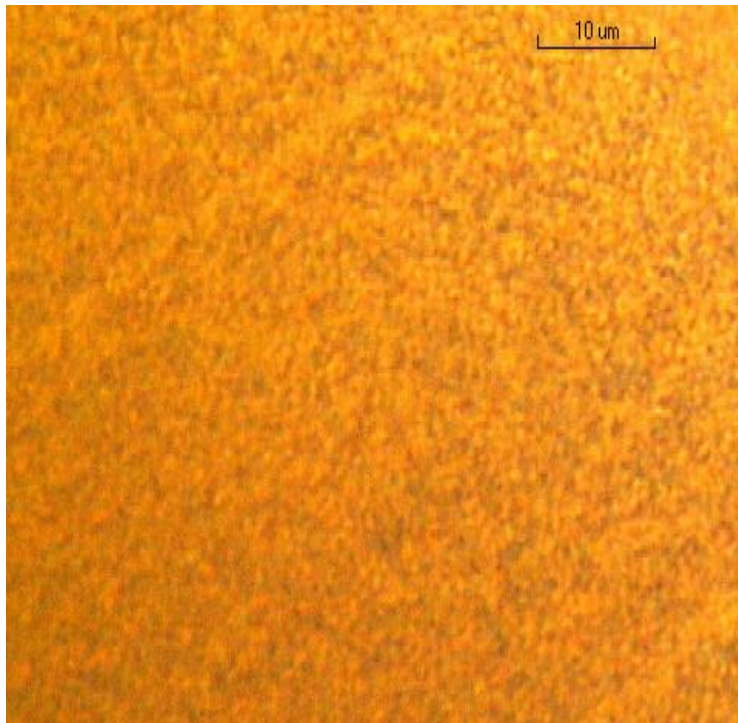


**FIGURE 3.3-3: CRYSTALS FORMED IN DYNAMIC DSC EXPERIMENTS ON PEEK FILM WHEN COOLED AT 10°C/MIN (100X)**

### 3.4 SUMMARY

Characterizing PEEK film material for the level of crystallinity due to isothermal or dynamic DSC experiments can be compared with crystallization kinetics models that have been investigated in the literature.

The PEEK material undergoes a parallel, two-stage crystallization process when it cools and solidifies. Generally, the literature has shown that the primary crystallization produces spheruletic shaped crystals and is more dominant for the dynamic crystallization process, while the secondary crystallization produces epitaxial shaped crystals is more dominant in the isothermal crystallization process.

When comparing the experimental data for both the isothermal and dynamic crystallization methods to the models in literature there was a variety of results. The isothermal data fit more accurately with the two-stage Avrami model. However, the same data still fit very well to the Nakamura model.

When fitting to the three models from literature: Cebe, Velisaris, and Tierney with the constants that each of these models found to fit their data, the models did not fit well to the DSC experimental data. However, when each of these models had the constants fit to the data by the method of least squares, the data fit well for the slower cooling rates (up to 5°C/min), but not as well at the faster cooling rates. However, the models did predict values close to the maximum crystallinity level.

The constants in the Nakamura model were fit to the dynamic DSC data as done with the other models. The data fit best to this model, but it fits even worse for the higher cooling rates than compared with the other three models. When considering the final crystallinity levels, the Velisaris and Tierney models with the literature constants can predict the final level of crystallinity closer to what is found from DSC experiments. However, Cebe's model with literature constants does not fit well to the experiments.

---

## CHAPTER 4: MANUFACTURING PROCESSING

ATP is a manufacturing technique where a robotic head heats up, lays down, and adds pressure to consolidate ply or tow composite layers on a mandrel or on pre-established layers to build up a material and part. The overall goal behind this project is to use ATP as an “*in-situ*” manufacturing practice for high performance thermoplastic materials. Usually the part is put into an autoclave oven where pressure and heat can further consolidate the composite layers together to create more uniformity through the layers. Using an autoclave adds cost and time to the manufacturing process and is especially cumbersome for large parts. This drives the research behind studying the methods for making ATP strictly an *in-situ* process.

This project examines the thermal aspects related to the ATP manufacturing process to produce high quality parts for an *in-situ* operation. First, one must know the temperatures that a part undergoes during the ATP process and second, one must understand how the consequent changes in cooling rates throughout the layers of the composite affect each layer’s crystallinity level. As mentioned in the literature review, the material cooling rate found in ATP for natural air cooling is 3000°C/min [29], but this needs to be validated with the following set of experiments.

If manufacturers understand the effects of the cooling rates of composite thermoplastic material on its crystallinity during the ATP process, they will be able to produce higher quality parts. The following sections discuss an experimental plan to measure both the temperatures and crystallinity levels that occur in a part during the manufacturing process along with the results and analysis of the measurements.

## 4.1 MATERIAL SELECTION

Chapter 3 examined the film material to characterize and model the crystallinity levels. The experimental work covered in this chapter on the ATP manufacturing process will use a composite material. The material used for the ATP experiments work were CYPEK APC2/PEEK and CYPEK APC/PEKK, which are carbon fiber/thermoplastic matrix tow tapes from Cytec Engineered Material Inc. The material tows are continuous, and both have a width of 0.635 cm (0.25 in).

The key processing temperatures for the PEEK and PEKK matrix composite materials can be found in Table 4.1-1.

TABLE 4.1-1: IMPORTANT TEMPERATURES FOR BOTH MATERIALS TO CONSIDER IN MANUFACTURING [45]

	$T_g$ [°C]	$T_m$ [°C]	$T_{Processing}$ [°C]
APC2/PEEK	143	343	380-400
APC/PEKK	154	308	340-370

## 4.2 EXPERIMENTAL PLAN

An ATP manufacturing process experiment was designed to determine the heating and cooling rates of the material to predict the crystallinity level through the thickness of the material due to the cooling rate. The ATP machine used was from Automated Dynamics, located at National Research Council Canada-Institute for Aerospace Research/Aerospace Manufacturing Technology Center (NRC-IAR/AMTC) in Montreal, Quebec.

During manufacturing, there are many parameters that can be changed in order to optimize material quality (Figure 4.2-1). The torch temperature provides the heat to melt the material. Since the material must be heated to over 380°C for PEEK and 340°C for PEKK, the gas torch

temperature must be set higher to melt the matrix completely. Due to the high temperatures that the material is subjected, the torch gas is nitrogen to prevent oxidation from occurring on the composite tow. The gas flow rate also is important as it will have an impact and influence on spreading the fibers when it is heating up the material. The speed at which the part is laid up will influence the heating and cooling rates. This particular machine combines the rotational speed and the feed rate of the material into one parameter for simplicity. The distance from the heating torch to the material also impacts the quality since the part could burn if the high temperature is too close to the material. Lastly, the compaction force from the roller plays an important role in the compaction of the layers to ensure the plies stick together.

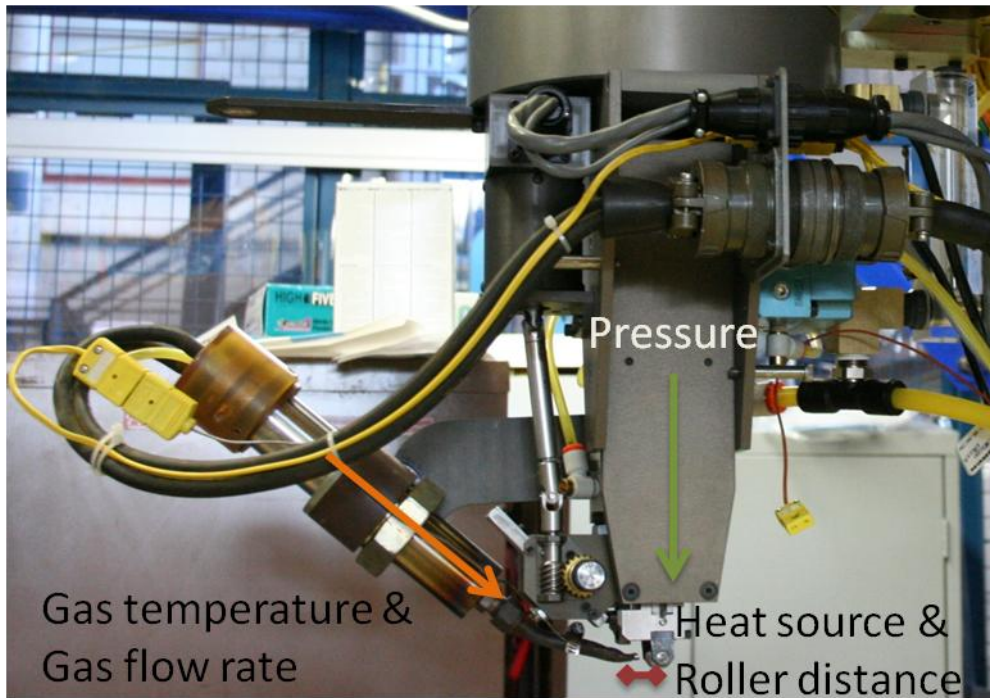


**FIGURE 4.2-1: ATP MANUFACTURING HEAD WITH A DESCRIPTION OF THE IMPORTANT MANUFACTURING PARAMETERS TO THE ATP PROCESS**

The manufacturing parameters were varied in order to optimize and make a high quality part. In order to do so, the temperature had to be high enough to allow for the polymer matrix to melt, while at the same time not burning the material. Next, the flow of the nitrogen gas coming from the torch had to be considered, so that the tows would not spread too much and that enough gas would be directed at the tow. The layup speed was also important for allowing the material enough time to consolidate. Distance between the heat source and roller was kept constant, which was sufficient so that the torch was not going to overheat the roller. Lastly, the compaction force had to be sufficient enough to allow for the layers to compact together to become one piece. A summary of the manufacturing parameters for both materials used in the project with the values for them are as follows:

**TABLE 4.2-1: ATP MANUFACTURING PARAMETERS FOR BOTH COMPOSITE TAPE MATERIALS**

	<b>APC2/PEEK</b>	<b>APC/PEKK</b>
Torch temperature-Nitrogen backed	900°C	800°C
Nitrogen gas flow rate	65 SLPM	65 SLPM
Layup speed	20 mm/sec	20 mm/sec
Distance between heat source and roller	3.81 cm (1.5 in)	3.81 cm (1.5 in)
Compaction force	40 kg	40 kg

To measure the part temperatures during manufacturing, both a geometry and a manufacturing method had to be created. In the literature, researchers have manufactured flat panels and ring shapes and used the methods of measuring the temperatures with infrared cameras and thermocouples [25, 29, 33, 36-37]. It was decided that the best option to measure the thermal profile of the material for this project was to manufacture a ring-geometry shape on a mandrel and to measure the part temperatures with thermocouples. The mandrel rotation during manufacturing must be considered as thermocouples are wires attached to a data collection unit that is attached to a computer. Rather than use wires

that were extremely long and wrapped around a spool, this problem was overcome by using a data-acquisition unit that had wireless capabilities to transmit the temperatures to a laptop computer across the room (Figure 4.2-2).

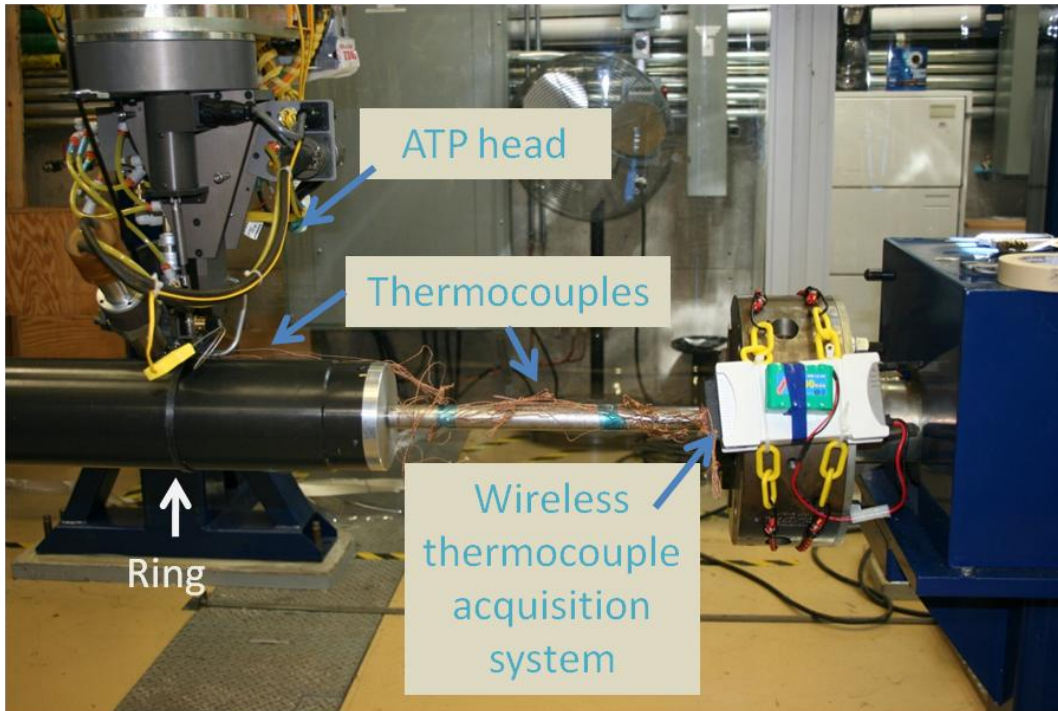


FIGURE 4.2-2: MANUFACTURING SETUP WITH THERMOCOUPLES AND WIRELESS DATA ACQUISITION SYSTEM

### 4.3 MANUFACTURING PROCEDURE

Before the process, the hollow, anodized aluminum mandrel was pre-heated with a ultra-violet lamp for an hour. This pre-heating step will expand the mandrel to remove the part post-processing easily once both the laminate ring and mandrel have cooled down. What occurs is the mandrel will shrink back to the original size while the composite will remain almost the same size, thus making the ring easy to remove from the mandrel.

The material tow was placed onto the mandrel using an ATP thermoplastic head. The ATP head remained stationary, i.e. no travel or rotation about any axis, to manufacture a simple geometry, called a “ring”

(Figure 4.3-1) of one tow width, which was 0.635 cm (0.25 in) and 80 layers thick. The inner diameter of the ring to start was set as 15.24 cm (6 in), as that was the diameter of the tool that the ring was manufactured on.

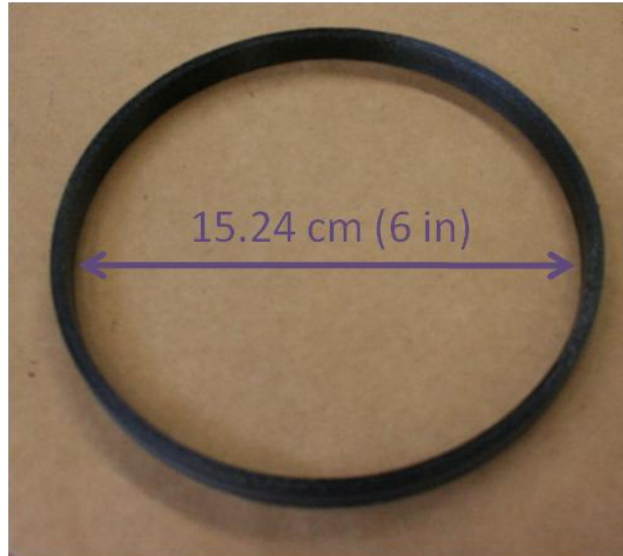


**FIGURE 4.3-1: ACTUAL CARBON FIBER/THERMOPLASTIC MATRIX RING MANUFACTURED BY ATP**

The ATP head laid the material onto the mandrel, with measurements of 1.12 cm (0.5 in) thickness and 15.24 cm (6 in) outer diameter (Figure 4.3-2). The combined rotational speed of mandrel with the rate at which the material was fed from the spool was set at a speed of 20 mm/sec.

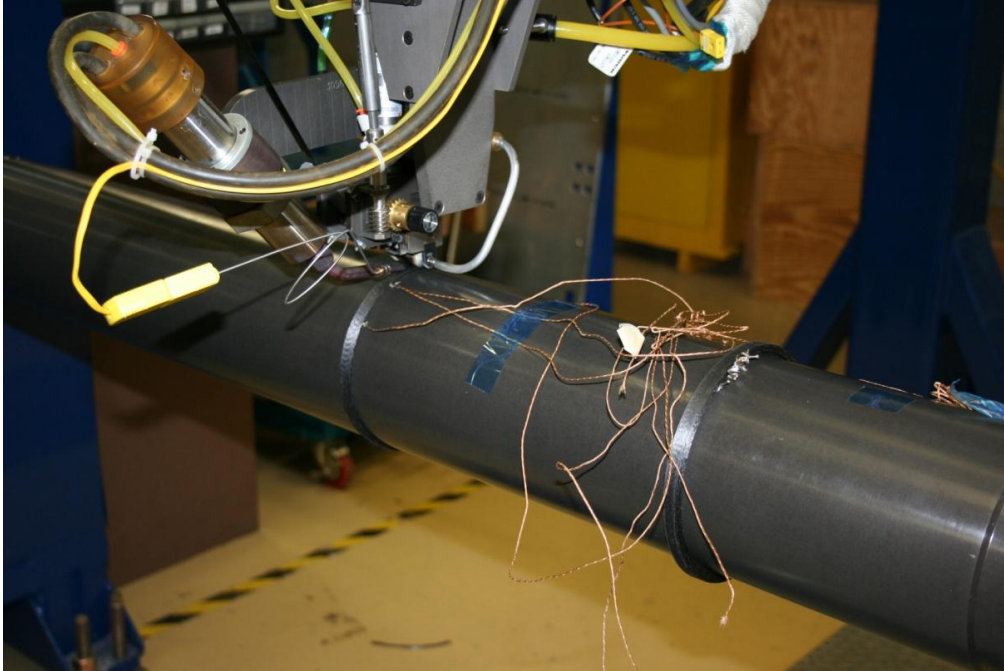


**FIGURE 4.3-2: MANUFACTURING SETUP THAT INCLUDES THE ATP HEAD, ANODIZED ALUMINUM MANDREL, AND THERMOCOUPLES IMBEDDED IN LAMINITE RING**

#### 4.3.1 MANUFACTURING CONSIDERATIONS FOR ATP

When starting the ATP process, it is imperative to ensure that the first layer of material will stick to the mandrel, and in the case of these experiments that the material will wrap properly around the mandrel. The other consideration is to prevent tow drift during the process (Figure 4.3-3). The tows need to stay perfectly aligned when manufacturing the ring, but there were instances where the tows were misaligned and thus the tows would drift off the intended manufacturing path.

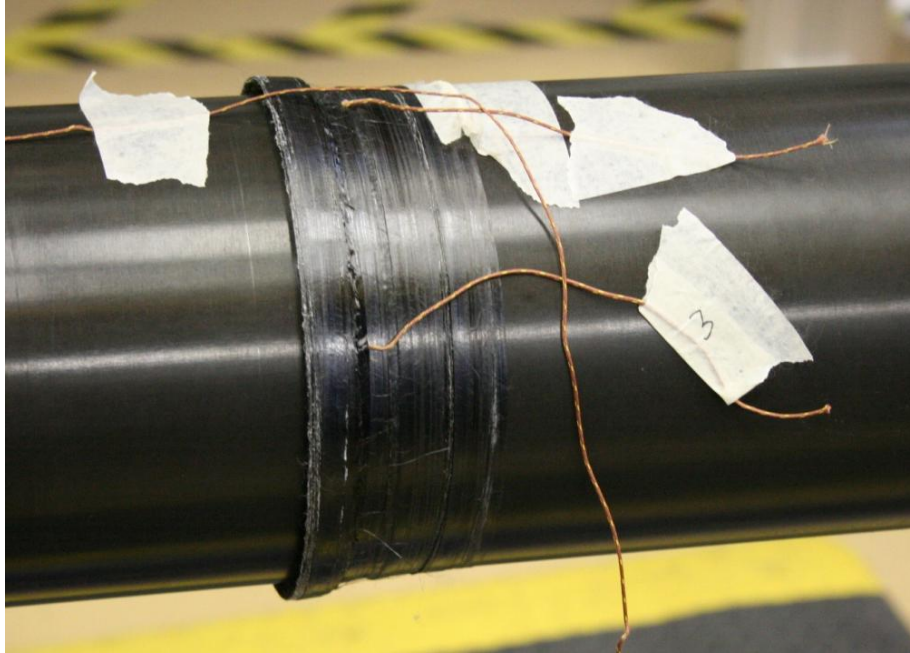


**FIGURE 4.3-3: EXAMPLE OF A POORLY MANUFACTURED RING THAT HAD SIGNIFICANT TOW DRIFT; THE WIRES ARE TRIMMED THERMOCOUPLE WIRES**

#### 4.3.2 MANUFACTURING MEASUREMENTS DURING ATP

K-type thermocouples were placed in between every 10 layers, starting with Layer 1 to Layer 80, to measure the temperature of the material during processing. Each thermocouple was placed along the same radial line through the ring thickness to keep a consistent location temperature reading (Figure 4.3-4).

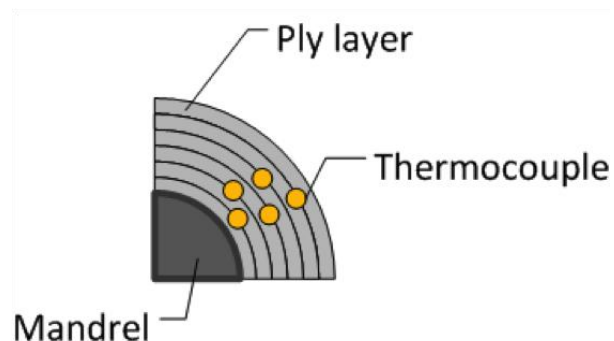


**FIGURE 4.3-4: GENERAL SECTION OF A RING MANUFACTURED OUT OF THERMOPLASTIC MATERIAL BY ATP THAT SHOWS THE GENERAL PLACEMENT OF THE THERMOCOUPLES THROUGH THE THICKNESS**

These temperature measurements are to be used to calculate the cooling rates of the material throughout the process as well as at the end of the process. One thermocouple was also placed on the mandrel to determine the heat sink effect that the mandrel had on the material. The thermocouple wires were connected to a wireless data acquisition unit that had an interface to a laptop computer to record the data.

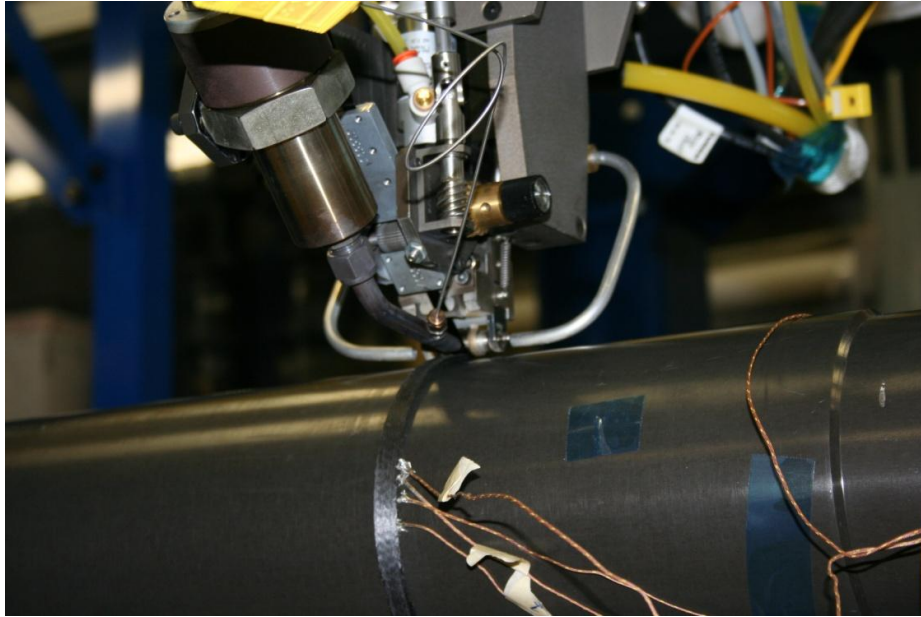


**FIGURE 4.3-5: MANUFACTURING RING PART ON MANDREL WITH THERMOCOUPLES IN PLACE**

#### 4.3.3 POST PROCESSING MEASUREMENTS

The crystallinity level of each laminate part was needed in order to verify and determine how the levels were affected by the processing parameters. Post-processing, both of the manufactured parts were cut into three different sections to find the percent crystallinity through the part thickness. The crystallinity level was measured with DSC (Figure 4.3-6).

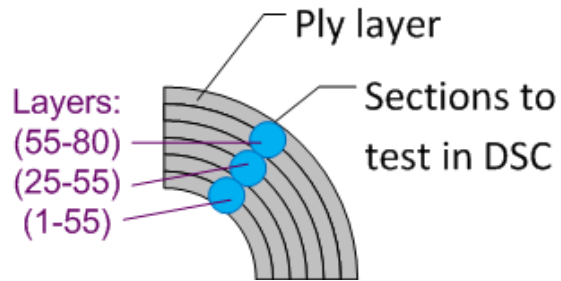


FIGURE 4.3-6: THE THREE SECTIONS OF THE ATP MANUFACTURED RING THAT WERE TESTED IN THE DSC

Three samples from each section were tested for crystallinity levels in the DSC. These results for each section were averaged to determine the correct crystallinity levels through the laminate thickness. The DSC method used to calculate the crystallinity level is as follows:

1. Heat the material from room temperature to 400°C at a heating rate of 10°C/min.
2. Hold at 400°C for 5 minutes.
3. Cool down at a rate of 10°C/min back to room temperature.

The peaks obtained from the DSC curves are a heat of crystallinity and heat of melting during the melting portion of the DSC method (Figure 4.3-7).

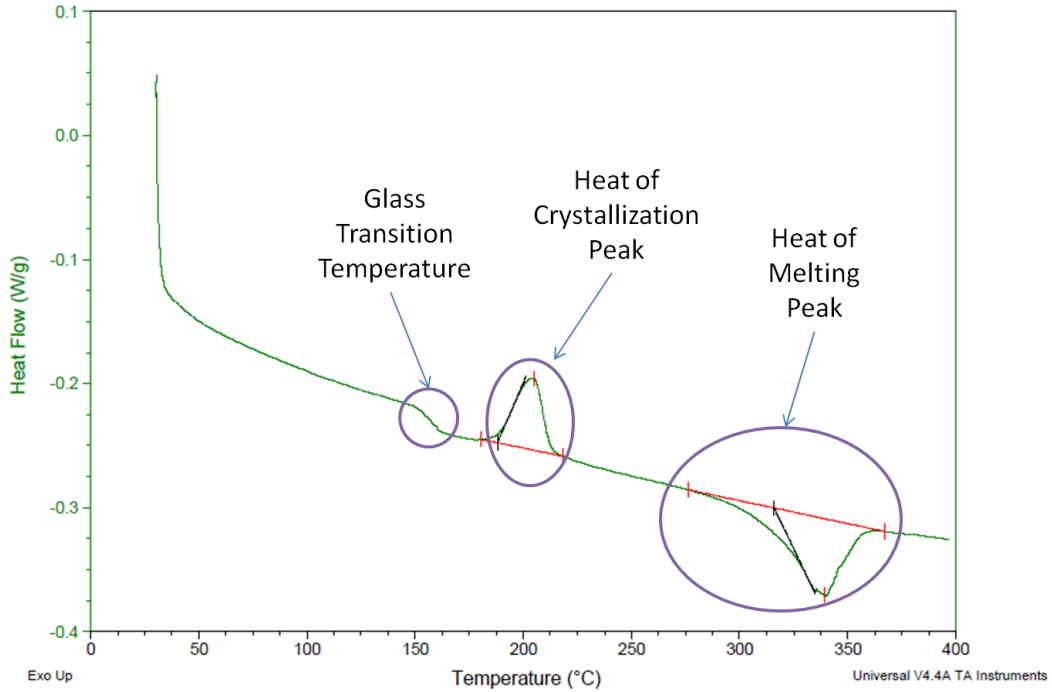


FIGURE 4.3-7: DSC CHART OBTAINED FOR A SECTION OF ATP MANUFACTURED RING

Before determining the crystallinity levels that were in the samples, the fiber volume in the composite laminate had to be neglected in the heat flow measurements. In order to do that, the resin weight fraction, which was taken to be 32% for both PEEK and PEKK composite tapes, was isolated from the total mass for the sample measured in the DSC.

$$m_{resin} = 0.32 m_{sample} \quad 20$$

The heat of crystallization for the resin can also be calculated after the heat of crystallization has been integrated. The same method was used to find the heat of melting:

$$H_{resin} = \frac{H_{sample}}{0.32} \quad 21$$

In order to determine the crystallinity level in the sample, the heat of crystallinity must be subtracted from the heat of melting to obtain the initial heat of reaction. Also, the fiber volume fraction had to be considered, so the percentage of the fibers, which was taken to be 61% [45] was removed, so that only the matrix volume was considered in the calculation of the crystallinity of the polymer matrix.

$$H_i = H_{c,resin} - H_{m,resin} \quad 22$$

This can then be applied to the total ultimate heat of reaction, 130 J/g, to calculate the percentage of crystals that have formed in the laminate during the ATP manufacturing process [5, 8].

$$X_i = \frac{H_i}{H_u} \quad 23$$

## 4.4 RESULTS

Since two things (temperature profiles and crystallinity levels) were examined during the ATP manufacturing process, the results have been broken down into two sections to clearly analyze both aspects that were tested. During ATP, the temperatures through the laminate were measured and after ATP the crystallinity levels through the laminate parts were measured.

### 4.4.1 TEMPERATURE PROFILE DURING THE PROCESS

Thermocouples measured the temperature changes through the laminate thickness and the mandrel during processing. While both PEEK and PEKK composite materials have similar temperature behavior, they both have different temperature peaks and cooling rates since the torch is set to different temperatures for each material. Thermocouple measurements were analyzed to understand the temperature changes through the part during ATP processing.

#### 4.4.1.1 EVOLUTION OF TEMPERATURE THROUGH MANUFACTURING

The nip point is where the tow material is heated under the torch (Figure 4.4-1). The first peak is the temperature of the torch when the thermocouple is placed immediately in between the layers.

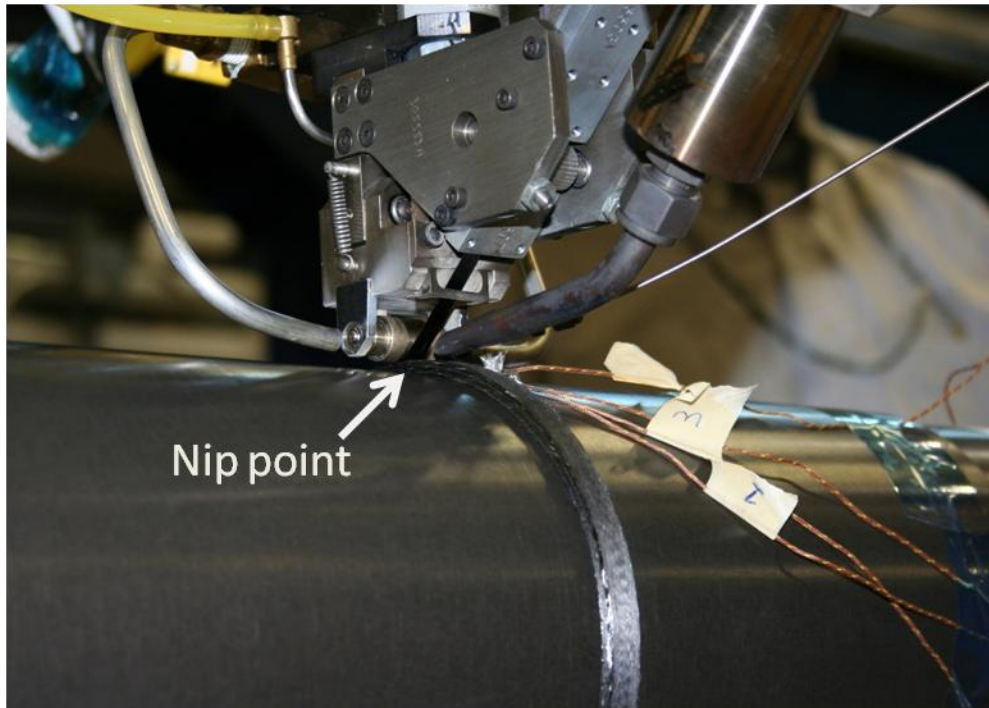


**FIGURE 4.4-1: CLOSEUP OF THE NIP POINT AND OF THE THERMOCOUPLE, WHICH LAYS IN BETWEEN THE LAMINATE LAYERS**

After the material completes the heating process it will begin the cooling process. Cooling occurs when the nip point moves away from the torch as the mandrel rotates. The part cools down to a temperature that is higher than room temperature. After a revolution, another layer is deposited. The layer with the thermocouple will rise in temperature after each revolution, as the material goes under the torch at the nip point. The temperature of the layer already laid down will rise, but not to such an extreme level as when it was initially laid down (Figure 4.4-2).

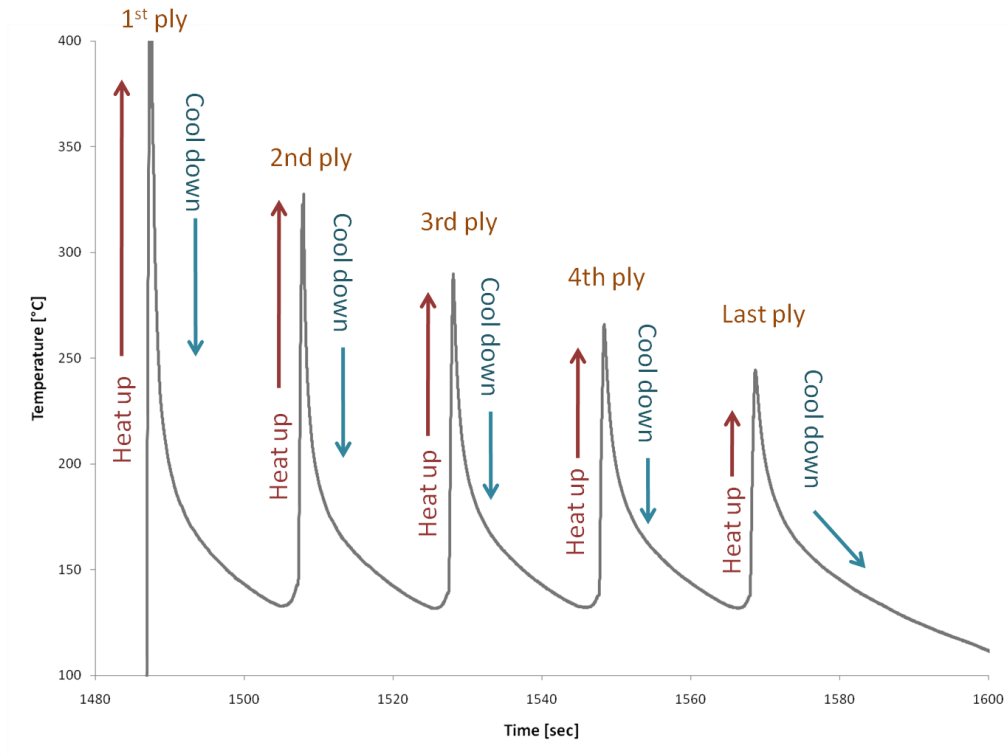


**FIGURE 4.4-2: GENERAL TEMPERATURE BEHAVIOR FOR ONE LAYER DURING ATP; THE MATERIAL REHEATS AFTER A MANDREL REVOLUTION WHEN THE TORCH PASSES OVER THE MATERIAL AT THE SAME POINT AGAIN**

As more layers are added to the laminate, the thermocouple results show two things about the heating and cooling behaviors: 1) the temperature which the part cools to after every revolution increases through the process and 2) the maximum temperature after each revolution gradually becomes lower as more material is consolidated onto the part (Figure 4.4-3).

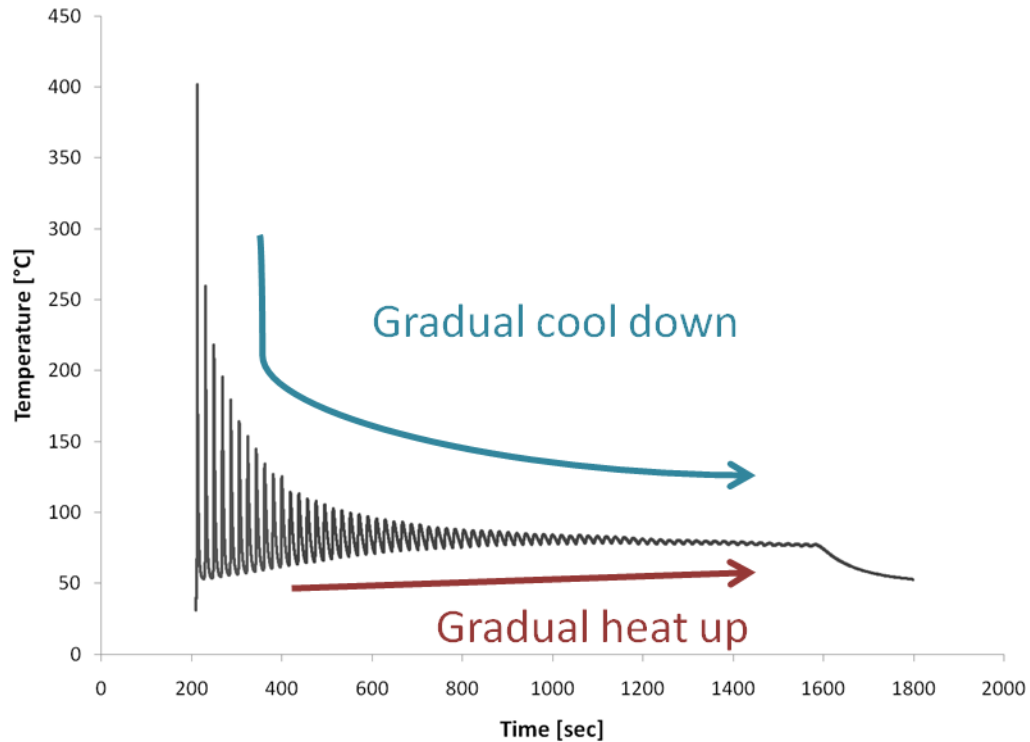


**FIGURE 4.4-3: TEMPERATURE WITH RESPECT TO PROCESSING TIME FOR ONE THERMOCOUPLE IN THE PEEK RING SHOWS THAT AS MORE LAYERS ARE DEPOSITED THE PEAK TEMPERATURE DECREASES, WHILE THE OVERALL TEMPERATURE GRADUALLY INCREASES**

All of the thermocouples placed into the ring during the process can be plotted together for each ring to examine how the temperatures through the manufacturing process evolved over time (Figure 4.4-4 and Figure 4.4-5). Since the PEEK-carbon fiber material was heated up to a higher temperature than the PEKK-carbon fiber material, the initial temperature of the material placed was higher for the PEEK than PEKK.

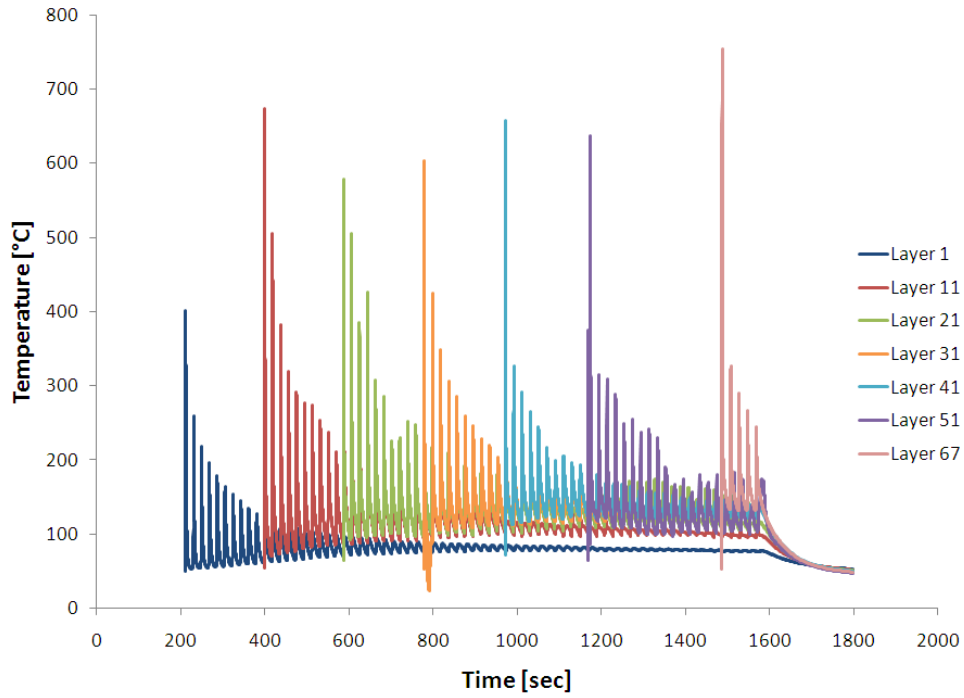


FIGURE 4.4-4: THERMOCOUPLE RESULTS FOR THE PEEK RING MANUFACTURED BY ATP FOR SEVEN LAYERS

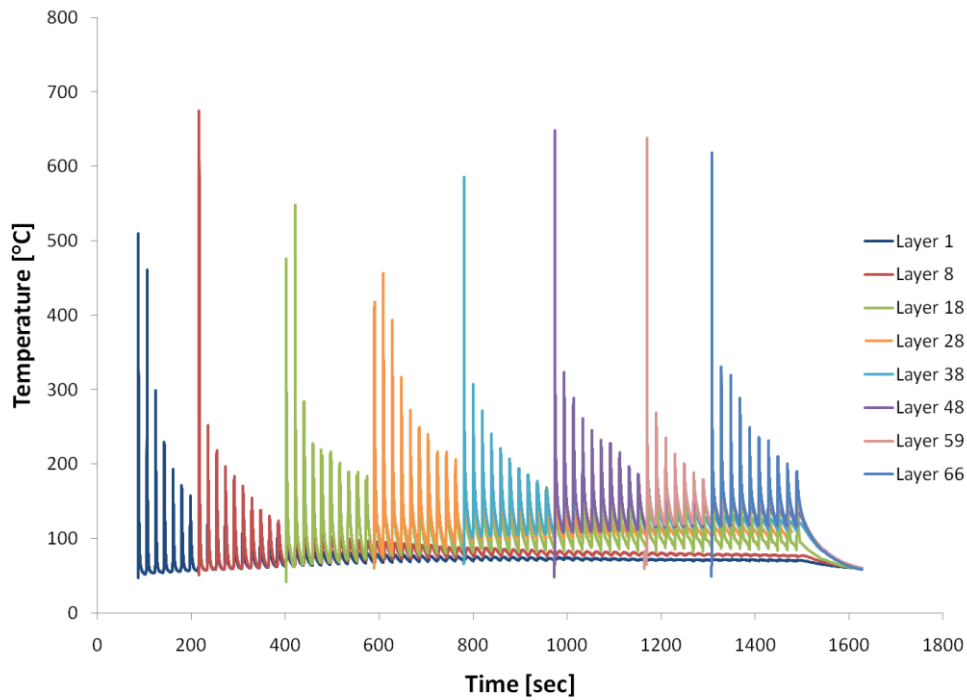
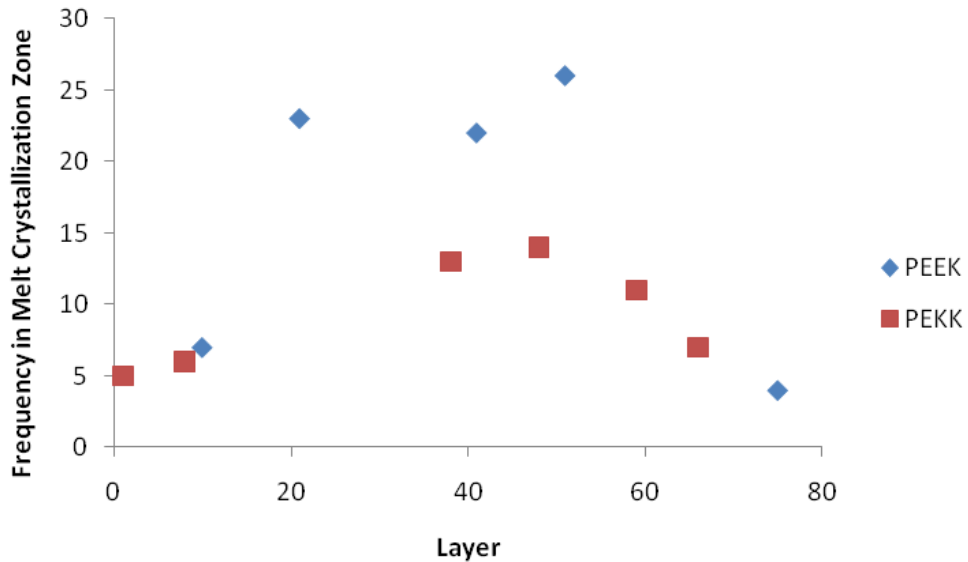


FIGURE 4.4-5: THERMOCOUPLE RESULTS FOR THE PEKK RING MANUFACTURED BY ATP FOR EIGHT LAYERS

For the first few revolutions after the thermocouple has been deposited, the material's temperature at that point raises back into the melt crystallization region, which is the temperature range between the melting temperature and the glass transition temperature. The layers deposited early in the process return to the melt crystallization region less frequently than the layers deposited later in the process. For the last layers, the frequency would be notably higher, however, the process ended when the layers were still being reheated into the melt crystallization region (Figure 4.4-6).



**FIGURE 4.4-6: FOR EACH LAYER MEASURED, THE FREQUENCY THAT THE TEMPERATURE PEAKS INTO THE MELT CRYSTALLIZATION ZONE; THE MIDDLE LAYERS SHOW A HIGHER FREQUENCY THAN THE FIRST AND LAST LAYERS**

The frequency that the laminate part layers returns to the melt crystallization temperature region during the process could have an influence on the final crystallinity level of the material for those layers. The middle layers in the PEEK ring was reheated more often into the melt crystallization region than for the layers in the PEKK ring, due to PEEK's

larger melt crystallization range. This would make it viable to predict that the crystallinity level will be highest in the middle section of the ring.

#### 4.4.1.2 MATERIAL HEATING AND COOLING RATES DURING MANUFACTURING

When the torch goes over the material, there is a sharp peak in temperature and then the laminate will cool down. The details of the material's initial heating and cooling stages shows changing heating and cooling rates through the process (Figure 4.4-7). For each of the subsequent times that the torch passes over the thermocouple, i.e. when another layer of tow is deposited onto the laminate, the peak temperature becomes less extreme. The temperature to which the part rises to influences the cooling rate of the layer after that revolution.

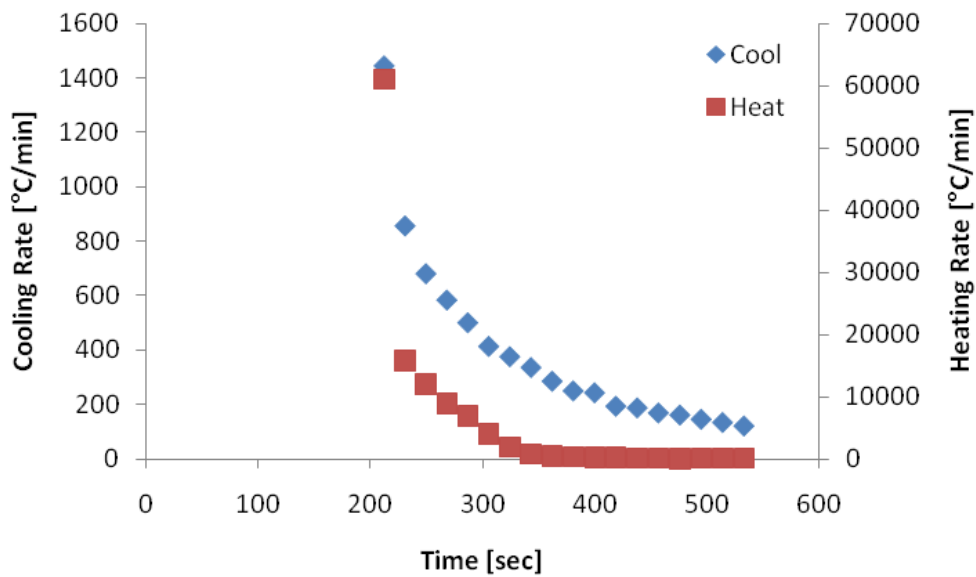
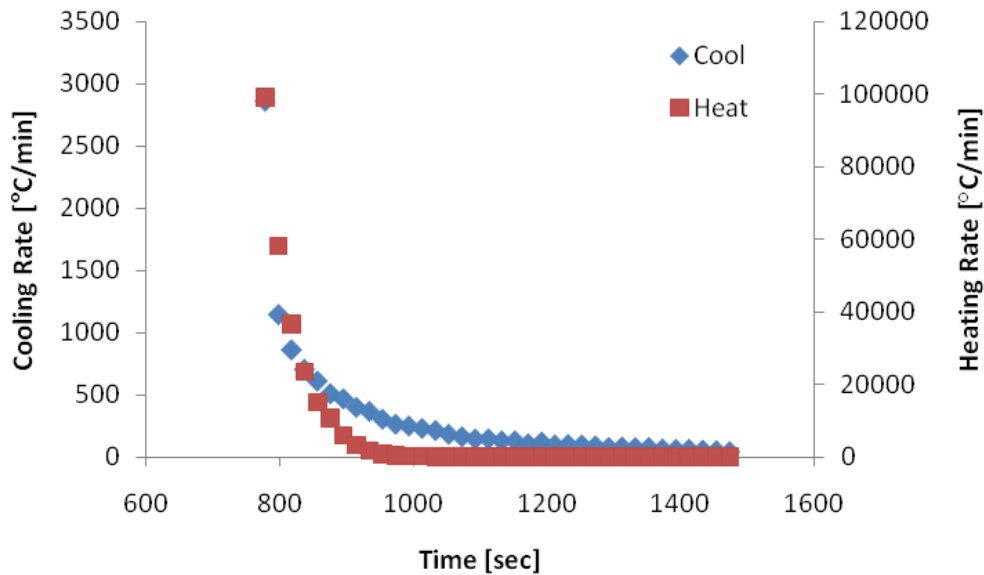


FIGURE 4.4-7: PEEK RING AT LAYER 10 - THE COOLING AND HEATING RATES WITH RESPECT TO THE PROCESSING TIME FOLLOW AN EXPONENTIAL TREND

The PEEK and PEKK composite laminate rings both show a similar pattern for all the layers graphs when they undergo the heating and cooling stages during manufacturing (Figure 4.4-8).



**FIGURE 4.4-8: PEEK RING AT LAYER 41 - THE COOLING AND HEATING RATES WITH RESPECT TO THE PROCESSING TIME FOLLOW AN EXPONENTIAL TREND**

The best way to calculate the cooling rate is to take the derivative, or slope, of the temperature as a function of time. However, the cooling rate is split up into sections since the cooling rate does not stay constant through cool down. The temperature follows a pattern that is not a constant line; rather, it is a set of transitions during the revolution that has a similar shape to an exponential function (Figure 4.4-9).

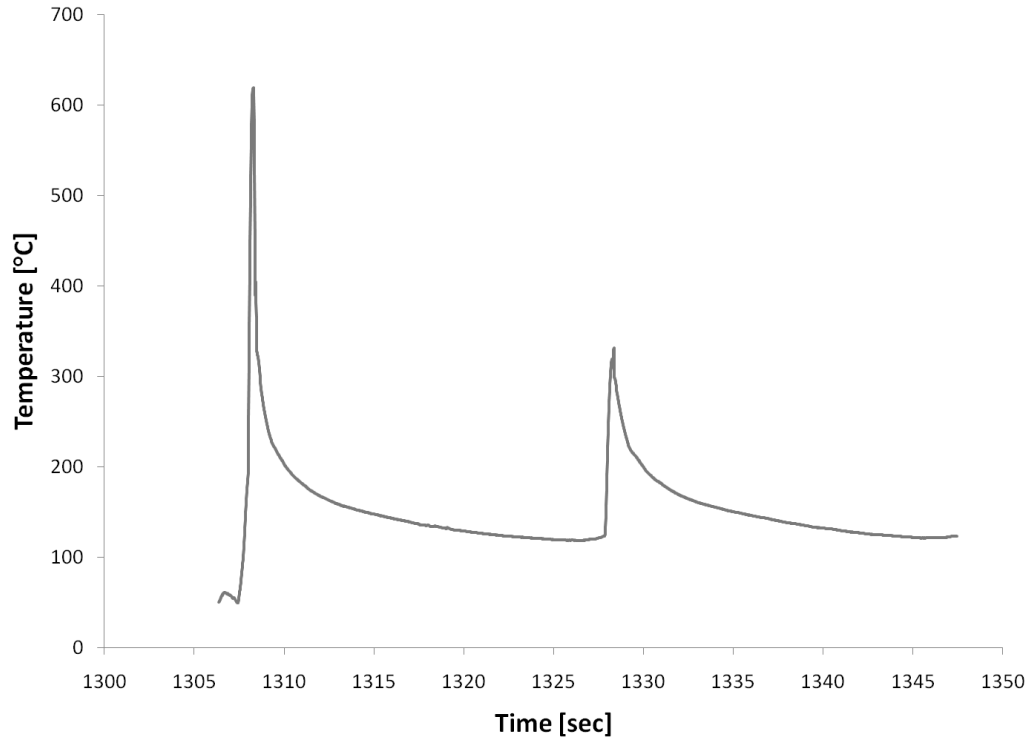


**FIGURE 4.4-9: A GENERAL THERMOCOUPLE CHART OF TEMPERATURE WITH RESPECT TO PROCESSING TIME, AFTER ONE REVOLUTION**

To calculate the cooling rate of the different sections of the “temperature versus time” charts, the sampling rate of how often the thermocouple records the data is used to extract the data to calculate the cooling rates. For these experiments, the sampling rate of the thermocouple acquisition unit was set at 150 Hz, meaning that 150 samples were taken every second. This was the fastest possible rate that could be obtained to take thermocouple temperature measurements for this system in a wireless mode. Thus, for the initial cool down portion of the curve, the cooling rate is taken to be the first 50 samples after the peak temperature. This correlates to a third of a second after the torch passed over the nip point section of the material, and is the significant section of the cooling rate that the material is subjected to.

The cooling rates of the subsequent torch passes on the layers that are reheated into the melt crystallization region needs to be highlighted as this effect will influence the final crystallinity level in the laminate (Figure 4.4-10 and Figure 4.4-11).

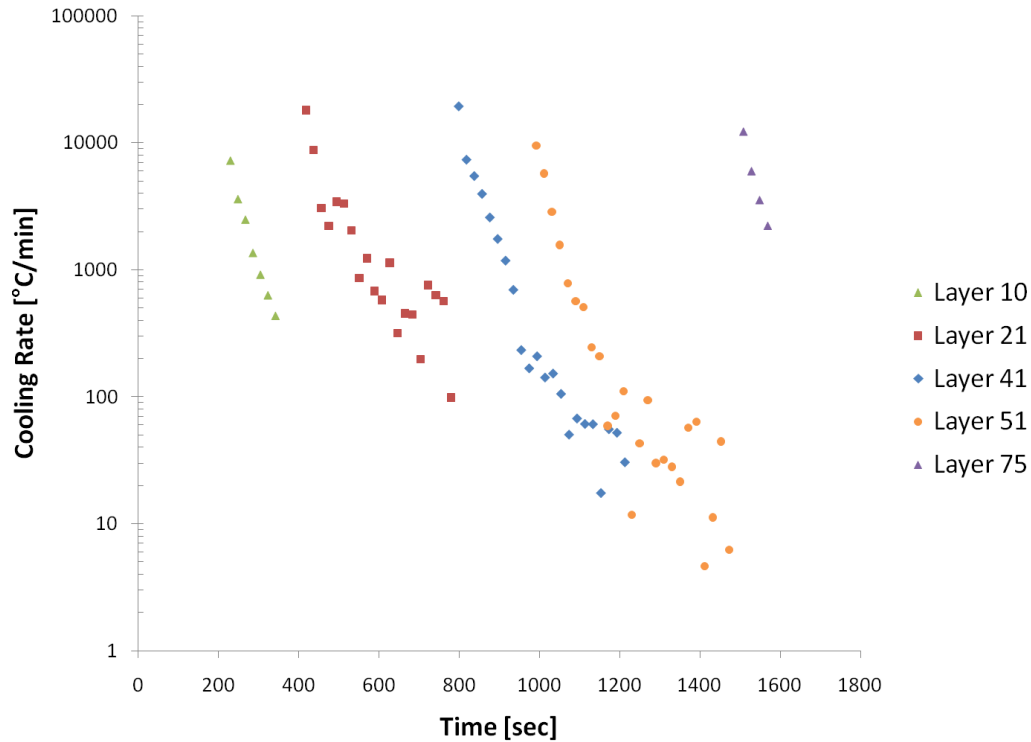


**FIGURE 4.4-10: THE COOLING RATES FOR THE VARIOUS LAYERS FOR THE PEEK RING AFTER EACH ROTATION WITH RESPECT TO THE PROCESSING TIME FOR ROTATIONS WHERE THE MATERIAL IS REHEATED INTO THE MELT CRYSTALLIZATION REGION**

The cooling rates for the PEKK ring will have similar behavior to the cooling rates in the PEEK ring. However, the PEKK ring will have different cooling rates though the layers since the temperature of the torch that the part is subjected to is set at a lower temperature due to PEKK's lower melting temperature.

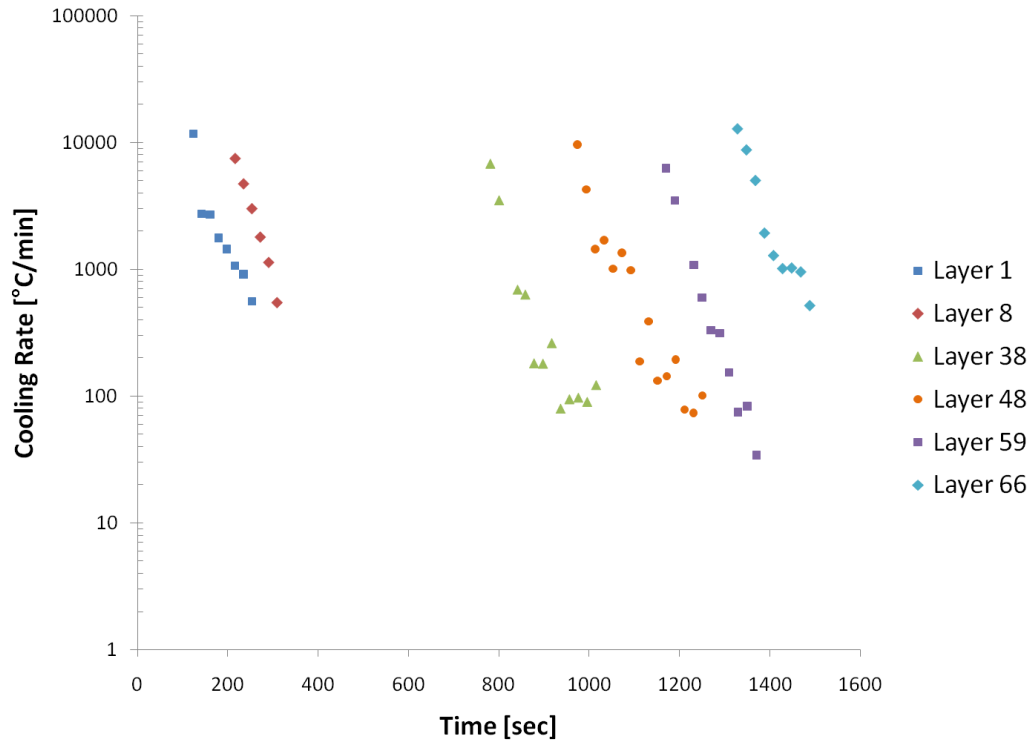


**FIGURE 4.4-11: THE COOLING RATES FOR THE VARIOUS LAYERS FOR THE PEKK RING AFTER EACH ROTATION WITH RESPECT TO THE PROCESSING TIME; ONLY DISPLAYING COOLING RATES FOR THE ROTATIONS WHERE THE MATERIAL IS REHEATED INTO THE MELT CRYSTALLIZATION REGION**

The previous figures make it apparent that the number of times the part is reheated into the melt crystallization region is fewer for the material that is closer to the mandrel than for the material that is deposited further from the mandrel. The cooling rates behave in a logarithmic manner with respect to the processing time. The fastest cooling rate occurs when the material is initially laid down, but as more layers are deposited, the layer measured will decrease in cooling rate by ten-fold.

#### 4.4.2 MANDREL EFFECT ON COOLING THE MATERIAL

During the ATP process, the temperature of the material tow is affected by the temperature of the surface that it is laid onto. Two things can affect this: the actual temperature of the material during the lay down and the ease of heat transfer to the other material. This would be a phenomenon known as the heat sink effect.

A material tow applied to a hotter surface will not drop in temperature as much as if it is consolidated onto a much cooler surface. The sections manufactured close to the mandrel cool down faster since the mandrel has a lower temperature than the temperature of the plies deposited. Thus, the sections manufactured later end up having a slower overall cool down since the composite material temperature is higher than the mandrel temperature. Essentially the cooling rate of the material will be faster since the heat will be drawn from the composite material into the cooler aluminum material from the mandrel. The cooling rate graphs from the previous section (Figure 4.4-10 and Figure 4.4-11) describe the influence of the temperature profile through the process.

During manufacturing one of the rings, a thermocouple measured the mandrel temperature. The thermocouple was placed about 10 cm away from where the laminate ring was being manufactured during the ATP process (Figure 4.4-12).

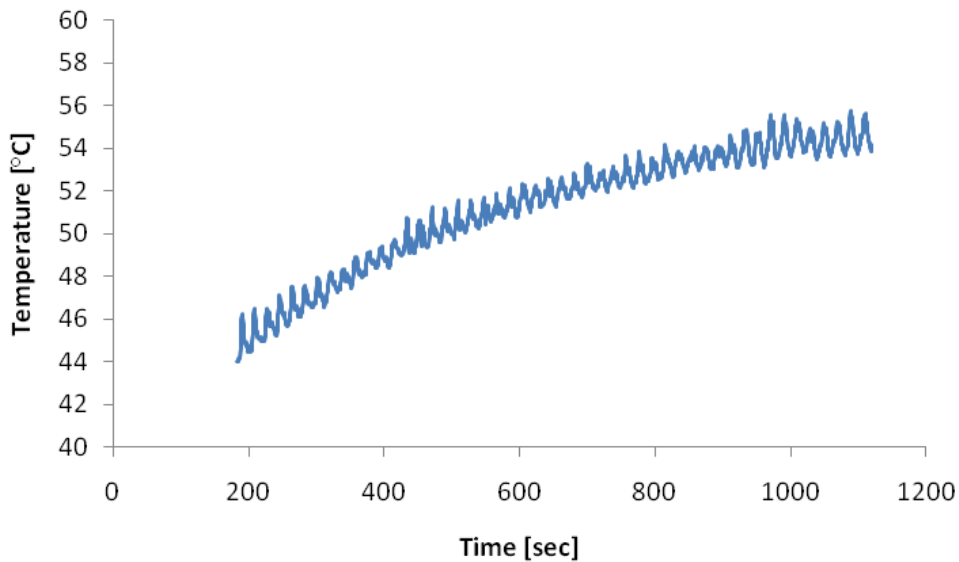


**FIGURE 4.4-12: THE MANDREL TEMPERATURES DURING THE ATP PROCESS GRADUALLY INCREASE DURING MANUFACTURING TIME**

The recorded mandrel temperature at the beginning of the manufacturing process was about 45°C and by the end it was 55°C. Even though the nitrogen torch was localized to flow over the tow material, the nitrogen gas would also heat up the mandrel which creates the “noise” peaks in the temperature graph. The peaks correlate to when the thermocouple was at the closest to the torch during the revolution. Another thing to consider is where the overall 10°C increase in the mandrel temperature comes from. It is most likely due to some of the heat being drawn from the part that was being laid up onto the mandrel into the mandrel to raise the temperature.

During the cool down, the section of the material laminate close to the mandrel cools down to about 50°C after a revolution and for the section that was laid down towards the end of the process the material cooled down to 100°C after a revolution (Figure 4.4-13 & Figure 4.4-14). The mandrel temperature is a considerably lower temperature than what the laminate part will have when it cools down after a few seconds of being heated by the torch.

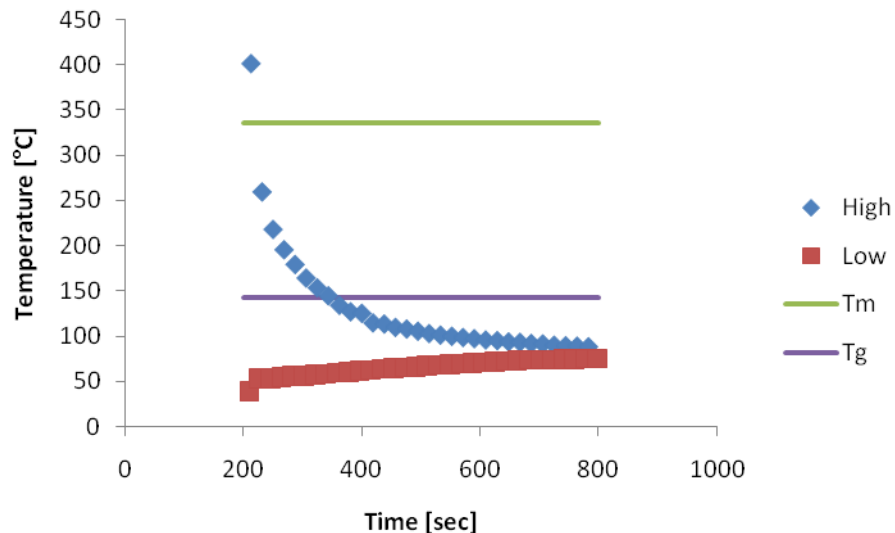


**FIGURE 4.4-13: PEEK RING AT LAYER 10 - THE “HIGH” TEMPERATURES AFTER EACH MANDREL REVOLUTION GRADUALLY DECREASES AND FALLS INTO THE MELT CRYSTALLIZATION RANGE FOR A PERIOD OF TIME WHILE THE “LOW” TEMPERATURES SLIGHTLY INCREASE WITH MANUFACTURING TIME**

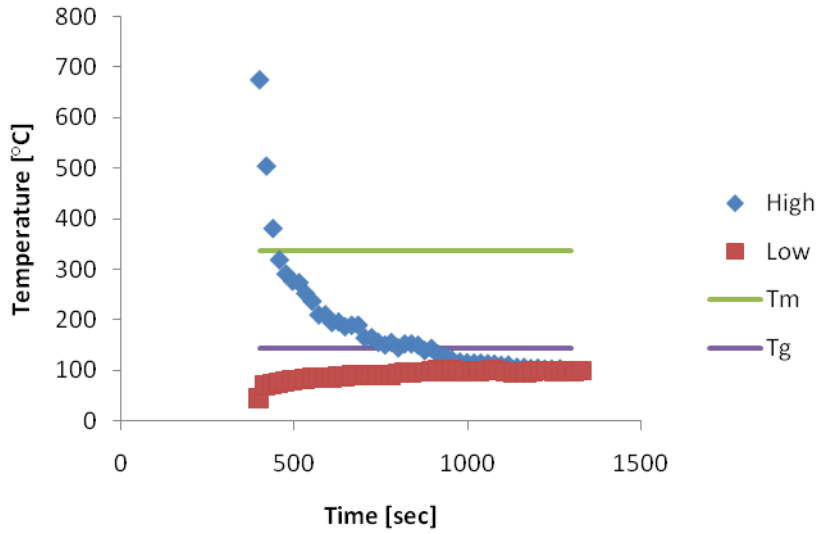


**FIGURE 4.4-14: PEEK RING AT LAYER 21 - THE “HIGH” TEMPERATURES AFTER EACH MANDREL REVOLUTION GRADUALLY DECREASES AND FALLS INTO THE MELT CRYSTALLIZATION RANGE FOR A PERIOD OF TIME WHILE THE “LOW” TEMPERATURES SLIGHTLY INCREASE WITH MANUFACTURING TIME**

There is a noticeable difference with layers deposited later on in the process, such as “Layer 75” in material PEEK (Figure 4.4-15) with “Layer 10” and “Layer 21”.

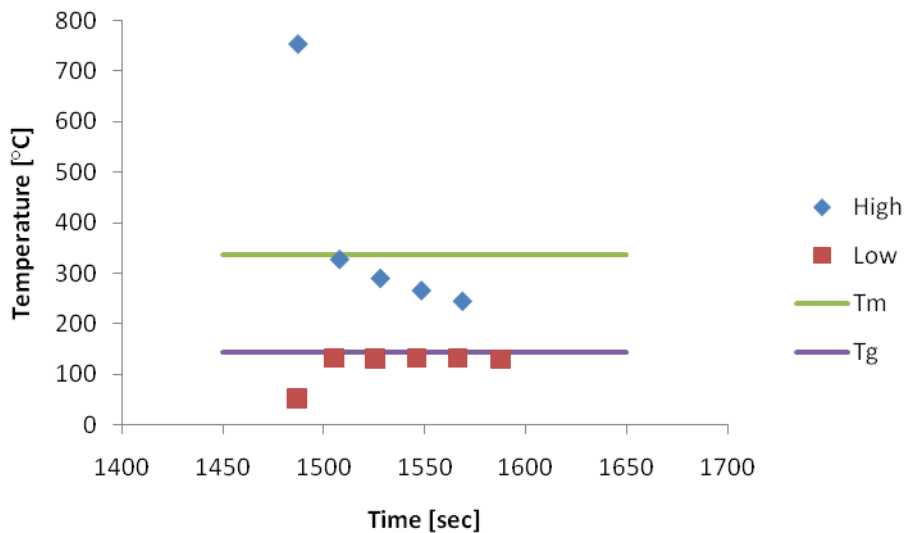


**FIGURE 4.4-15: PEEK RING AT LAYER 75 - THE “HIGH” TEMPERATURES AFTER EACH MANDREL REVOLUTION GRADUALLY DECREASES AND FALLS INTO THE MELT CRYSTALLIZATION RANGE FOR A PERIOD OF TIME WHILE THE “LOW” TEMPERATURES SLIGHTLY INCREASE WITH MANUFACTURING TIME**

When examining the temperature histories of all the layers during manufacturing, it is possible to correlate the material's cooling rate at each layer with the heat-sink effect. The temperature that the material goes down to is higher for both of these cases than for the layers placed earlier on. The graphs of the cooling rates with respect to the manufacturing time show that the cooling rates level off for layers deposited at the beginning of the ATP process. The remaining images of the other remaining layers for the PEEK ring and all of the images for the PEKK ring are found in Appendix B.

While the heat is being drawn from the composite material into the mandrel the overall composite material also heats up through the process. These effects combined together will impact the overall cooling rate of the material.

#### 4.4.3 COOLING RATE SUMMARY

Based on the cooling rate behavior found, it could be predicted that the laminates would have a gradient of the crystallinity level. The average cooling rates of the different sections for both rings were taken and can be summarized in the following table.

**TABLE 4.4-1: COOLING RATES OF THE THREE SECTIONS OF THE COMPOSITE RINGS**

	<b>PEEK</b> Cooling rate [°C/min]	<b>PEKK</b> Cooling rate [°C/min]
Inside (Layers 1-25)	21000	20000
Middle (Layers 25-55)	19000	8500
Outside (Layers 55-80)	12000	7000

Since the cooling rates are faster for the inside section there is reason to predict that the inside of the ring would have a lower crystallinity level than the outside of the ring. Another point to consider is that the part is not reheated into the melt crystallization region as often as for the layers that are placed at the very end of the process as the middle layers are reheated into the region. Thus, for predicting the general crystallinity level through the ring's thickness, it is possible that the middle would be highest, the inside with the lowest, and the outside being in the between.

#### 4.5 CRYSTALLINITY MEASUREMENTS OF PART POST PROCESSING

Post-processing, the laminate ring part was left alone to cool for a few hours to room temperature, and then removed from the mandrel. Then sections from the ring were cut out and tested in the DSC. The sections are named through the thickness of the material, as the "Inside (Layers 1-25)", "Middle (Layers 25-55)", and "Outside (Layers 55-80)". The "Inside" is designated as the part that was manufactured closest to the mandrel, the "Middle" is the middle of the thickness, and the "Outside" is the section that was manufactured last (Figure 4.5-1).

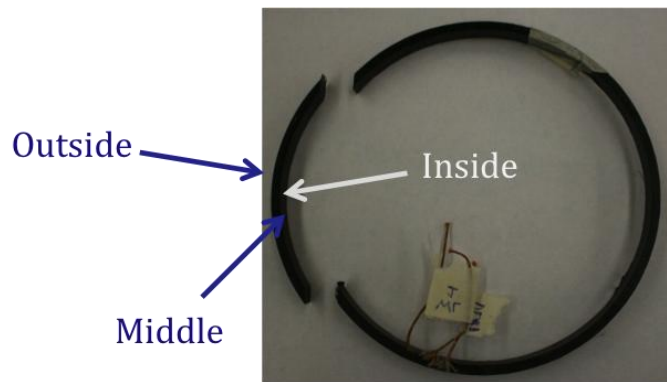
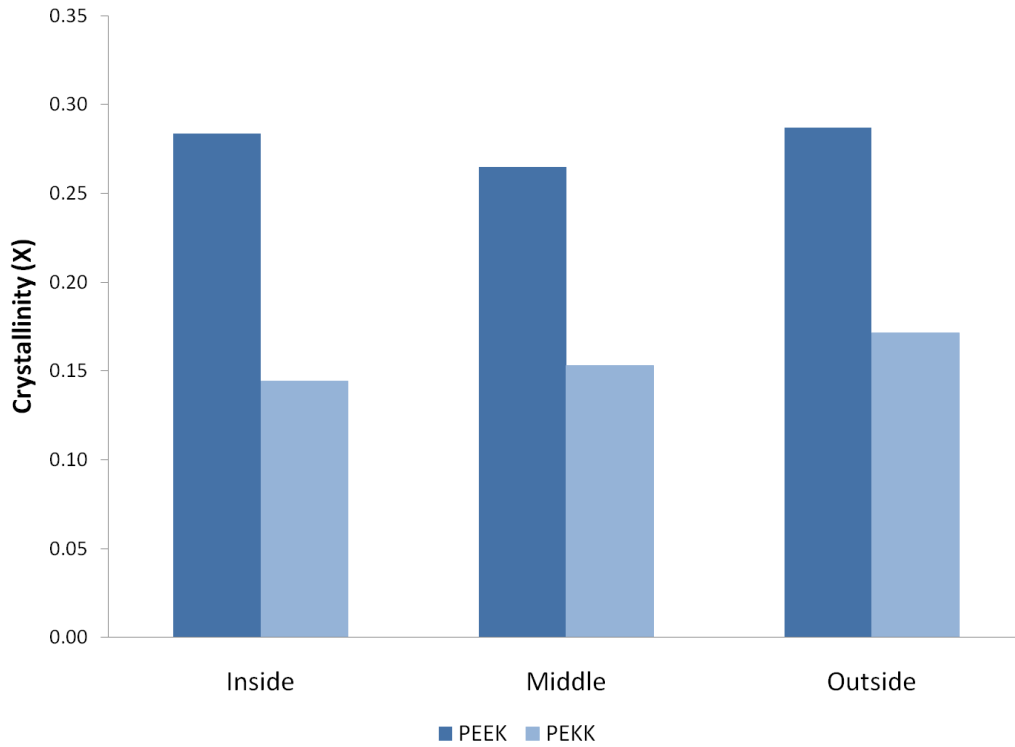


FIGURE 4.5-1: ACTUAL RING, DESCRIBING THE LOCATION OF WHERE EACH SAMPLE WAS TAKEN

The heat of crystallinity peaks and heat of melting peaks for all of the materials were integrated and used to determine the crystallinity level through the thickness of the laminate ring. Then the initial crystallinity

levels of the sections of the ring were calculated. Since there were three samples from each section, “Inside”, “Middle”, and “Outside”, the average crystallinity level is what is used for comparing through the thickness. The results from the DSC measurements are summarized in a bar chart (Figure 4.5-2).



**FIGURE 4.5-2: MEASURED CRYSTALLINITY LEVELS OF THE THREE SECTIONS OF BOTH LAMINATE RINGS**

The crystallinity level for the PEEK ring retained a high crystallinity level even at very rapid cooling rates. PEKK had a lower crystallinity level which is due to the polymer structure. This form of PEKK is a high crystallinity grade. The profile shows that there is no real gradient for the PEEK ring but a small one is present for the PEKK ring. There is a 3% change in the crystallinity level for the inside location with the outside location for both of the rings.

However, it was found that there was a slight gradient in crystallinity levels for the PEKK ring and no gradient was found for the PEEK ring. It is important to note that the crystallinity levels through the thickness were very close together, and at the very high cooling rates, the difference of a few thousand °C/min would not affect the crystallinity level drastically since the material grade allowed for high crystallinity levels at fast cooling rates.

#### 4.6 SUMMARY

After observing the ATP process by looking at the thermal profiles through the thickness of a laminate ring some of the following conclusions can be made:

- Cooling rates on a ATP manufactured part are rapid
- Both the initial cooling rate and temperature that the material cools to depends on the material onto which the laminate is deposited
- The cooling rate during a mandrel revolution is not constant and follows a pattern that is similar to an exponential decay
- The cooling rate is fastest when the layer is first deposited and it gradually becomes slower as more layers are added
- The material is reheated into the melt crystallization temperature region for a few rotations after the initial layer deposition
- The temperature of the part gradually increases during the manufacturing process

The thermal profile displays that the cooling rates may have a slight impact on the crystallinity level through the thickness of the part. The effect of the material's crystallinity level due to the reheat into the melt crystallization region was not looked at into detail in the present work, but

could be in a future project. From analyzing the cooling rates, it could be predicted that there would be a crystallinity gradient through the laminate thickness, since the cooling rate was faster on the inside of the ring than on the outside. However, when actually testing the parts manufactured for the crystallinity levels through the thickness it was found that there is not a significant crystallinity gradient through the thickness even though the cooling rates were different. This lends to the fact that the material is a high crystallizing material even at the fast cooling rates, so it is no longer dependent on the cooling rate at the extremely high rates that are obtained in ATP.

---

## CHAPTER 5: CONCLUSIONS

Understanding the thermal and crystallinity profiles of a thermoplastic composite laminate manufactured by the ATP manufacturing process will aid engineers to design better parts. Crystallization is essential for thermoplastic polymers and affects the material's mechanical properties. The poly (aryl) ketone thermoplastics crystallize to a high level even at fast cooling rates, which make them desirable for high performance applications where the material will need to have high strength. This work was split into two parts: modeling the crystallinity level of a thermoplastic film and a manufacturing process for a thermoplastic matrix composite with the same thermoplastic polymer as the film that was modeled in the first section.

Chapter 3 examined modeling the crystallinity levels of a thermoplastic PEEK film due to both an isothermal crystallization process and a dynamic crystallization process. The crystallinity models from literature are derived from Avrami's equation. PEEK film crystallizes in two-stages, so the models were based on such an approach that used a weight factor for each type of crystal that formed. Models were fit to both crystallization processes: isothermal and dynamic. DSC experiments on these processes were used to compare with the models. For both sets of data the method of least squares was used to find proper constants to fit the data to the models. The results of the tests are summarized as follows:

- Isothermal DSC data fit well to Avrami and Nakamura models.
- Dynamic DSC data compared with literature constants for the models by Velisaris, Cebe, and Tierney did not fit well.
- Nakamura's, Cebe's, and Tierney's models were fit to both sets of DSC data by the method of least squares:

- The data fit nicely for the slower cooling rates.
- At fast cooling rates, the models predicted too low; thus the models will fit to materials that will have low crystallinity levels at fast cooling rates.

Chapter 4 covered manufacturing parts by ATP in order to determine the cooling rates that occur on the part and subsequently the crystallinity levels through the final part thickness. A high thickness, ring geometry made by the ATP manufacturing process was instrumented for temperature measurements made through the thickness during the processing. The composite materials, with the high performance thermoplastic matrix chosen for this thesis were APC2/PEEK and APC/PEKK. Thermocouples measured the temperatures changes during the process, which was used to calculate the cooling rates of the material. These measurements showed:

- The cooling rates changed through the thickness of the part.
- The mandrel acted as a heat sink during the manufacturing process.
- The temperature of the material that the composite tow is laid down onto affects the temperature that the material will cool to, which impacts the cooling rate behavior of the material.
- Both PEEK and PEKK rings maintained a level of crystallinity that is close to the maximum level that can be obtained at the rapid cooling rates that the materials were subjected to in ATP.
- There was no significant crystallinity gradient through the final part thickness.

## 5.1 FUTURE WORK

After examining all that has been completed in this thesis, it is clear that this project leaves some unanswered questions that should be addressed in future work and projects.

First off, since the models examined in Chapter 3 did not fit perfectly to the experimental crystallinity data obtained by DSC, another model should be considered. Recall that the fit fell off especially at the faster cooling rates; this must be amended so that the model can fit a wider range of cooling rates. Also, it would be desirable for the model to not have so many different constants that will vary depending on the isothermal hold temperature or the dynamic cooling rate. A simple model is ideal for predicting the crystallinity level of a material. For instance, the best model would be straightforward, where one could input the cooling rate to output the maximum crystallinity level.

To further validate the models, PEKK film could be examined. Tierney's model [22, 25] has been used for PEKK film, but as was found in this thesis, the model itself must work properly before modeling another material.

Lastly, for the manufacturing process, it could be beneficial to see how the cooling rate was affected by the edges. Thus a shape, such as a cylinder, could be manufactured in order to better understand how the edges could influence the cooling rate and how the material consolidated next to what is currently being consolidated (instead of through the thickness) is affected. This geometry is also more applicable to a part geometry that is normally manufactured.

ATP provides a manufacturing method that will continue to aid in manufacturing composite laminates for the aerospace and automotive industries. A thermoplastic matrix composite in ATP process manufacturing process provides a cheaper alternative to the current material choice that uses a thermoset matrix, since the need for an autoclave becomes lost. Hopefully this thesis has provided an insight for modeling crystallinity levels in thermoplastics and the ATP manufacturing process in order to benefit the entirety of the composites industry.

---

## REFERENCES

1. Paul, D. and D. Pratt, *History of Flight Vehicle Structures 1903–1990*. Journal of Aircraft, 2004. **41**(5): p. 969-977.
2. McCormick, C. (2008) *How nickel contributes to more sustainable air transportation*. Nickel **23**.
3. Callister, W.D., *Fundamentals of Materials Science and Engineering: An Integrated Approach, 5th Edition*. 2001: Wiley.
4. Painter, P.C. and M.M. Coleman, *Fundamentals of polymer science : an introductory text*. 2nd ed. 1997, Lancaster, Pa.: Technomic Pub. Co. xv, 478 p.
5. Blundell, D.J. and B.N. Osborn, *The morphology of poly(aryl-ether-ether-ketone)*. Polymer, 1983. **24**(8): p. 953-958.
6. Price, F.P., *A phenomenological theory of spherulitic crystallization: Primary and secondary crystallization processes*. Journal of Polymer Science Part A: General Papers, 1965. **3**(9): p. 3079-3086.
7. Velisaris, C.N. and J.C. Seferis, *Crystallization kinetics of polyetheretherketone (peek) matrices*. Polymer Engineering & Science, 1986. **26**(22): p. 1574-1581.
8. Lee, W.I., et al., *Effects of Cooling Rate on the Crystallinity and Mechanical Properties of Thermoplastic Composites*. Journal of Reinforced Plastics and Composites, 1987. **6**(1): p. 2-12.
9. Avrami, M., *Kinetics of Phase Change. I General Theory*. The Journal of Chemical Physics, 1939. **7**(12): p. 1103-1112.
10. Hillier, I.H., *Modified avrami equation for the bulk crystallization kinetics of spherulitic polymers*. Journal of Polymer Science Part A: General Papers, 1965. **3**(9): p. 3067-3078.
11. Ozawa, T., *Kinetics of non-isothermal crystallization*. Polymer, 1971. **12**(3): p. 150-158.
12. Silva Spinacé, M.A. and M.A. De Paoli, *Characterization of poly(ethylene terephthalate) after multiple processing cycles*. Journal of Applied Polymer Science, 2001. **80**(1): p. 20-25.

13. Ahn, S.H., C.B. Cho, and K.Y. Lee, *The Kinetics of Shear-Induced Crystallization in Poly(Ethylene Terephthalate)*. Journal of Reinforced Plastics and Composites, 2002. **21**(7): p. 617-628.
14. Di Lorenzo, M.L. and C. Silvestre, *Non-isothermal crystallization of polymers*. Progress in Polymer Science, 1999. **24**(6): p. 917-950.
15. Nakamura, K., K. Katayama, and T. Amano, *Some aspects of nonisothermal crystallization of polymers. II. Consideration of the isokinetic condition*. Journal of Applied Polymer Science, 1973. **17**(4): p. 1031-1041.
16. Nakamura, K., et al., *Some aspects of nonisothermal crystallization of polymers. I. Relationship between crystallization temperature, crystallinity, and cooling conditions*. Journal of Applied Polymer Science, 1972. **16**(5): p. 1077-1091.
17. Tobin, M.C., *Theory of phase transition kinetics with growth site impingement. I. Homogeneous nucleation*. Journal of Polymer Science: Polymer Physics Edition, 1974. **12**(2): p. 399-406.
18. Tobin, M.C., *The theory of phase transition kinetics with growth site impingement. II. Heterogeneous nucleation*. Journal of Polymer Science: Polymer Physics Edition, 1976. **14**(12): p. 2253-2257.
19. Tobin, M.C., *Theory of phase transition kinetics with growth site impingement. III. Mixed heterogeneous-homogeneous nucleation and nonintegral exponents of the time*. Journal of Polymer Science: Polymer Physics Edition, 1977. **15**(12): p. 2269-2270.
20. Williams, M.L., R.F. Landel, and J.D. Ferry, *The Temperature Dependence of Relaxation Mechanisms in Amorphous Polymers and Other Glass-forming Liquids*. Journal of the American Chemical Society, 1955. **77**(14): p. 3701-3707.
21. Seferis, J.C., *Polyetheretherketone (PEEK): Processing-structure and properties studies for a matrix in high performance composites*. Polymer Composites, 1986. **7**(3): p. 158-169.
22. Ferrara, J.A., J.C. Seferis, and G. Vassilatos, *Processing Characteristics of PEKK Matrices and Their Composites*, in *23rd International SAMPE Technical Conference*. 1991. p. 1137-1148.
23. Cebe, P. and S.-D. Hong, *Crystallization behaviour of poly(ether-etherketone)*. Polymer, 1986. **27**(8): p. 1183-1192.

24. Velisaris, C.N. and J.C. Seferis, *Heat transfer effects on the processing-structure relationships of polyetheretherketone (PEEK) based composites*. Polymer Engineering & Science, 1988. **28**(9): p. 583-591.
25. Tierney, J., *Material Quality Development During the Automated Tow Placement Process*, in *Materials Science*. 2003, University of Delaware.
26. Mantell, S.C. and G.S. Springer, *Manufacturing Process Models for Thermoplastic Composites*. Journal of Composite Materials, 1992: p. 2348-2377.
27. Tierney, J.J. and J.W. Gillespie Jr, *Crystallization kinetics behavior of PEEK based composites exposed to high heating and cooling rates*. Composites Part A: Applied Science and Manufacturing, 2004. **35**(5): p. 547-558.
28. Cebe, P., *Application of the parallel Avrami model to crystallization of poly(etheretherketone)*. Polymer Engineering & Science, 1988. **28**(18): p. 1192-1197.
29. Tierney, J. and J.W. Gillespie, *Modeling of Heat Transfer and Void Dynamics for the Thermoplastic Composite Tow-Placement Process*. Journal of Composite Materials, 2003. **37**(19): p. 1745-1768.
30. The Boeing Company. *Development Work on Boeing 787 Noses Ahead*. 2005; Available from: <http://boeing.mediaroom.com/index.php?s=13&cat=27&page=8&item=694>.
31. Bourban, P.E., et al., *Material phenomena controlling rapid processing of thermoplastic composites*. Composites Part A: Applied Science and Manufacturing, 2001. **32**(8): p. 1045-1057.
32. Lee, W.I. and G.S. Springer, *A Model of the Manufacturing Process of Thermoplastic Matrix Composites*. Journal of Composite Materials, 1987. **21**(11): p. 1017-1055.
33. Tierney, J. and J.W. Gillespie, *Modeling of In Situ Strength Development for the Thermoplastic Composite Tow Placement Process*. Journal of Composite Materials, 2006. **40**(16): p. 1487-1506.
34. Ghasemi Nejjhad, M.N., R.D. Cope, and S.I. Güceri, *Thermal Analysis of in-situ Thermoplastic Composite Tape Laying*. Journal of Thermoplastic Composite Materials, 1991. **4**(1): p. 20-45.

35. Shih, P.-J. and A.C. Loos, *Heat Transfer Analysis of the Thermoplastic Filament Winding Process*. Journal of Reinforced Plastics and Composites, 1999. **18**(12): p. 1103-1112.
36. Guan, X. and R. Pitchumani, *Modeling of spherulitic crystallization in thermoplastic tow-placement process: heat transfer analysis*. Composites Science and Technology, 2004. **64**(9): p. 1123-1134.
37. Guan, X. and R. Pitchumani, *Modeling of spherulitic crystallization in thermoplastic tow-placement process: spherulitic microstructure evolution*. Composites Science and Technology, 2004. **64**(9): p. 1363-1374.
38. Joshi, S.C. and Y.C. Lam, *Integrated approach for modelling cure and crystallization kinetics of different polymers in 3D pultrusion simulation*. Journal of Materials Processing Technology, 2006. **174**(1-3): p. 178-182.
39. Talbott, M.F., G.S. Springer, and L.A. Berglund, *The Effects of Crystallinity on the Mechanical Properties of PEEK Polymer and Graphite Fiber Reinforced PEEK*. Journal of Composite Materials, 1987. **21**(11): p. 1056-1081.
40. Chang, I.Y. and J.K. Lees, *Recent Development in Thermoplastic Composites: A Review of Matrix Systems and Processing Methods*. Journal of Thermoplastic Composite Materials, 1988. **1**(3): p. 277-296.
41. Hojjati, M., J. Chen, and A. Yousefpour, *Crystallization Kinetics of Poly(ether ketone ketone) PEKK*, in *SAMPE*. 2008: Long Beach.
42. Hojjati, M., et al., *Crystallization Kinetics of CYPEK Poly Ether Ketone Ketone*, in *SAMPE*. 2007: Baltimore.
43. Cytec Industries Inc. *CYTEC-Engineered Materials*. October 7, 2010]; Available from: [www.cytec.com/engineered-materials/thermoplastics.htm](http://www.cytec.com/engineered-materials/thermoplastics.htm).
44. Motz, H. and J.M. Schultz, *The Solidification of PEEK. Part I: Morphology*. Journal of Thermoplastic Composite Materials, 1989. **2**(4): p. 248-266.
45. Cytec Fiberite Inc., *Thermoplastic Composite Materials Handbook*. 1999: Havre de Grace.

---

# APPENDIX A: MODELING

## 6.1 ISOTHERMAL MODELING

The experimental data was fit for both the Avrami model and the Nakamura model by using the method of least squares. The table below outlines the actual “ $k_1$ ” and “ $k_2$ ” values that were solved for in the Avrami equation and were fit to the data to make an appropriate fitting line.

TABLE 6.1-1: ISOTHERMAL K1 AND K2 VALUES IN AVRAMI MODEL

	323°C	325°C	327°C
$k_1$	7.28e-10	1.75e-10	5.36e-11
$k_2$	8.29e-7	3.64e-7	1.38e-7

For the Nakamura model, each constant was then fit to the “ $k$ ” values, by again, using the method of least squares. The data was fit appropriately and the set of constants is described here:

TABLE 6.1-2: THE NAKAMURA CONSTANTS SOLVED FOR BY METHOD OF LEAST SQUARES FOR FITTING THE MODEL TO THE ISOTHERMAL DSC DATA

	323°C	325°C	327°C
$A_1$	103.0	103.0	103.0
$B_1$	1483.053	1483.053	1483.053
$C_1$	196.987	196.987	196.987
$A_2$	8.17	8.56	9.24
$B_2$	1318.62	1318.61	1318.60
$C_2$	102.74	102.71	102.63
$w_1$	0.005	0.005	0.004
$w_2$	0.995	0.995	0.996

## 6.2 DYNAMIC MODELING

The method of least squares was used to fit the Cebe, Tierney, and Nakamura models to dynamic crystallization data for each of the constants for all of the cooling rates measured in DSC experiments. Each cooling rate has a different value which was the downfall in using these models.

**TABLE 6.2-1: BEST FIT CONSTANTS FOR FITTING THE CEBE MODEL TO EXPERIMENTAL DSC DATA**

	0.5°C/min	1°C/min	2°C/min	5°C/min	10°C/min	20°C/min	30°C/min
C <sub>11</sub>	1.44e3	1.49e3	1.50e3	1.51e3	1.53e3	1.65e3	1.81e3
C <sub>21</sub>	1572.6	1262.0	1148.3	1074.6	986.1	105.2	-1128.2
C <sub>31</sub>	1.00e6	1.00e6	1.00e6	1.00e6	1.00e6	1.00e6	1.00e6
C <sub>12</sub>	4.54e8	4.54e8	4.54e8	4.54e8	4.54e8	4.54e8	4.54e8
C <sub>22</sub>	5666.6	5299.6	4969.4	4714.2	4448.2	4356.8	4254.0
C <sub>32</sub>	5.96e5	5.96e5	5.96e5	5.96e5	5.96e5	5.96e5	5.96e5
w <sub>1</sub>	0.749	0.745	0.751	0.628	0.245	0.084	0.065
w <sub>2</sub>	0.251	0.255	0.285	0.372	0.755	0.916	0.935

**TABLE 6.2-2: BEST FIT CONSTANTS FOR FITTING THE TIERNEY MODEL TO EXPERIMENTAL DSC DATA**

	0.5°C/min	1°C/min	2°C/min	5°C/min	10°C/min	20°C/min	30°C/min
C <sub>11</sub>	-9.44	-5.68	0.732	11.1	15.8	3.89	4.68
C <sub>21</sub>	1497.2	1498.5	1496.4	1474.1	1451.2	1501.9	1501.8
C <sub>31</sub>	-9.78e1	-8.87e1	1.63e0	2.63e2	3.92e2	2.43e0	6.69e0
C <sub>12</sub>	2.45e1	2.26e1	2.09e1	1.83e1	1.51e1	1.64e1	1.65e1
C <sub>22</sub>	1312.0	1311.6	1310.6	1314.9	1323.7	1313.7	1313.7
C <sub>32</sub>	3.72e2	3.70e2	3.78e2	3.16e2	2.19e2	2.65e2	2.65e2
w <sub>1</sub>	0.575	0.462	0.364	0.344	0.335	0.419	0.412
w <sub>2</sub>	0.425	0.538	0.636	0.656	0.665	0.581	0.588

**TABLE 6.2-3: BEST FIT CONSTANTS FOR FITTING THE NAKAMURA MODEL TO EXPERIMENTAL DSC DATA**

	0.5°C/min	1°C/min	2°C/min	5°C/min	10°C/min	20°C/min	30°C/min
A <sub>1</sub>	-9.44	-5.68	0.73	11.07	15.83	3.89	6.34
B <sub>1</sub>	1.5e3	1.5e3	1.5e3	1.47e3	1.45e3	1.5e3	1.5e3
C <sub>1</sub>	-97.8	-88.7	1.63	263.0	392.0	2.43	4.34
A <sub>2</sub>	24.5	22.6	20.9	18.3	15.1	16.4	14.8
B <sub>2</sub>	1.31e3	1.31e3	1.31e3	1.31e3	1.32e3	1.31e3	1.24e3
C <sub>2</sub>	3.72e2	3.70e2	3.78e2	3.16e2	2.19e2	2.65e2	1.76e2
w <sub>1</sub>	0.57	0.46	0.36	0.34	0.34	0.42	0.32
w <sub>2</sub>	0.43	0.54	0.64	0.66	0.66	0.58	0.68

# APPENDIX B: ATP MANUFACTURING

## 7.1 COOLING RATE WITH RESPECT TO PROCESSING TIME

The temperature profiles of the laminate rings are what was looked at through the experiments in this project. In the Chapter 4, regarding the measurements of the temperatures through the thickness of the laminate, the cooling rates were calculated. While in the chapter, for clarity only the charts of the cooling rates with respect to the time for each revolution for each layer where the maximum temperatures had fallen into the melt crystallization. However, the following graphs show all of the cooling rates for the revolutions in both of the rings.

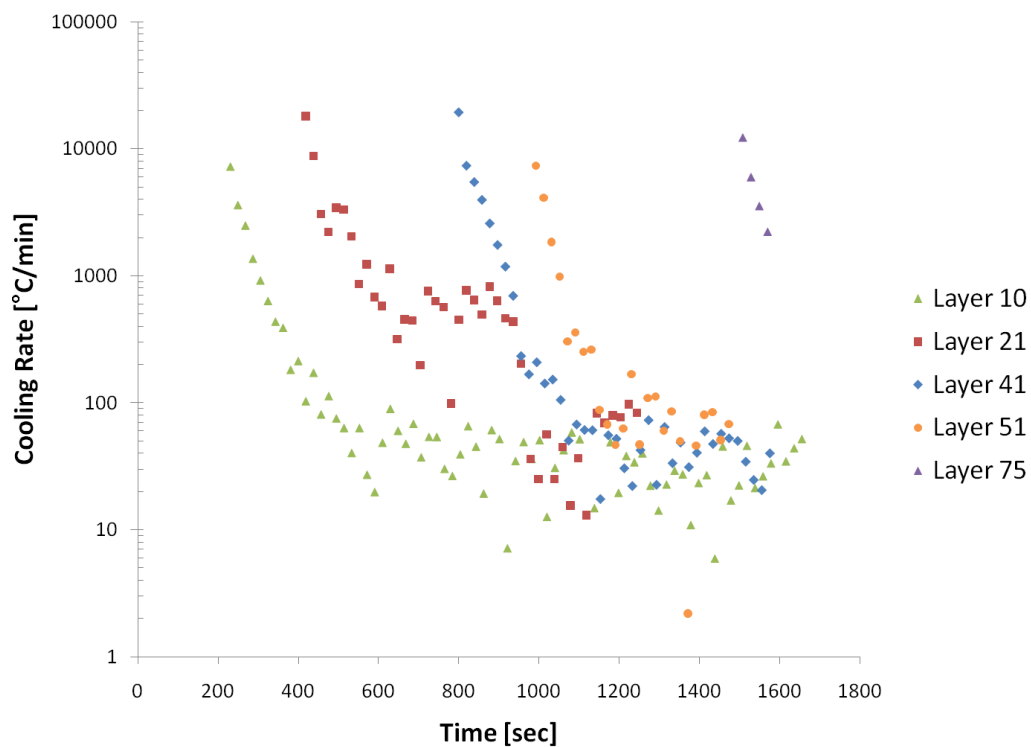


FIGURE 7.1-1: PEEK RING COOLING RATE AT EACH LAYER VERSUS ATP PROCESSING TIME WHERE EACH DOT REPRESENTS ONE MANDREL ROTATION

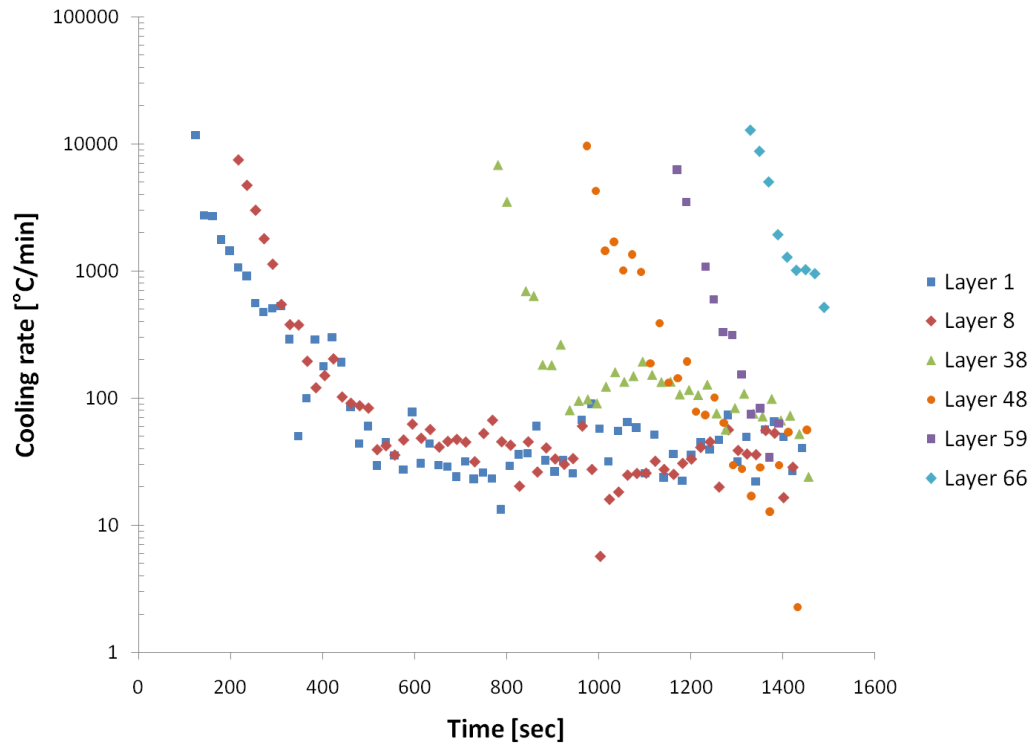
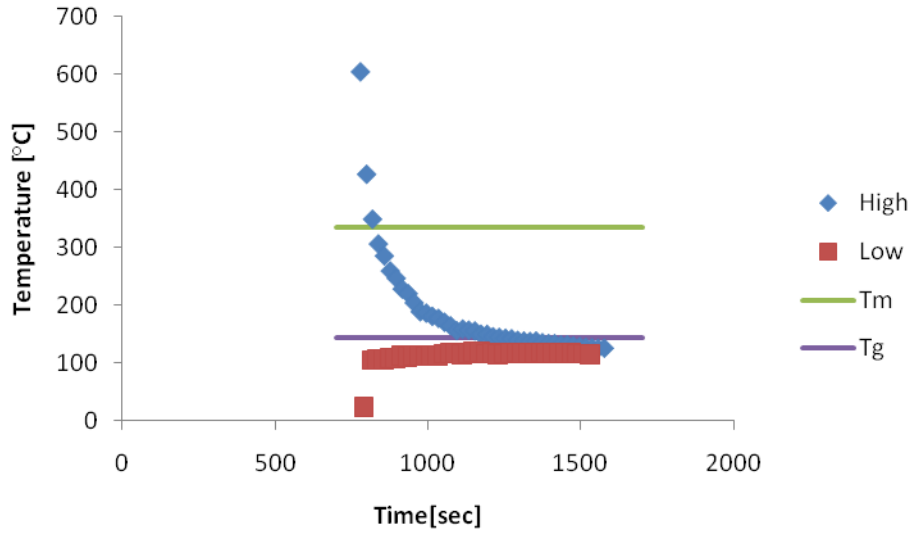


FIGURE 7.1-2: PEKK RING COOLING RATE AT EACH LAYER VERSUS ATP PROCESSING TIME, WHERE EACH DOT REPRESENTS ONE MANDREL ROTATION

## 7.2 TEMPERATURE WITH RESPECT TO PROCESSING TIME

The “High” and “Low” temperatures to which the material was brought to during the process for each of the revolutions plays an impact to really be able to clearly see the transition of how the temperatures were through the part. The  $T_m$  and  $T_g$  lines are included in the graphs to aid in visualizing where the material was reheated back into the melt crystallization region. The remaining layers for the PEKK ring and all of the layers for the PEKK ring are displayed here.

### 7.2.1 PEEK RINGS:



**FIGURE 7.2-1: PEEK RING AT LAYER 41 - THE "HIGH" TEMPERATURES AFTER EACH MANDREL REVOLUTION GRADUALLY DECREASES AND FALLS INTO THE MELT CRYSTALLIZATION RANGE FOR A PERIOD OF TIME WHILE THE "LOW" TEMPERATURES SLIGHTLY INCREASE WITH MANUFACTURING TIME**

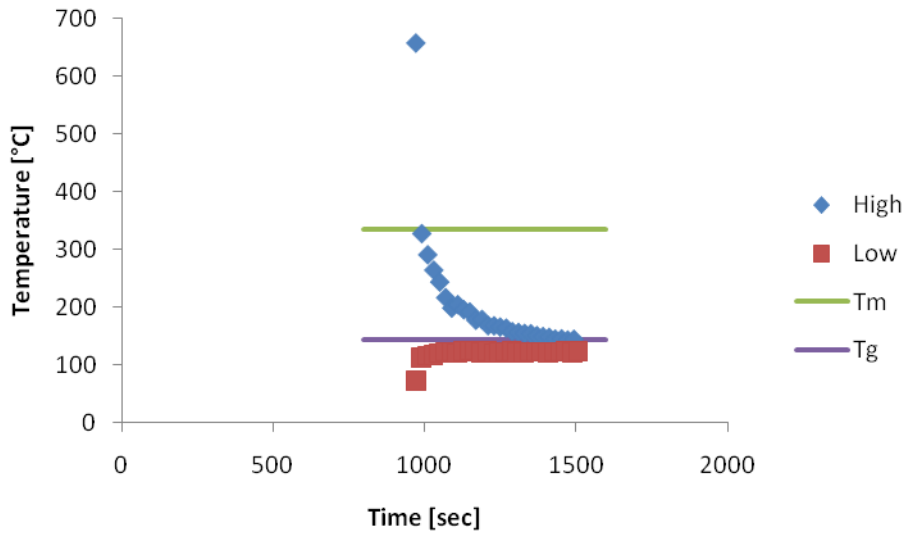


**FIGURE 7.2-2: PEEK RING AT LAYER 51 - THE "HIGH" TEMPERATURES AFTER EACH MANDREL REVOLUTION GRADUALLY DECREASES AND FALLS INTO THE MELT CRYSTALLIZATION RANGE FOR A PERIOD OF TIME WHILE THE "LOW" TEMPERATURES SLIGHTLY INCREASE WITH MANUFACTURING TIME**

7.2.2 PEKK RINGS:

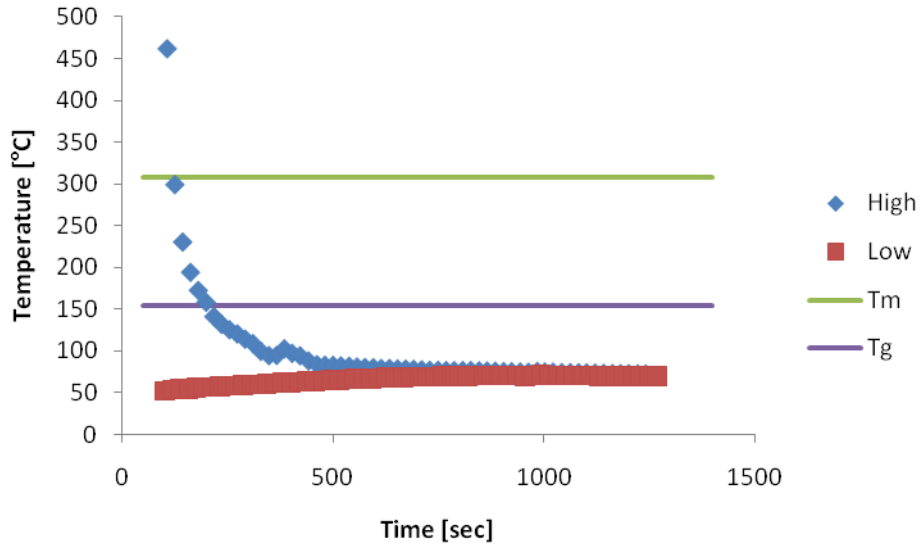


FIGURE 7.2-3: PEKK RING AT LAYER1 - THE “HIGH” TEMPERATURES AFTER EACH MANDREL REVOLUTION GRADUALLY DECREASES AND FALLS INTO THE MELT CRYSTALLIZATION RANGE FOR A PERIOD OF TIME WHILE THE “LOW” TEMPERATURES SLIGHTLY INCREASE WITH MANUFACTURING TIME

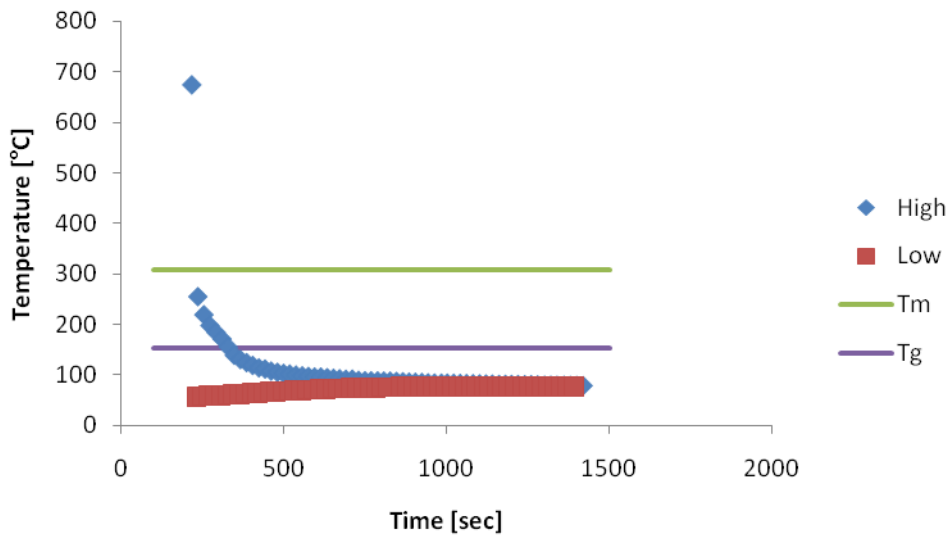
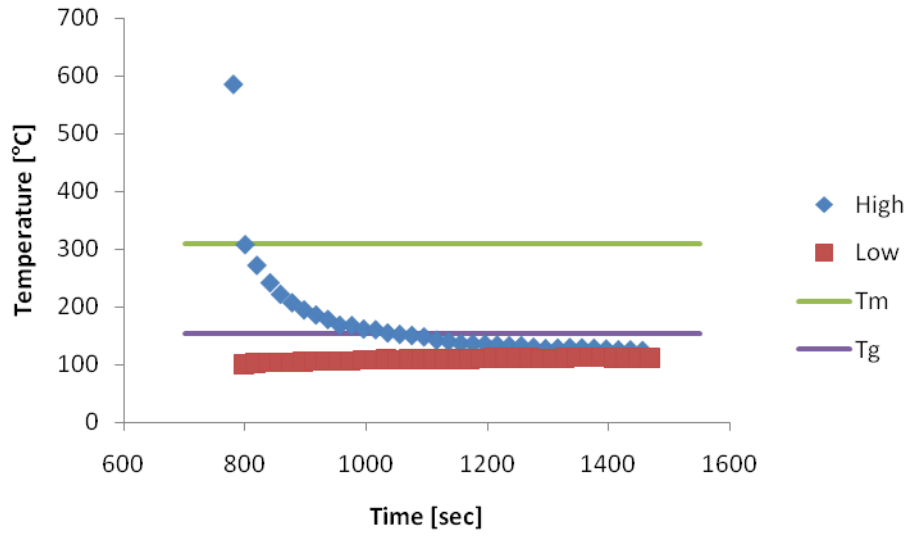
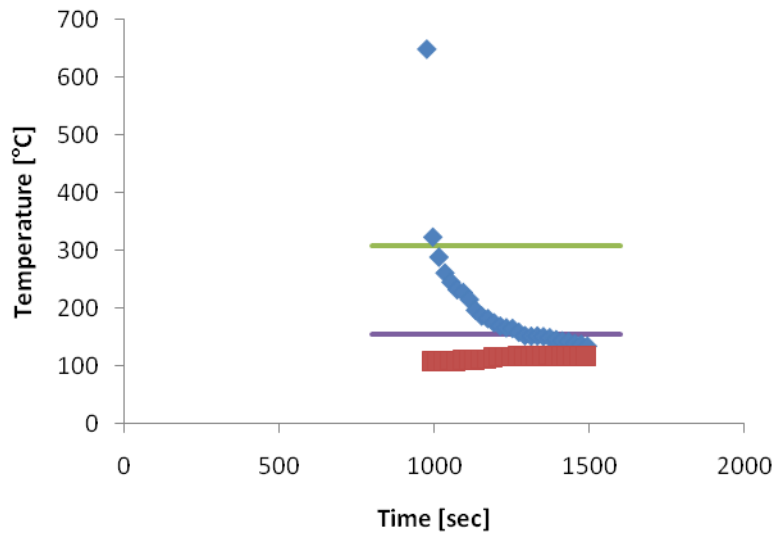


FIGURE 7.2-4: PEKK RING AT LAYER 8 - THE “HIGH” TEMPERATURES AFTER EACH MANDREL REVOLUTION GRADUALLY DECREASES AND FALLS INTO THE MELT CRYSTALLIZATION RANGE FOR A PERIOD OF TIME WHILE THE “LOW” TEMPERATURES SLIGHTLY INCREASE WITH MANUFACTURING TIME



**FIGURE 7.2-5: PEKK RING AT LAYER 38 - THE "HIGH" TEMPERATURES AFTER EACH MANDREL REVOLUTION GRADUALLY DECREASES AND FALLS INTO THE MELT CRYSTALLIZATION RANGE FOR A PERIOD OF TIME WHILE THE "LOW" TEMPERATURES SLIGHTLY INCREASE WITH MANUFACTURING TIME**



**FIGURE 7.2-6: PEKK RING AT LAYER 48 - THE "HIGH" TEMPERATURES AFTER EACH MANDREL REVOLUTION GRADUALLY DECREASES AND FALLS INTO THE MELT CRYSTALLIZATION RANGE FOR A PERIOD OF TIME WHILE THE "LOW" TEMPERATURES SLIGHTLY INCREASE WITH MANUFACTURING TIME**

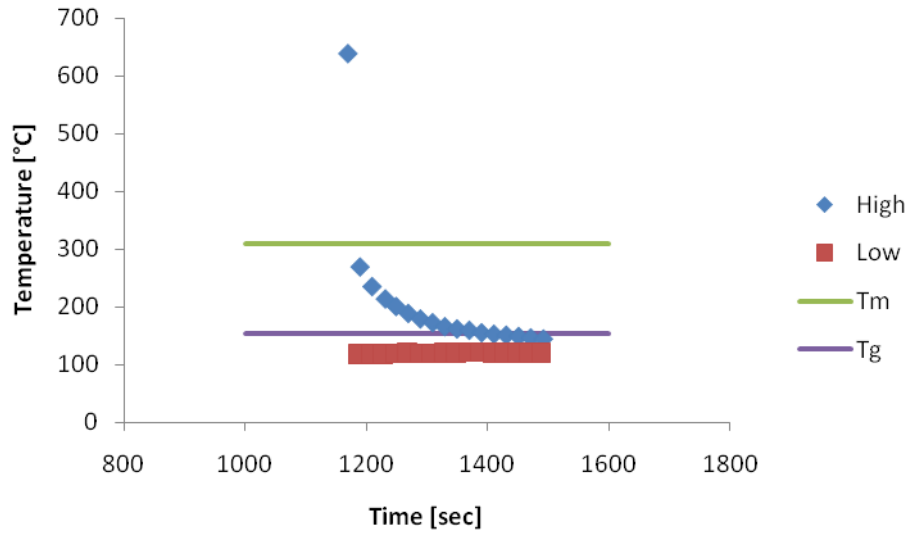


**FIGURE 7.2-7: PEKK RING AT LAYER 59 - THE “HIGH” TEMPERATURES AFTER EACH MANDREL REVOLUTION GRADUALLY DECREASES AND FALLS INTO THE MELT CRYSTALLIZATION RANGE FOR A PERIOD OF TIME WHILE THE “LOW” TEMPERATURES SLIGHTLY INCREASE WITH MANUFACTURING TIME**

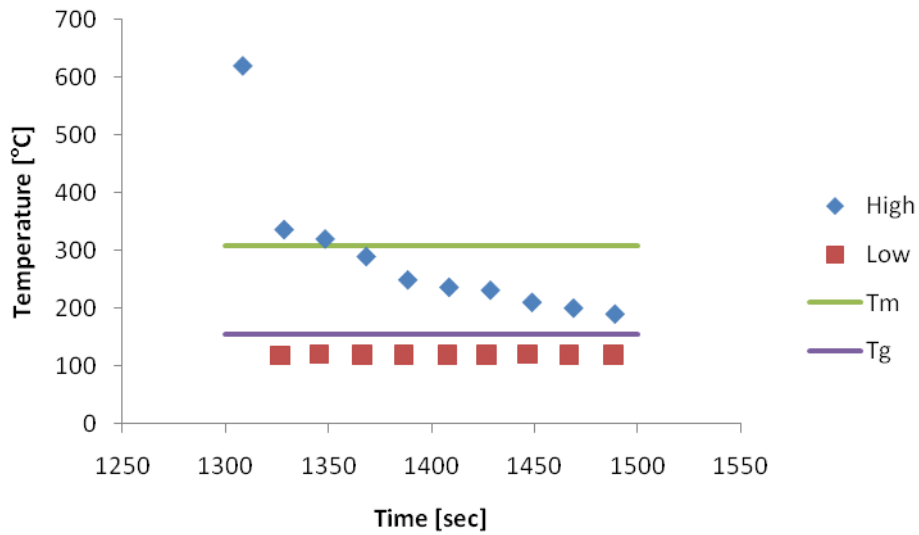


**FIGURE 7.2-8: PEKK RING AT LAYER 66 - THE “HIGH” TEMPERATURES AFTER EACH MANDREL REVOLUTION GRADUALLY DECREASES AND FALLS INTO THE MELT CRYSTALLIZATION RANGE FOR A PERIOD OF TIME WHILE THE “LOW” TEMPERATURES SLIGHTLY INCREASE WITH MANUFACTURING TIME**